

# **Stony Brook University**



OFFICIAL COPY

**The official electronic file of this thesis or dissertation is maintained by the University Libraries on behalf of The Graduate School at Stony Brook University.**

**© All Rights Reserved by Author.**

**Identification of Novel Interaction Sites between Myosin Phosphatase (MP) subunits  
PP1c  $\beta$  and MYPT1.**

A Dissertation Presented

by

**Elizabeth Scotto-Lavino**

to

The Graduate School

In Partial Fulfillment of the

Requirements

for the Degree of

**Doctor of Philosophy**

in

**Molecular and Cellular Pharmacology**

Stony Brook University

**May 2009**

**Stony Brook University**

The Graduate School

**Elizabeth Scotto-Lavino**

We, the dissertation committee for the above candidate for the  
Doctor of Philosophy degree, hereby recommend  
acceptance of this dissertation.

**Michael A. Frohman, M.D., Ph.D., Professor and Interim Chair  
Dissertation Advisor  
Department of Pharmacological Sciences**

**Nancy C. Reich, Ph.D., Professor  
Chairperson of Defense  
Department of Molecular Genetics and Microbiology**

**Howard Crawford, Ph.D., Assistant Professor  
Department of Pharmacological Sciences**

**Carol Carter, Ph.D., Professor  
Department of Molecular Genetics and Microbiology**

This dissertation is accepted by the Graduate School.

Lawrence Martin  
Dean of the Graduate School

Abstract of the Dissertation

**Identification of Novel Interaction Sites between Myosin Phosphatase (MP) subunits  
PP1c  $\beta$  and MYPT1.**

by

**Elizabeth Scotto-Lavino**

**Doctor of Philosophy**

in

**Molecular and Cellular Pharmacology**

Stony Brook University

**2009**

Myosin II association with actin, which triggers contraction, is regulated by orchestrated waves of phosphorylation / dephosphorylation of the myosin regulatory light chain (MLC). Modulation of myosin activity by small molecule inhibitors that inhibit the kinase step alter the cellular shape, adhesion and migration of many cancer cells. The dephosphorylation step is mediated by myosin phosphatase (MP), an enzyme complex that consists of a catalytic subunit (protein phosphatase 1, PP1c), a large subunit (myosin phosphatase targeting subunit, MYPT, also called MBS or M130) and a 20-kDa small subunit of unknown function. MYPT functions by targeting the PP1c catalytic subunit on its substrate, phosphorylated myosin II.

MP plays a function in muscle contraction and relaxation and plays a role in many smooth muscle-associated functions. The individual subunits of MP such as MYPT1 affect cell migration by regulating myosin phosphorylation and actin assembly. There have been implications indicating the importance MP in the inhibition of apoptosis, and the role of myosin phosphatase in the regulation of signaling events and in the ablation of tumor suppressor cascades.

In our lab, it has been illustrated that MP subunits PP1c  $\beta$  and MYPT1 are interdependent. Using both RNAi or retroviral shRNA expression systems, we have shown that when knocking down one of the subunits, the other subunit is knocked down.

Upon subunit knockdown, there appears to be a change in cell shape and cell number. Cells become larger and appear flattened out. There appears to be change in cell number due to the increased number of apoptotic cells. We observe that upon knockdown of the subunits, there is an increase in actin based structures along the perimeter of the cell.

There are three different isoforms of PP1c:  $\alpha$ ,  $\beta$ , and  $\gamma$ . When aligning the protein sequences of PP1c  $\beta$  from the three different species mouse, human and rat, the sequences are highly conserved. Using immunoprecipitation assays, I was able to show that MYPT1 binding is specific to the PP1c  $\beta$  isoform. MYPT1 does not interact with the PP1  $\alpha$  or  $\gamma$  isoforms. We were interested in studying how the MYPT1 and PP1c  $\beta$  subunits of myosin phosphatase interact and the reason for PP1c isoform specificity.

In order to address this question, we made two sets of PP1c chimera constructs swapping different regions between PP1c  $\beta$  and PP1c  $\gamma$ . From this data, I concluded that our region of interest between residues 121 and 303 of PP1c  $\beta$  was required for its interaction with MYPT1. The next approach taken to investigate this interaction was mutation of the divergent residues between PP1c  $\beta$  and  $\gamma$  isoforms in this region to the corresponding residue in the other isoform and then looking at the affects of these mutations on MYPT1 interaction was studied using immunoprecipitation assays. The only PP1c  $\beta$  mutation that had an effect on PP1c  $\beta$  binding to MYPT1 was the T197Q mutation. This mutation greatly decreased the capability of PP1c  $\beta$  to bind to MYPT1. This indicates that PP1c  $\beta$  residue 197 plays a role in the interaction with MYPT1. When analyzing the results from the PP1c  $\gamma$  mutants made, the only construct that rescues the binding affinity for PP1c  $\gamma$  is the construct in which residues 237 and 238 are mutated to the corresponding residues found in PP1c  $\beta$  (H237N/K238R,  $\gamma$ 2x). Based on this data I have identified novel binding sites for MYPT1 on PP1c  $\beta$ , which has implications for potential screening strategies for cancer therapeutic agents.

Dedicated to everyone in my life who have supported my endeavors in science;  
my husband Anthony, my parents, siblings and loved ones.

## Table of Contents

|   |             |
|---|-------------|
| <b>List of Figures.....</b>   | <b>viii</b> |
| <b>List of Tables.....</b>  | <b>xi</b>   |
| <b>List of Abbreviations.....</b>   | <b>xii</b>  |
| <b>Chapter 1: Introduction.....</b>   | <b>1</b>    |
| <b>Myosin Phosphatase and Cancer.....</b>   | <b>1</b>    |
| <b>Ras and Cancer.....</b>  | <b>2</b>    |
| <b>I. Identification of Novel Interaction Sites between Myosin Phosphatase (MP) subunits PP1c <math>\beta</math> and MYPT1.....</b>         | <b>4</b>    |
| <b>II. Investigation of the differential accumulation of H-Ras and K-Ras within the cell.....</b>   | <b>5</b>    |
| <b>III. Identification of Specific Determinants in the Regulation of Ras Ubiquitination.....</b>  | <b>6</b>    |
| <b>Chapter 2: Identification of Novel Interaction Sites between Myosin Phosphatase (MP) subunits PP1c <math>\beta</math> and MYPT1.....</b> | <b>7</b>    |
| <b>Introduction.....</b>  | <b>7</b>    |
| <b>Materials and Methods.....</b>   | <b>15</b>   |
| <b>Results.....</b>   | <b>19</b>   |
| <b>Discussion.....</b>  | <b>26</b>   |
| <b>Future Directions.....</b>   | <b>30</b>   |
| <b>Figures.....</b>   | <b>31</b>   |

|  |            |
|--|------------|
| <b>Chapter 3: Investigation of the differential accumulation of H-Ras and K-Ras within the cell.....</b> | <b>57</b>  |
| <b>Abstract.....</b>   | <b>57</b>  |
| <b>Introduction.....</b>   | <b>58</b>  |
| <b>Materials and Methods.....</b>  | <b>59</b>  |
| <b>Results and Discussion.....</b>   | <b>60</b>  |
| <b>Summary and Future Directions.....</b>  | <b>62</b>  |
| <b>Figures.....</b>  | <b>63</b>  |
| <b>Chapter 4: Identification of Specific Determinants in the Regulation of Ras Ubiquitination.....</b>   | <b>67</b>  |
| <b>Introduction.....</b>   | <b>67</b>  |
| <b>Background and Significance.....</b>  | <b>69</b>  |
| <b>Materials and Methods.....</b>  | <b>72</b>  |
| <b>Results and Discussion.....</b>   | <b>74</b>  |
| <b>Summary and Future Directions.....</b>  | <b>79</b>  |
| <b>Figures.....</b>  | <b>89</b>  |
| <b>Tables.....</b>   | <b>97</b>  |
| <b>References.....</b>   | <b>100</b> |
| <b>Appendix - Rapid Amplification of cDNA (RACE) Methods.....</b>  | <b>108</b> |
| <b>A. 5' RACE.....</b>   | <b>108</b> |
| <b>B. 3' RACE.....</b>   | <b>108</b> |
| <b>C. "New" RACE.....</b>  | <b>109</b> |



## List of Figures

|   |           |
|---|-----------|
| <b>Figure II-1. Myosin Phosphatase (MP).....</b>  | <b>31</b> |
| <b>a. Representation of Myosin Phosphatase</b>  |           |
| <b>Figure II-2. Myosin Phosphatase and Merlin Signaling.....</b>  | <b>33</b> |
| <b>Figure II-3. Myosin Phosphatase and Lipid Signaling.....</b>   | <b>35</b> |
| <b>a,b. PLD2 overexpression leads to accumulation of myosin phosphatase at the cell periphery</b>   |           |
| <b>Figure II-4. Myosin Phosphatase (MP).....</b>  | <b>37</b> |
| <b>a. Representation of Myosin Phosphatase</b>  |           |
| <b>b. MYPT1 Specificity for PP1c <math>\beta</math> Isoform</b>   |           |
| <b>Figure II-5. Interdependence of PP1c <math>\beta</math> and MYPT1.....</b>   | <b>39</b> |
| <b>a. RNAi Results</b>  |           |
| <b>b. Morphological Changes Present Following MYPT1 Knockdown</b>   |           |
| <b>c. Quantitation of Morphological Changes</b>   |           |
| <b>Figure II-6. MYPT1 and PP1c <math>\beta</math> are required for the stability of each other.....</b>   | <b>41</b> |
| <b>Figure II-7. Changes in Cell Number and Cell Shape Following PP1c <math>\beta</math> Knockdown in MDA-MB-231 cells.....</b>                          | <b>43</b> |
| <b>a. Live Cell Analysis</b>  |           |
| <b>b. Immunofluorescence Microscopy</b>   |           |
| <b>c. Quantitation of decrease in cell number</b>   |           |
| <b>d. Quantitation of increase in filopodia per cell</b>  |           |
| <b>Figure II-8. Schematic of PP1 Hybrid Constructs.....</b>   | <b>45</b> |
| <b>a. Alignment of Human PP1 Isoforms</b>   |           |
| <b>b. Structure of PP1 Chimera Constructs</b>   |           |
| <b>Figure II-9. Identification of the PP1c Domain Required for Interaction with MYPT1 – Immunoprecipitation Results.....</b>                            | <b>47</b> |
| <b>Figure II-10. Identification of the PP1c Domain Required for Interaction with MYPT1 - PP1 Hybrid Constructs and Immunoprecipitation Results.....</b> | <b>49</b> |

|   |           |
|---|-----------|
| <b>Figure II-11. Site-directed Mutagenesis of PP1c <math>\beta</math> and PP1c <math>\gamma</math>.....</b>                           | <b>51</b> |
| <b>a. Schematic of PP1c <math>\beta</math> and PP1c <math>\gamma</math> site-directed mutants</b>                                     |           |
| <b>b. Immunoprecipitation Results</b>   |           |
| <b>c. Quantitation of PP1c <math>\beta</math> T197Q mutant MYPT1 binding</b>  |           |
| <b>Figure II-12. MYPT1 Binding Capability of Double and Triple PP1c <math>\beta</math> and <math>\gamma</math> Mutants.....</b>       | <b>53</b> |
| <b>a. Immunoprecipitation Results</b>   |           |
| <b>b. Quantitation of PP1c <math>\beta</math> and <math>\gamma</math> Double and Triple Mutant MYPT1 binding</b>                      |           |
| <b>Figure II-13. PP1<math>\beta</math> residues that allow for interaction with MYPT1.....</b>  | <b>55</b> |
| <b>a. Space-filling model of MYPT1 and PP1c b Interaction</b>   |           |
| <b>b. PP1c <math>\beta</math> Residues 197, 232, 236, and 237 are necessary for MYPT1 binding</b>                                     |           |
| <b>Figure III-1. Expression Profiles and Metabolic Stability of H-Ras and K-Ras.....</b>  | <b>63</b> |
| <b>a. K-Ras is expressed at significantly lower level than H-Ras irrespective of the cell-type, promoter, or activating mutation.</b> |           |
| <b>b. Differential accumulation of K-Ras and H-Ras in the cell is a result of the difference in their metabolic stability.</b>        |           |
| <b>Figure III-2. Hypervariable region contains the determinants of Ras stability.....</b>   | <b>65</b> |
| <b>Figure III-3. Oncogenic H-Ras and K-Ras induce different morphological changes in mouse primary embryo fibroblasts (MEFs).....</b> | <b>66</b> |
| <b>Figure IV-1. HRas is ubiquitinated.....</b>  | <b>89</b> |
| <b>Figure IV-2. H and NRas but not KRas is ubiquitinated.....</b>   | <b>90</b> |
| <b>Figure IV-3. Ubiquitination of HRas occurs through Lysine63-linked ubiquitin chains.....</b>                                       | <b>91</b> |
| <b>a. Schematic diagram of unique diglycine signature peptides for Lys63-linked polyubiquitin chains</b>                              |           |
| <b>b. Schematic representation of arginine to lysine mutation at position 63 in UBK0 R63K</b>   |           |
| <b>c. Immunoprecipitation Results</b>   |           |

|  |           |
|--|-----------|
| <b>Figure IV-4. H-Ras hypervariable region (HVR) lysine mutants are ubiquitinated.....</b> | <b>92</b> |
| <b>a. The hypervariable region (HVR) of HRas</b>   |           |
| <b>b. Table of the HVR lysine mutants constructed</b>                                      |           |
| <b>c. Immunoprecipitation Results</b>  |           |
| <b>Figure IV-5. Ubiquitination deficient HRas 8RK.....</b>                                 | <b>93</b> |
| <b>a. Schematic representation of lysine mutations in HRas8RK</b>                          |           |
| <b>b. Immunoprecipitation Results</b>  |           |
| <b>Figure IV-6. Location Specific Ubiquitination within the Cell.....</b>                  | <b>94</b> |
| <b>Figure IV-7. Localization of KDELR-HRas SS.....</b>                                     | <b>95</b> |
| <b>a. Localization of YFP-<math>\beta</math>1,4-galactosidase to the Golgi</b>             |           |
| <b>b. Localization of HRasV12</b>  |           |
| <b>c. Localization of HRasV12 and YFP-<math>\beta</math>1,4-galactosidase</b>              |           |
| <b>d. Localization of Golgi-localized KDELR-HRas SS</b>                                    |           |
| <b>e. Co-localization of KDELR-HRas SS and YFP-<math>\beta</math>1,4-galactosidase</b>     |           |
| <b>Figure IV-8. KDELR-HRas SS Ubiquitination Assay.....</b>                                | <b>96</b> |

## List of Tables

|   |           |
|---|-----------|
| <b>Table 1: Constructs proposed in Thesis Proposal (August 2005).....</b>                   | <b>97</b> |
| <b>Table 2: Peptide sequences used to target Ras to specific subcellular locations.....</b> | <b>97</b> |
| <b>Table 3: All Ras targeting constructs used by Piero Crespo.....</b>                      | <b>98</b> |
| Arozarena, I. et al.; MCB (2004); 24 (4): 1516-1530.  |           |
| Matallanas D. et al.; MCB (2006); 26 (1): 100-16.   |           |
| <b>Table 4: Additional published Ras targeting constructs.....</b>                          | <b>99</b> |

## **List of Abbreviations**

myosin phosphatase (MP)

protein phosphatase 1 (PP1c)

myosin phosphatase targeting subunit (MYPT, also called MBS or M130)

20-kDa small subunit of unknown function (M20)

RNA interference (RNAi)

short hairpin RNA (shRNA)

rapid amplification of cDNA ends (RACE)

hypervariable region (HVR)

mouse embryo fibroblasts (MEFs)

mass spectrometry (MS)

endoplasmic reticulum (ER)

ubiquitin-mediated fluorescence complementation (UbFC)

fluorescence resonance energy transfer (FRET)

deubiquitinating enzyme (DUB)

plasma membrane (PM)

trans-golgi network (TGN)

## **Acknowledgements**

I would like to begin by first thanking my advisor, Michael A. Frohman. He accepted me into his laboratory when I was in need of a “home” and allowed me to continue working towards my doctorate. He has always been a very supportive and helpful advisor. Secondly, I would to thank Guangwei Du. When I first joined the lab, he worked with me until experiments were started and was always available for intense scientific discussion of my results.

I would also like to thank the members of my thesis committee: Carol Carter, Howard Crawford, and Nancy C. Reich. These faculty members have gone above and beyond their duties and supported my decision to change laboratories.

In addition, I would like to recognize my parents for their undying love and support. Lastly but certainly not least, I would like to thank my husband Anthony for always being there for me, as a shoulder to cry on, or as someone just to sit and laugh with.

## **Chapter 1: Introduction**

In this dissertation, I will be presenting two topics. For the first topic I will be describing the identification of novel interaction sites between myosin phosphatase (MP) subunits MYPT1 and PP1c  $\beta$ . In the second part of the dissertation, I will be describing the investigation of the differential accumulation of H-Ras and K-Ras within the cell. In the third part of the dissertation, I will be describing the identification of specific determinants in the regulation of Ras ubiquitination. Described below is the relationship between myosin phosphatase, Ras and their link to cancer regulation. In addition, please find below an additional description of the topics to be discussed in this dissertation.

### **Myosin Phosphatase and Cancer:**

The myosin phosphatase protein consists of three different subunits (**Figure II-1**). The first subunit is the catalytic subunit, type 1 protein phosphatase, PP1c. There are three different isoforms of PP1c: PP1c  $\alpha$ , PP1  $\beta/\delta$ , PP1c  $\gamma$ . The second subunit is the myosin light chain (MLC) targeting subunit (MYPT). This subunit is also sometimes called the myosin binding subunit, MBS. The third subunit is a 20 kDa subunit of unknown function termed M20 (Ito, Nakano et al. 2004).

Myosin phosphatase plays a role in smooth muscle contraction (Dimopoulos, Semba et al. 2007). In addition to the regulation of smooth muscle contraction, myosin phosphatase also plays a role in other smooth muscle associated functions such as: vascular tone, blood pressure control, gastrointestinal motility, airway resistance, erectile function and uterine contraction (Ito, Nakano et al. 2004).

In addition to its roles in smooth muscle control, myosin phosphatase has been shown to play a role in the regulation of several signaling pathways and in the ablation of tumor suppressor cascades. There are several publications indicating the role of myosin phosphatase in the regulation of signaling events and in the ablation of tumor suppressor cascades. Merlin is a plasma membrane-cytoskeletal scaffolding protein. It has been shown that the phosphorylation status of merlin is important for regulating the Ras-ERK pathway (Jung, Kim et al. 2005). An inhibitor of myosin phosphatase, CPI-17, leads to tumorigenic transformation (Jin, Sperka et al. 2006).

Merlin is encoded by the NF2 gene and becomes phosphorylated through the action of Akt (**Figure II-2**). Merlin becomes dephosphorylated at serine 518 through the action of myosin phosphatase. This leads to the activation of merlin. CPI-17 is a negative inhibitor of myosin phosphatase, allowing for the phosphorylation of merlin. Phosphorylated merlin can lead to Ras activation and cellular transformation.

In addition to the role of myosin phosphatase in the regulation of signaling events, there is also evidence that some subunits of myosin phosphatase are overexpressed in certain cancers. It has been shown that the MYPT1 gene, PPP1R12A, is upregulated in some cancer cell lines including the HCC1954 breast carcinoma cancer cell line (Schlabach, Luo et al. 2008). Using retroviral short hairpin RNA (shRNA) mediated genetic screens in mammalian cells can be a powerful tool for discovering loss-of-function phenotypes. Using shRNA directed against MYPT1, it was shown that knockdown of the MYPT1 gene causes a decrease in HCC1954 cancer cell viability (Schlabach, Luo et al. 2008). Therefore, MYPT1 can be used as a possible target for cancer therapeutics.

### **Ras and Cancer:**

The Ras family of small GTPases play critical roles in several biological pathways. Ras proteins cycle between an inactive GDP-bound and an active GTP-bound state. Ras proteins are essential components of signal transduction pathways that link extracellular stimuli with a diverse range of biological outcomes such as cell proliferation, differentiation and survival. Ras isoforms are nearly 90% homologous to one another, and differ only in a C-terminal domain termed the hypervariable region (HVR). The hypervariable region is composed of a membrane targeting domain and a linker domain. Both H and KRas contain a C-terminal CAAX motif that becomes farnesylated on the cysteine residue. HRas also contains two additional cysteine residues upstream of the CAAX box that become palmitoylated. This palmitoylation allows HRas to associate with the Golgi apparatus in route to the plasma membrane. KRas does not contain these cysteine residues but instead has a poly-lysine stretch upstream of the CAAX box. It is thought that this positively charged stretch of amino acids allows for electrostatic interactions of KRas with the negatively charged plasma membrane. Therefore, the



hypervariable region (HVR) is required for the proper trafficking and localization of Ras proteins to the plasma membrane.

H and KRas also differentially activate downstream effector pathways of Ras. It has been shown that HRas can engage effectors on the endomembrane, not only on the plasma membrane (Chiu, Bivona et al. 2002). Inactive HRas associates with lipid rafts and caveolae, and upon activation, HRas is redistributed from rafts and caveolae to the disordered plasma membrane (Roy, Wyse et al. 2002). KRas, however, is predominantly localized to the disordered plasma membrane regardless of its activation state (Chiu, Bivona et al. 2002). Therefore, KRas is capable of activating downstream effector pathways at an increased rate in comparison to HRas (Jura, Scotto-Lavino et al. 2006). This may be one possible reason that KRas activates certain downstream effector pathways at an increased rate in comparison to HRas. In particular, certain effector pathways leading to cellular transformation. It has been shown that HRas but not KRas requires endocytosis and endocytic recycling to signal through the Raf/MEK/MAPK cascade (Roy, Wyse et al. 2002). It is interesting to note that KRas is preferentially mutated in colon and pancreatic cancers, whereas HRas is infrequently mutated in human tumors. It is well recognized that the functional versatility of Ras proteins is accomplished through their differential compartmentalization, but the mechanisms that control their spatial segregation are not fully understood. Since the modification of proteins by the covalent attachment of ubiquitin has been widely implicated in the regulation of protein trafficking (Di Fiore, Polo et al. 2003), we explored the role of ubiquitination in controlling the compartmentalization of Ras proteins and subcellular localization of Ras ubiquitination.

## **I. Identification of Novel Interaction Sites between Myosin Phosphatase (MP) subunits PP1c $\beta$ and MYPT1.**

Myosin II association with actin, which triggers muscle contraction, is regulated by orchestrated waves of phosphorylation / dephosphorylation of the myosin regulatory light chain (MLC). Modulation of myosin activity by small molecule inhibitors that inhibit the kinase step alter the cellular shape, adhesion and migration of many cancer cells. The dephosphorylation step is mediated by myosin phosphatase (MP), an enzyme complex that consists of a catalytic subunit (protein phosphatase 1, PP1c), a large subunit (myosin phosphatase targeting subunit, MYPT, also called MBS or M130) and a 20-kDa small subunit of unknown function. I have shown that PP1c  $\beta$  and MYPT1 are interdependent: RNAi knock-down of one of the subunits diminishes the expression level of the other and causes increases in actin-based structures along the cell perimeter. Three different highly conserved isoforms of PP1c exist,  $\alpha$ ,  $\beta$ , and  $\gamma$ . However, immunoprecipitation assays revealed that MYPT1 binds only to the PP1 $\beta$  isoform. This finding led me to investigate how the MYPT1 and PP1c subunits of myosin phosphatase interact and the reason for PP1 isoform specificity. PP1 constructs chimeric for different regions of PP1  $\beta$  and  $\gamma$  were generated and studied, leading to the conclusion that the site of interaction with MYPT1 lies between residues 121 and 303. Swapping of the few divergent residues between the PP1  $\beta$  and  $\gamma$  isoforms in this region were then made, identifying Threonine 197 as a key residue for PP1  $\beta$  interaction. In contrast, swapping of residues 237 and 238 in PP1  $\gamma$  to the corresponding residues found in PP1  $\beta$  gave it the capacity to interact with MYPT1. Based on these results, I have identified novel binding sites for MYPT1 on PP1  $\beta$ , which has implications for potential screening strategies for cancer therapeutic agents.

## **II. Investigation of the differential accumulation of H-Ras and K-Ras within the cell.**

Ras proteins, which are represented by three isoforms: H-, N- and K-Ras, are small GTPases that cycle between active and inactive states. In its active, GTP-bound state, Ras mediates the signal from cell surface receptors to intracellular effector molecules. Ras proteins are critical regulators of signaling pathways that control cell proliferation and survival. In over 30% of human cancers, the activating mutation in Ras, glycine 12 to valine, has been detected. In the majority of cases, the mutation is in the splicing variant of K-Ras, K-Ras4B gene, referred to hereafter as K-Ras. The incidence of H-Ras mutations in cancer are not prevalent, however H-Ras is the most common isoform utilized in *in vitro* studies of cell transformation (Giehl 2005; Hancock and Parton 2005).

All Ras isoforms are nearly 90% homologous to one another and differ only in the hypervariable region (HVR) located at the C-terminus. At the N-terminus, there is a GTP-binding domain followed by an effector binding domain and a C-terminal tail ending in a CAAX box. The C-terminal domain of H-Ras contains two cysteine residues upstream of the CAAX box that becomes palmitoylated during processing. H-Ras is targeted to the plasma membrane through the Golgi. The C-terminal domain of K-Ras contains a polybasic region upstream of the CAAX box. K-Ras is targeted to the plasma membrane through an unknown mechanism. K-Ras is either mutated or absent in 90% of all pancreatic, colon and lung cancers. Here, we describe the targeting function for the HVR in RAS isoforms.

Additionally, I also investigated whether K-Ras and H-Ras exerted different biological functions dependent on the level of Ras signaling intensity. In primary mouse embryo fibroblasts (MEFs) high levels of oncogenic Ras have been shown to induce cell cycle arrest – senescence (Bringold and Serrano 2000). The role of K-Ras in MEFs has not been investigated in detail. Using a retroviral infection system, we have shown that K-Ras induces distinct morphological changes than H-Ras in MEFs.

Overall, the goals of these experiments included the investigation of the specific determinants of Ras stability, the determination if Ras stability is conferred within the hypervariable region (HVR), and to study the effects of oncogenic H- and K-Ras in mouse primary embryo fibroblasts (MEFs). These data will help us understand the role of Ras signaling and expression in primary cells.

### **III. Identification of Specific Determinants in the Regulation of Ras Ubiquitination.**

The Ras family of small GTPases play critical roles in several biological pathways. There are three different isoforms of Ras named H-Ras, N-Ras and K-Ras. Ras isoforms are nearly 90% homologous to one another, and differ only in the hypervariable region (HVR) at their C-terminus. The hypervariable region (HVR) is required for the proper trafficking and localization of Ras proteins to the plasma membrane. Ras proteins are preferentially mutated in 30% of all human cancers. H- and K-Ras traffic and localize to different subdomains of the plasma membrane and also differentially activate downstream effector pathways of Ras (Chiu, Bivona et al. 2002; Roy, Wyse et al. 2002).

Ras proteins are essential components of signal transduction pathways that control cell proliferation, differentiation and survival. It is well recognized that the functional versatility of Ras proteins is accomplished through their differential compartmentalization, but the mechanisms that control their spatial segregation are not fully understood. Ubiquitination of membrane-associated proteins and receptors often serves to target proteins to the endocytic pathway (Finley, Sadis et al. 1994; Hicke 2001; Di Fiore, Polo et al. 2003). Recent studies in the lab have identified ubiquitination as a novel modification of HRas whose significance has not yet been determined. We have observed that H-Ras is subject to ubiquitin conjugation whereas K-Ras is not. Ubiquitin attachment to H-Ras modulates its ability to activate the Raf/MAPK signaling pathway. Therefore, differential ubiquitination of Ras proteins may control their location-specific signaling activities.

The proposed purpose of these studies was to analyze the exact site of ubiquitin attachment to H-Ras, and to determine the subcellular location of H-Ras ubiquitination within the cell. The identity of the E3 ubiquitin ligase and the deubiquitinating enzyme (DUB) for Ras was also to be determined. In further characterizing the mechanism of Ras ubiquitination, it is our hope to understand the specific determinants in the regulation of Ras ubiquitination, and the effects of Ras ubiquitination on the interaction of Ras with its downstream effectors and signaling.

## **Chapter 2: Identification of Novel Interaction Sites between Myosin Phosphatase (MP) subunits PP1c $\beta$ and MYPT1.**

### **INTRODUCTION:**

This dissertation will be about a multi-subunit protein named myosin phosphatase (MP) that is most known for its role in cellular contraction. Myosin II association with actin, which triggers contraction, is regulated by orchestrated waves of phosphorylation / dephosphorylation of the myosin regulatory light chain (MLC) (Hartshorne, Ito et al. 1998). Modulation of myosin activity by small molecule inhibitors that inhibit the kinase step alter the cellular shape, adhesion and migration of many cancer cells (Kaneko, Satoh et al. 2002). The dephosphorylation step is mediated by myosin phosphatase (MP), an enzyme complex that consists of a catalytic subunit (protein phosphatase 1, PP1c), a large subunit (myosin phosphatase targeting subunit, MYPT, also called MBS or M130) and a 20-kDa small subunit of unknown function (Matsumura and Hartshorne 2008). MYPT functions by targeting the PP1c catalytic subunit on its substrate, phosphorylated myosin II (Hartshorne, Ito et al. 1998).

### **Functions of Myosin Phosphatase (MP):**

#### **I. Smooth-Muscle Associated Functions.**

There are many publications indicating the importance of myosin phosphatase in the regulation of smooth muscle relaxation. For example, myosin phosphatase regulation has been shown to play a role in pulmonary arterial relaxation (Dakshinamurti 2005). In addition, it has been published that myosin phosphatase plays a role in many smooth muscle associated functions including: vascular tone, blood pressure control, gastrointestinal motility, airway resistance, erectile function and uterine contraction (Ito, Nakano et al. 2004).

#### **II. Myosin Phosphatase and Smooth Muscle Contraction.**

As stated, myosin phosphatase is required for regulation of the contraction and subsequent relaxation of smooth muscle. Dimopoulos and Semba *et al.* (2007) describe smooth muscle contraction as follows: increases in the levels cytosolic  $[Ca^{2+}]_i$  initiate smooth muscle contraction by binding to the universal intracellular  $Ca^{2+}$  receptor protein,

calmodulin (CaM) which in turn binds to and activates smooth muscle light chain kinase (MLCK). Activated MLCK catalyzes the phosphorylation serine-19 of the regulatory myosin light chain (MLC) thereby increasing cross-bridge cycling and the rate of tension development (Dimopoulos, Semba et al. 2007) required for contraction.

Dephosphorylation of MLC is catalyzed by smooth muscle specific myosin light chain phosphatase (MLCP or MP). Decreases in cytosolic  $[Ca^{2+}]_i$  and MLC dephosphorylation are considered salient events in smooth muscle relaxation. It has now become apparent that decreased  $[Ca^{2+}]_i$ , and MLC dephosphorylation are separate events that are independently controlled (Dimopoulos, Semba et al. 2007). Therefore, the regulation of MP activity plays a role in smooth muscle contraction (Dimopoulos, Semba et al. 2007).

### **III. Actin-Based Myosin Motors.**

The actin-based myosin motors generate motions associated with intracellular trafficking, cell division, and muscle contraction. Myosin acts to convert energy from adenosine triphosphate into protein motion using a conformational change strategy described below (Vale and Milligan 2000).

Vale and Milligan (2000) describe the action of actin-based myosin motors as follows. Muscle myosin is a dimer of two identical motor heads, which are anchored to the thick filament by a coiled coil. In the ADP-Pi-bound state, the catalytic core binds weakly to actin. One head docks properly onto the actin binding site. The two myosin heads act independently, and only one attaches to actin at a time. Actin docking causes phosphate release from the active site. The lever arm then swings to the post-stroke, ADP-bound state, which moves the actin filament  $\sim 100$  angstroms. After completing the stroke, ADP dissociates and ATP binds to the active site, which rapidly reverts the catalytic core to its weak-binding actin state. The lever arm will then move back to its prestroke state (Vale and Milligan 2000). As described, this mechanism acts to move actin filaments approximately 100 angstroms per cycle.

### **IV. Myosin Phosphatase and Lipid Signaling.**

Phospholipase D2 is the enzyme that catalyzes the reaction converting phosphatidylcholine to phosphatidic acid (PA) and choline (Du and Frohman 2008). Recent evidence in the lab has indicated that MP is regulated by a plasma membrane

signaling lipid. It was shown that cells in suspension exhibit high levels of Phospholipase D2 (PLD2). This elevates the production of the lipid second messenger Phosphatidic Acid (PA) at the plasma membrane (PM). This in turn recruits MP and stores it at the PM in an inactive state. As described below, there is also a change in cell shape upon PLD2 overexpression similar to cells that are rounded in appearance (**Figure II-3**) (Du and Frohman 2008). Upon cell attachment, downregulation of PLD2 activity decreases PA production, leading to MP release, myosin dephosphorylation and, actomyosin disassembly (Du and Frohman 2008).

### **V. Effects on Cell Morphology and Migration.**

As stated, myosin phosphatase is regulated by a plasma membrane signaling lipid. It has been observed that in CHO cells overexpressing PLD2, myosin phosphatase accumulates at the cell periphery (Du and Frohman 2008). This causes a redistribution of myosin phosphatase subunits MYPT1 and PP1c  $\beta$  from the cytoplasm and bottom of the cell to the cell periphery (**Figure II-3**). There is also a change in the shape of the cells, in that the cells contract and become very round in shape (Du and Frohman 2008).

In contrast, it has been shown that in HeLa cells expressing siRNA against the MYPT1 subunit of myosin phosphatase also show a change in cell morphology (Xia, Stull et al. 2005). Upon siRNA knockdown of MYPT1, there is an increase in the amount of actin stress fibers in the cell in addition to an increase in the number of focal adhesions (Xia, Stull et al. 2005). This data illustrates how regulation of myosin phosphatase subunit expression can lead to changes in cellular morphology.

Recently, a siRNA migration screen using a wound healing approach was performed using MCF-10A breast cancer cells (Simpson, Selfors et al. 2008). In this study several pools of RNAi representing different libraries of kinases, phosphatases and migration and adhesion related (MAR) genes were screened (Simpson, Selfors et al. 2008). Interestingly, upon 70-80% knockdown of protein phosphatase 1 beta (PP1c  $\beta$ ) in MCF-10A cells, there was little to no change in wound healing and cell morphology in comparison to control cells (Simpson, Selfors et al. 2008). This is different from our data in which PP1c  $\beta$  knockdown causes a change in cell shape and morphology. Based on our data, we predict that there will also be a deficit in cell migration and wound healing.

## **VI. Apoptosis.**

Apoptosis is a form of programmed cell death. In order for apoptosis to take place, several characteristic changes of a cell have to occur. These include: cell shrinkage, membrane blebbing, condensation of chromatin, and DNA fragmentation (Mills, Stone et al. 1998). It has been shown that actin-myosin-based contraction of the cell is responsible for apoptotic nuclear disintegration (Croft, Coleman et al. 2005). It has also been shown that the membrane blebbing that occurs during apoptosis is regulated by myosin light chain (MLC) phosphorylation (Mills, Stone et al. 1998). As discussed, myosin phosphatase dephosphorylates active myosin light chain (MLC), preventing cellular contraction. In our studies, upon knockdown on myosin phosphatase subunit levels, there is an increase in cellular apoptosis. This is based mainly on the presence of rounded, floating cells. It is therefore possible that upon myosin phosphatase knockdown, myosin light chain remains phosphorylated, allowing for cellular contraction and actin-based processes such as cell rounding and blebbing required for apoptosis to occur.

There are publications indicating the importance of myosin phosphatase in the inhibition of apoptosis. Myosin phosphatase dephosphorylates a histone deacetylase protein, HDAC7, inhibiting its nucleocytoplasmic shuttling in thymocytes (Parra, Mahmoudi et al. 2007). HDAC7 dephosphorylation promotes its nuclear localization, leading to the repression of the HDAC7 target, *Nur77*, and the inhibition of apoptosis in CD4<sup>+</sup>CD8<sup>+</sup> thymocytes (Parra, Mahmoudi et al. 2007). Therefore, myosin phosphatase acts to inhibit apoptosis (Parra, Mahmoudi et al. 2007).

## **VII. Regulation of Signaling Events and Merlin Signaling.**

There are several publication indicating the role of myosin phosphatase in the regulation of signaling events and in the ablation of tumor suppressor cascades. Merlin is a plasma membrane-cytoskeletal scaffolding protein. It has been shown that the phosphorylation status of merlin is important for regulating the Ras-ERK pathway (Jung, Kim et al. 2005). An inhibitor of myosin phosphatase, CPI-17, leads to tumorigenic transformation (Jin, Sperka et al. 2006).

Merlin is encoded by the NF2 gene and becomes phosphorylated through the action of Akt (**Figure II-2**). Merlin becomes dephosphorylated at serine 518 through the action of



myosin phosphatase. This leads to the activation of merlin. CPI-17 is a negative inhibitor of myosin phosphatase, allowing for the phosphorylation of merlin. Phosphorylated merlin can lead to Ras activation and cellular transformation.

### **VIII. Role of MYPT1 in Cancer.**

It has been shown that the MYPT1 gene, PPP1R12A, is upregulated in some cancer cell lines including the HCC1954 breast carcinoma cancer cell line (Schlabach, Luo et al. 2008). Using retroviral short hairpin RNA (shRNA) mediated genetic screens in mammalian cells can be a powerful tool for discovering loss-of-function phenotypes. Using shRNA directed against MYPT1, it was shown that knockdown of the MYPT1 gene causes a decrease in HCC1954 cancer cell viability (Schlabach, Luo et al. 2008). Therefore, MYPT1 can be used as a possible target for cancer therapeutics.

### **IX. The Three Different Isoforms of PP1c: $\alpha$ , $\beta$ , and $\gamma$ .**

#### **A. Overview.**

The four mammalian *PP1c* gene products initially identified were PP1c  $\alpha$ , PP1c  $\beta$  (sometimes referred to as PP1c  $\delta$ ), PP1c  $\gamma_1$  and PP1 $\gamma_2$ , the latter two arising from alternative splicing (Cohen 1988). An additional PP1 $\alpha$  variant, PP1 $\alpha_2$ , is similar to the PP1 $\alpha$  isoforms in that it is predicted from the human genome sequence. This indicates that alternative splicing also gives rise to at least two  $\alpha$  isoforms (Durfee, Becherer et al. 1993; Yoshida, Watanabe et al. 1999). Of these isoforms it is thought that MYPT1 bind specifically to PP1c  $\beta$  (Ito, Nakano et al. 2004).

The isoforms differ mainly in the C-terminal sequences, for about 30 amino acids. Some variation is found in the N-terminal sequences, but the bulk of the molecule is highly conserved between isoforms with over 95% identity (Hartshorne and Hirano 1999). Differences in function associated with the N- and C-terminal sequences have not been identified (Hartshorne and Hirano 1999). However, the role of differing sequences is not appreciated with respect to PP1c function and interactions. It is possible that the sequences unique to each isoforms are involved in interactions with specific target/regulatory subunits (Ito, Nakano et al. 2004). Mammalian PP1c isoforms possess distinct tissue distributions and subcellular localizations as described below.

## **B. Cellular Localization of PP1c Isoforms.**

Much work has been done on determining the localization of the three different isoforms of PP1c:  $\alpha$ ,  $\beta$ ,  $\gamma$ . In the rat brain, PP1c  $\alpha$  has been shown to colocalize with cytoskeletal elements and with the nucleolus (Colbran, Bass et al. 1997). In fibroblasts and smooth muscle cells, PP1c  $\beta$  is well known to also be in the nucleus and focal adhesions (Andersen, Lyon et al. 2002). In mammalian cells, PP1c  $\gamma$  has been shown to be in the nucleus, but then shuttles between the cytoplasm and nucleolus during mitosis (Andreassen, Lacroix et al. 1998).

## **C. Tissue distribution of PP1c Isoforms.**

Among the different PP1c isoforms there are some differences in tissue distribution. As described above, PP1c  $\alpha$  is found in high levels in the brain. For example, PP1c  $\gamma_1$  is high in the brain and PP1c  $\gamma_2$  is high in the testis (Shima, Hatano et al. 1993). The PP1c  $\beta$  isoforms is found in smooth muscle and was detected bound to myosin (Okubo, Ito et al. 1994). The PP1c  $\beta$  isoforms from different tissues appear to be very highly conserved (Hartshorne, Ito et al. 1998).

## **D. PP1c $\gamma$ Knockout Mice.**

Although there are few differences between the three isoforms of PP1c in terms of function, there is one published report on a PP1c  $\gamma$  knockout mouse. Male mice with a homozygous null mutation in the protein phosphatase 1c gamma gene (PP1c  $\gamma$ ) display the following phenotype (Hrabchak, Henderson et al. 2007). They are infertile, and display a severe deficit in spermatogenesis (Hrabchak, Henderson et al. 2007). This deficit is not compensated by the expression of PP1c  $\alpha$  and PP1a  $\beta$  in mutant testis (Hrabchak, Henderson et al. 2007). It is also indicated that a testis specific isoform of endophilin B1, interacts specifically with PP1c  $\gamma$  in mouse testis and is overexpressed in PP1c  $\gamma$  null mice (Hrabchak, Henderson et al. 2007).

## **X. Myosin Phosphatase Crystal Structure.**

As mentioned, there are three different isoforms of PP1c: PP1 $\alpha$ , PP1 $\beta$ , and PP1 $\gamma$ . It has previously been published that MYPT1 interacts specifically with the beta form of

PP1c (PP1  $\beta$ ) (Eto, Kirkbride et al. 2005). When aligning the sequences of PP1c  $\beta$  from mouse, rat, and human, these sequences are nearly 100% homologous.

Previously published papers of the PP1c  $\beta$  structure included those of PP1c  $\beta$  protein complexed with the toxin microcystin (Goldberg, Huang et al. 1995), and with the tumor-promoter okadaic acid (Maynes, Bateman et al. 2001). PP1c  $\gamma$  has been crystallized in complex with the marine toxin calyculin A (Kita, Matsunaga et al. 2002), and tungstate (Egloff, Cohen et al. 1995). In general, these crystal structures have resolutions ranging from 1.9 angstroms to 2.5 angstroms. These crystal structures of PP1c were not in complex with the remaining subunits of myosin phosphatase, MYPT1 and M20. In 2004, a crystal structure of the complex between PP1c  $\beta$  and residues 1-299 of MYPT1 (Terrak, Kerff et al. 2004) isolated from chicken gizzard was published. From this structure, it was predicted that MYPT1 interacts with PP1c  $\beta$  at three separate regions: 1. the N-terminal arm, 2. the RVxF motif located in the central region of the protein, and 3. the second group of ankyrin repeats, which interact mainly with PP1c  $\beta$  residues Tyr A305 and Tyr A307 located at its C-terminus. I will present findings that suggest that this conclusion needs to be reevaluated. In this paper it is shown that PP1c  $\beta$  and MYPT1 do interact at MYPT1 residue F38 located in the PP1-binding site of MYPT1 (Terrak, Kerff et al. 2004). From these data, it is predicted that PP1c  $\beta$  interacts with MYPT1 through its C-terminal domain. We were interested in studying how the MYPT1 and PP1c  $\beta$  subunits of myosin phosphatase interact and the reason for PP1c isoform specificity.

When aligning the amino acid sequences of PP1c  $\alpha$ ,  $\beta$ , and  $\gamma$  from human species, three things are evident. First, there is a region of divergence between the three isoforms at the N-terminus. Second, there is also a region of sequence divergence at the extreme C-terminus. Third, there is not much sequence divergence in the central portion of the protein, with the exception of a few amino acids. Based on both the structural data and sequence analysis data presented, I sought out to determine the region of PP1c  $\beta$  that confers its specificity for interaction with MYPT1.

## **XI. Research Aims.**

As described earlier, the first research aim of this project was to determine the consequence of using RNAi to knock down the myosin phosphatase (MP) subunits PP1c and MYPT1 on the morphology and migration capability of cells. The second research aim was to determine the molecular mechanism of MYPT1 and PP1c interdependence and stability. The first approach taken was to confirm the interaction between MYPT1 and PP1c. Upon confirmation of this interaction, I sought out to determine the site of interaction between MYPT1 and PP1c.

## **XII. Research Goals and Future Implications.**

The overall goal of this project was to determine the role of the myosin phosphatase signaling pathway in cellular morphology and migration in tumor cells as the initial step in developing a new approach for cancer therapeutics. Future implications of these data are to use this information to drive the development and potential screening strategies of chemotherapeutic agents such as Taxol<sup>®</sup>, which target components of the cell infrastructure, i.e. microtubules, particularly important for tumor cell metastasis.

## **MATERIALS AND METHODS:**

### **1. Protein Sequence Alignments.**

Alignment of the protein sequences of PP1c  $\beta$  from the three different species mouse, human and rat as well as the alignment of the three different isoforms of human PP1c were performed using the Network Protein Sequence Analysis: Multalin Alignment algorithm (Corpet 1988).

### **2. Analysis of the expression of PP1c isoforms in different cell types and immunoblotting.**

CHO cells were cultured in Ham's F12 media supplemented with 10% fetal bovine serum (FBS). HEK 293, HeLa R19, HeLa and MDCK cells were cultured in Dulbecco's Modified Eagle's Medium (DMEM) supplemented with 10% bovine calf serum (CS). MDA-MB-231 breast cancer cells were cultured in Dulbecco's Modified Eagle's Medium (DMEM) supplemented with 10% fetal bovine serum (FBS). Cells were cultured on 60 mm tissue culture plates (Falcon) for 48 hours. Cells were then lysed in RIPA buffer (50 mM Tris-HCl, pH 7.4, 1% Triton X-100, 150 mM NaCl, 0.5% Na-deoxycholate, 0.1% SDS, 1 mM EDTA, 1mM EGTA) containing a protease inhibitor cocktail (Roche, Basel, Switzerland) as well as 1 mM  $\text{Na}_3\text{VO}_4$  and 1mM NaF. Equal amounts of cell lysates were then analyzed for endogenous expression of the three PP1c isoforms using SDS-PAGE gel electrophoresis and western blotting technique. The antibodies used were: monoclonal anti-protein phosphatase 1 alpha (Sigma, St. Louis, MO), polyclonal anti-PP1 gamma 1 (Stratagene, La Jolla, CA), polyclonal anti-PP1 delta (beta) (Upstate Biotechnology, Long Island, NY). Blotting lysates with anti-tubulin antibody served as a loading control.

### **3. PP1 immunoprecipitation and immunoblotting.**

HeLa cells were cultured in Dulbecco's Modified Eagle's Medium (DMEM) supplemented with 10% bovine calf serum (CS). Cells were transiently transfected with the indicated plasmids using Lipofectamine and Plus reagents (Invitrogen, Carlsbad, CA). Cell lysis and immunoprecipitation of PP1 with c-myc polyclonal antibody (Santa Cruz Biotechnology, Santa Cruz, CA) was carried out as described (Corbalan-Garcia, Margarit et al. 1998). Cells were lysed and harvested in 500  $\mu\text{L}$  RIPA buffer containing protease

inhibitors (please see above). After collection, lysates were passed through a 25<sup>5/8</sup> gauge needle 5 times. Lysates were then spun at 4°C at 14,000 rpm for 10 minutes. Supernatant was then removed and placed into a fresh eppendorf tube. Anti-myc monoclonal antibody (#M5546, Sigma) was then added to the supernatants and incubated at 4°C on a shaker for 1 hour. Following antibody incubation, a 50:50 slurry of Protein A Sepharose (Sigma-Aldrich, St. Louis, MO) was added to the supernatant and then incubated at 4°C on a shaker for 1 hour. Samples were then spun down at 14,000 rpm for 1 minute and the Protein A Sepharose is washed and the supernatant is aspirated 3 times with RIPA buffer excluding protease inhibitors. Following the wash steps, any residual buffer is removed using a needle. Protein A Sepharose is then resuspended in SDS-PAGE sample buffer. Prior to sample analysis, Protein A Sepharose must be boiled at 95°C for 5 minutes. Immunoblotting was performed using the following primary antibodies: monoclonal anti-myc (1:1000, #9B11, Cell Signaling), and polyclonal anti-GFP (1:1000, abcam). Secondary antibodies used were either IR dye 800 anti-mouse (1:5000, Rockland) or Alexa 680 anti-rabbit (1:5000; Molecular Probes). Western blots were then analyzed using the Odyssey Infrared Imaging System (LI-COR Biosciences).

#### **4. Cloning of PP1 Chimera Constructs.**

PP1 Chimera constructs were generated using a PCR-based strategy and then subcloned into a GFP-tag containing expression vector (pQCXIP-GFP).

#### **5. Cloning of PP1 site-directed mutants.**

PP1c  $\beta$  (T197Q, S232A, N236H/R237K, G280A) and PP1c  $\gamma$  (Q198T, A233S, H237N/K238R, A281G) site-directed mutants were generated by substituting corresponding amino acids in PP1c  $\beta$  or PP1c  $\gamma$  using a PCR-based strategy. All mutations and fusion constructs were confirmed by sequencing.

#### **6. Retroviral Infection.**

On day 1, GP2 retroviral packaging cells were passaged into 6 10 cm plates at 1:7. On day 2, GP2 cells were transfected with shRNAi constructs + VSVG using Lipofectamine and Plus reagent (Invitrogen, Carlsbad, CA). After 4 hours incubation, medium is then replaced with DMEM supplemented with 10% FBS. On day 3, cells to be infected were passaged into a 6 well plate. On day 4, virus was harvested (collected) and added to cells

to be infected. In addition, 2  $\mu$ L of polybrene (stock 6 mg/mL) is added to infected cells in each well. On day 6, cells were selected with puromycin for future analysis and study.

### **7. RNAi Transfection and Analysis.**

CHO cells were cultured in F-12 Nutrient Mixture (Ham) supplemented with 10% fetal bovine serum (FBS). Cells were transiently transfected with the indicated RNAi oligonucleotides (Invitrogen, Carlsbad, CA) using Lipofectamine RNAi/MAX transfection reagent (Invitrogen, Carlsbad, CA). Cells were incubated in 1 mL PBS containing 5 mM EDTA on ice for 10 minutes. Cells were harvested and spun down at 14,000 rpm for 1 minute in a table top microcentrifuge. Supernatant was aspirated and cells were lysed in 60  $\mu$ L RIPA buffer containing protease inhibitors (please see above). Lysates were then spun at 4°C at 14,000 rpm for 5 minutes. Supernatant was then removed and mixed with 5x sample buffer placed in a fresh eppendorf tube. Immunoblotting was performed using the following primary antibodies: polyclonal anti-MYPT1 (1:10,000; Covance), monoclonal anti-PP1 alpha (1:500, Sigma), polyclonal anti-PP1 delta (beta) (1:500, Upstate) and monoclonal anti- $\alpha$  tubulin (1:1000, Sigma). Secondary antibodies used were either IR dye 800 anti-mouse (1:5000, Rockland) or Alexa 680 anti-rabbit (1:5000; Molecular Probes). Western blots were then analyzed using the Odyssey Infrared Imaging System (LI-COR Biosciences).

### **8. Live cell analysis.**

CHO cells were cultured in F-12 Nutrient Mixture (Ham) supplemented with 10% fetal bovine serum (FBS). Cells were transiently transfected with the indicated RNAi oligonucleotides (Invitrogen, Carlsbad, CA) using Lipofectamine RNAi/MAX transfection reagent (Invitrogen, Carlsbad, CA). At 24 and 48 hours following transfection, live cells were viewed using a Nikon Eclipse TS100 light microscope (Nikon Corporation, Melville, NY) and photographed using a Nikon Digital Sight camera (Nikon Corporation, Melville, NY). Images were analyzed using NIS-Elements F v2.30 Imaging Software (Nikon Instruments, Melville, NY).

### **9. Immunofluorescence microscopy.**

MDA-MB-231 breast cancer cells were infected with retrovirus against PP1c  $\beta$ . 48 hours following infection, cells were fixed in 3.7% paraformaldehyde and stained with an antibody against phalloidin (actin) conjugated to rhodamine (Invitrogen, Carlsbad, CA).



## **RESULTS:**

### **Myosin Phosphatase (MP):**

As discussed, myosin phosphatase (MP) is an enzyme complex that consists of a catalytic subunit (protein phosphatase 1, PP1c), a large subunit (myosin phosphatase targeting subunit, MYPT, also called MBS or M130) and a 20-kDa small subunit of unknown function (Matsumura and Hartshorne 2008) (**Figure II-1**). In our studies, I sought to explore the following: 1. the interdependence of MP subunits MYPT1 and PP1c  $\beta$  through studying the effect of subunit knockdown on cellular morphology and proliferation, and 2. the molecular mechanism of the interaction between MYPT1 and PP1c  $\beta$ .

### **MYPT1 Specificity for PP1c $\beta$ Isoform:**

It has previously been published that MYPT1 interacts specifically with the beta form of PP1c (PP1  $\beta$ ) (Eto, Kirkbride et al. 2005). In order to confirm this observation, we performed immunoprecipitation assays with an anti-myc antibody (Cell Signaling, Danvers, MA) on cell lysates from cells expressing myc-tagged MYPT1 and GFP-tagged PP1 constructs. The immunoprecipitate generated was then immunoblotted with an anti-GFP antibody (abcam). As indicated, wild-type MYPT1 interacts specifically with the  $\beta$  isoform of PP1 (**lane 7**) and not the  $\alpha$  or  $\gamma$  isoforms (**Figure II-4b**). PP1c  $\beta$  did not interact with a MYPT1 construct that has a mutation in the PP1 binding site of MYPT1 (MYPT1 38A) (**lane 11**). This mutation is located in the RvXF motif of MYPT1. Based on these data, we sought to determine the exact site of PP1c  $\beta$  required for MYPT1 binding.

### **Interdependence of PP1c $\beta$ and MYPT1:**

Little is known about the interaction between the MYPT1 and PP1c subunits of MP (Hartshorne, Ito et al. 1998). We sought out to explore this interaction. First, through the transfection of CHO cells with commercially available RNAi oligonucleotides (Invitrogen, Carlsbad, CA) using a lipid based transfection method, it was shown that when PP1c  $\beta$  is knocked down, a corresponding decrease in MYPT1 levels was also observed (**Figure II-5a**).

Secondly, using a retrovirus infection system for shRNA encoding sequences against MYPT1 or PP1c  $\beta$  in CHO and MDA-MB-231 cells, it was shown that when PP1c  $\beta$  is knocked down, there is a corresponding decrease in MYPT1 levels (**Figure II-6**). When MYPT1 is knocked down, there is also a corresponding decrease in PP1c  $\beta$  levels (**Figure II-6**). In summary, using commercially available RNAi against PP1c  $\beta$  or shRNA directed against human MYPT1 or PP1c  $\beta$ , knockdown of PP1c  $\beta$  caused a decrease in MYPT1 levels. These data illustrate that the MYPT1 and PP1c  $\beta$  subunits are interdependent on one another.

#### **Changes in Cell Number and Cell Shape Following PP1c $\beta$ Knockdown:**

In addition to the interdependence of the two subunits, it was also observed that knockdown of PP1c  $\beta$  and MYPT1 caused a change in CHO cell morphology. Fully confluent control CHO cells had a well defined fibroblast morphology with smooth, ordered cell borders and were of an average cell size (**Figure II-5b**). Upon knockdown of MYPT1, cells are more spread out or flattened (**Figure II-5b**). In fact, the number of CHO cells displaying this morphology approximately doubles when transfected with PP1c  $\beta$  RNAi (**Figure II-5c**). This has been observed in other cell types as well including MDCK cells (not shown), MCF-7 (not shown), and MDA-MB-231 (**Figure II-7b**) cell lines.

In MDA-MB-231 cells infected with shRNA directed against PP1c  $\beta$ , a decrease in cell number is also observed (**Figure II-7a**). When quantitating these data, the number of cells per field decreased by approximately two and a half times when infected with shRNA directed against PP1c  $\beta$  (**Figure II-7c**). There was also an increase in cell death upon knockdown of MYPT1 and PP1c  $\beta$  (not shown). This was evident from the number of apoptotic cells present upon PP1c  $\beta$  knockdown. The reasoning for this observation is fully described in the introduction.

In addition to the above phenomena, there is also a change in the shape of cellular protrusions from MDA-MB-231 cells infected with shRNA directed against PP1c  $\beta$  (**Figure II-7b**). In control cells, the edges of the cells are smooth and have very few filopodium protrusions (see inset). It is important to note here that control cells lack

filopodia even at a lower cell density. In comparison, infected cells show an increased number of filopodia per cell (see inset). In fact, the number of filopodia per cell increases approximately five times (**Figure II-7d**).

**Working Model of the Cellular Phenotype observed upon MYPT1 and PP1c  $\beta$  Knockdown:**

Upon PP1c  $\beta$  and MYPT1 knockdown, myosin phosphatase levels in the cell are decreased. Therefore, myosin phosphatase cannot dephosphorylate myosin light chain (MLC) leading to cell contraction. This could be a possible reason for increase in filopodia extensions in PP1 c  $\beta$  and MYPT1 knockdown cells. As the cells contract, the formation of actin filopodia structures occur.

**Molecular Mechanism of PP1c  $\beta$  and MYPT1 Interdependence:**

Thus far, I have shown the interdependence of myosin phosphatase subunits MYPT1 and PP1c  $\beta$ . Since RNAi changed the morphology of the cell types studied, we were interested in uncovering the molecular mechanism of PP1c  $\beta$  and MYPT1 interdependence and their interaction. Based on my knockdown data, we were interested in understanding the structural interaction between myosin phosphatase subunits MYPT1 and PP1c  $\beta$ . In understanding the interaction between these subunits, we may be able to lead to the development of small molecules that interrupt this interaction. This would be helpful in making cells more susceptible to certain chemotherapeutic agents, such as those that target parts of the cell infrastructure like Taxol®.

**Alignment of Human PP1 Isoforms and the Formation of PP1 Hybrid Constructs:**

As mentioned, there are three different isoforms of PP1c: PP1 $\alpha$ , PP1 $\beta$ , and PP1 $\gamma$ . The sequences of PP1c  $\beta$  from mouse, rat, and human are nearly 100% homologous. It is also interesting to note that the sequences from PP1c  $\alpha$  and PP1c  $\gamma$  from these three different species are also highly homologous. As described earlier, this sequence homology allows for the specificity of the reactions in which these proteins are involved. When aligning the three different isoforms of human PP1c three things are present: 1. a somewhat divergent region at the extreme N-terminus, 2. a highly conserved region in the center of the protein, and 3. the sequence diverges between the three isoforms approximately

within the last 30 amino acids at the C-terminus (**Figure II-8a**). In 2004, a crystal structure of the complex between PP1c  $\beta$  and residues 1-299 of MYPT1 (Terrak, Kerff et al. 2004) isolated from chicken gizzard was published. From this structure, it was predicted that MYPT1 interacts with PP1c  $\beta$  at three separate regions: 1. the N-terminal arm, 2. the RVxF motif, and 3. the second group of ankyrin repeats, which interact mainly with PP1c  $\beta$  residues Tyr A305 and Tyr A307 located at its C-terminus. From these data, it is predicted that PP1c  $\beta$  interacts with MYPT1 through its C-terminal domain. From these data, it was hypothesized that the specificity of MYPT1 for PP1c  $\beta$  lies within the sequence located at the C-terminus.

In order to address this question, PP1 hybrid constructs were made by swapping different regions of the C-terminal domain of PP1c  $\beta$  with the C-terminal domain of PP1c  $\gamma$  and vice versa. Two sets of constructs were made. In the first pair of constructs, PP1c protein was split right down the center and the corresponding C-terminal domains of PP1c  $\beta$  and PP1c  $\gamma$  were switched. This pair of constructs was made to address the role of the somewhat divergent region of PP1 at the N-terminus. In the second set of constructs, the extreme C-terminus (approximately the last 30 amino acids) was swapped between PP1c  $\beta$  and PP1c  $\gamma$  (**Figure II-8b**). These constructs would address the role of the C-terminus in the interaction of MYPT1 and PP1c  $\beta$ .

#### **Identification of the PP1c Domain Required for the Interaction with MYPT1:**

As expected, the construct containing the C-terminal half of PP1c  $\beta$  was able to interact with MYPT1 as determined through immunoprecipitation assays while the construct containing the C-terminal half of PP1c  $\gamma$  was unable to interact with MYPT1. Surprisingly, the construct containing the last 30 amino acids of PP1c  $\gamma$  (and not that containing the last 30 amino acids of PP1c  $\beta$ ) was able to interact with MYPT1. These data illustrate that the interaction between PP1c  $\beta$  and MYPT1 is not specific for the C-terminal domain of the protein, but instead specific for a small region upstream of the C-terminal domain. As expected, PP1c  $\beta(\gamma1)$  (**lane 6**) (**Figure II-9**) was not capable of binding MYPT1 while PP1c  $\gamma(\beta1)$  (**lane 8**) was able to interact with MYPT1. Surprisingly, PP1c  $\beta(\gamma2)$  (**lane 10**) was capable of binding MYPT1 while PP1c  $\gamma(\beta2)$

(lane 12) was not. Based on this information, we deduced that the specificity of MYPT1 and PP1c  $\beta$  interaction does not lie within the C-terminal domain of PP1c  $\beta$  but instead in a region further upstream. The site of interaction is most likely in the region between residues 121-303 for PP1c  $\beta$ .

From the data described above, it was concluded that the interaction between PP1c  $\beta$  and MYPT1 occurs in the region between residues 121-303 for PP1c  $\beta$ . To further investigate this interaction, two different approaches were utilized. First, protein chimeras were made in PP1c  $\beta$  switching this region with residues 199-301 for PP1c  $\gamma$ . As expected, the construct containing this “center” region of PP1c  $\beta$  was capable of interacting with MYPT1 while the construct containing this region of PP1c  $\gamma$  was not. As predicted, PP1c  $\beta\gamma\beta$  (lane 4) was not capable of binding MYPT1 while PP1c  $\gamma\beta\gamma$  (lane 6) was able to bind MYPT1 (Figure II-10). This indicates that the site of interaction between PP1c  $\beta$  and MYPT1 is in the region between residues 121-303 for PP1c  $\beta$ . Therefore, we have identified a novel binding region for MYPT1 on PP1c  $\beta$ .

#### **Site-directed Mutagenesis of PP1c $\beta$ and PP1c $\gamma$ :**

The second approach taken to investigate this interaction was mutation of the divergent residues between PP1c  $\beta$  and  $\gamma$  isoforms in this region to the corresponding residues in the other isoform and then looking at the effects of these mutations on MYPT1 interaction using immunoprecipitation assays. In this fashion, it was thought that specific residues required for the MYPT1 and PP1c  $\beta$  interaction could be determined. The mutations made in PP1c  $\beta$  isoform were; T197Q, S232A, N236H/R237K, and G280A. The mutations made in the PP1c  $\gamma$  isoform were; Q198T, A233S, H237N/K238R, and A281G (Figure II-11a). In this fashion, it was thought that the exact site of interaction between PP1c  $\beta$  and MYPT1 could be uncovered.

The only PP1c  $\beta$  mutation that had an effect on PP1c  $\beta$  binding to MYPT1 was the T197Q mutation (lane 4) (Figure II-11b). This mutation greatly decreased the capability of PP1c  $\beta$  to bind to MYPT1 by almost one-hundred percent. It is important to note that although the  $\beta$ T197Q mutation greatly decreased binding to MYPT1, there is still a residual amount of protein interacting with MYPT1 of about five percent (Figure II-

**11c).** This indicates that PP1c  $\beta$  residue 197 plays a role in the interaction with MYPT1. The other two PP1c  $\beta$  mutations (S232A, G280A) had no effect on MYPT1 binding. In analyzing the PP1c  $\gamma$  mutants, none of the mutants were able to rescue the capability of binding to MYPT1. To further address this point, double and triple mutants were made introducing the T197Q mutation into the PP1c  $\beta$  mutant plasmids S232A, N236H/R237K, and G280A. Plasmids were also made introducing the Q198T mutation into the PP1c  $\gamma$  mutants A233S, H237N/K238R, and A281G. In this fashion, it was thought that I could gently alter the shape of PP1c  $\gamma$  through these mutations to allow for interaction with MYPT1.

Interestingly, when expressing a PP1c  $\beta$  construct with mutations T197Q and S232A, the ability of PP1c  $\beta$  to interact with MYPT1 was rescued (**lane 4**) (**Figure II-12**). The ability of this construct to bind MYPT1 was approximately twenty percent. Similarly, a PP1c  $\beta$  construct with mutations N236H and R237K ( $\beta$ 2x) was able to interact with MYPT1 (**lane 5**) (**Figure II-12**). This construct was able to bind MYPT1 with an affinity of approximately sixty percent. Conversely, a PP1c  $\beta$  construct with mutations T197Q and  $\beta$ 2x was unable to interact with MYPT1 (**lane 6**) (**Figure II-12**). Similarly, a PP1c  $\beta$  construct with mutations T197Q and G280A was also unable to interact with MYPT1 (**lane 7**) (**Figure II-12**). These data illustrates that residue 197 of PP1c  $\beta$  enables its interaction with MYPT1. Curiously, in PP1c  $\beta$  the mutation of residue 232 from serine to the corresponding alanine found in PP1c  $\gamma$  rescues the ability of PP1c  $\beta$  to interact with MYPT1. Concurrently, the mutation of residues 236 and 237 in PP1c  $\beta$  to the corresponding residues in PP1c  $\gamma$  also rescues the ability of PP1c  $\beta$  to interact with MYPT1.

When analyzing the results from the PP1c  $\gamma$  mutants made, the only construct that rescues the binding affinity for PP1c  $\gamma$  is the construct in which residues 237 and 238 are mutated to the corresponding residues found in PP1c  $\beta$  (H237N/K238R,  $\gamma$ 2x) (**lane 9**) (**Figure II-12**). This construct was able bind MYPT1 with an affinity of approximately five percent. The remainder of the PP1c  $\gamma$  mutant constructs failed to interact with MYPT1. Taking all of these data into account, one can say that residue 197 of PP1c  $\beta$  is needed for its interaction with MYPT1. In addition, from the PP1c  $\gamma$  mutant data, it can

be stated that mutation of residues 237 and 238 in PP1c  $\gamma$  to the corresponding residues of PP1c  $\beta$  236 and 237 enables the interaction between PP1c  $\beta$  and MYPT1. Therefore, residues 236 and 237 of PP1c  $\beta$  enable the interaction between PP1c  $\beta$  and MYPT1 (**Figure II-12**).

As mentioned, there are three different isoforms of PP1c: PP1 $\alpha$ , PP1 $\beta$ , and PP1 $\gamma$ . The sequences of PP1c  $\beta$  from mouse, rat, and human are nearly 100% homologous. In 2004, a crystal structure of the complex between PP1c  $\beta$  and residues 1-299 of MYPT1 (Terrak, Kerff et al. 2004) isolated from chicken gizzard was published. From this structure, it was predicted that MYPT1 interacts with PP1c  $\beta$  at three separate regions: 1. the N-terminal arm, 2. the RVxF motif, and 3. the second group of ankyrin repeats, which interact mainly with PP1c  $\beta$  residues Tyr A305 and Tyr A307 located at its C-terminus. In this paper it is shown that PP1c  $\beta$  and MYPT1 do interact at MYPT1 residue 38A located in the PP1-binding site of MYPT1 (MYPT1 38A) (Terrak, Kerff et al. 2004). From these data, it is predicted that PP1c  $\beta$  interacts with MYPT1 through its C-terminal domain.

Based on our mutant data, we then looked to molecular modeling to visualize our residues of interest. This work was done in collaboration with Miguel Garcia-Diaz, Department of Pharmacological Sciences, Stony Brook University. In contrast to the published structure, our data indicate that MYPT1 interacts with PP1c  $\beta$  through residues 197, 232, 236 and 237 (**Figure II-13a**). In our structure, residues 1-299 of MYPT1 are illustrated in red as previously published. Full-length PP1c  $\beta$  is shown in blue. Manganese ions are illustrated in magenta. The published PP1-binding region residue F38 of MYPT1 is illustrated in green. The area of interest is indicated in the black box (**Figure II-13a**). Residues 197, 232, 236 and 237 are illustrated in yellow, as are the predicted van der Waal's interactions (**Figure II-13b**).

## **DISCUSSION:**

In this body of work, I was able to show that two subunits of myosin phosphatase (MP) are interdependent on one another. When knocking down the PP1c  $\beta$  subunit using either RNAi or shRNA we are able to observe a decrease in the protein levels of MYPT1. In addition to their interdependence, we were also able to show that knocking down PP1c  $\beta$  and MYPT1 levels causes a change in cell morphology, size, number, and the abundance of cortical actin structures present at the plasma membrane.

As mentioned, there are three different isoforms of PP1c: PP1 $\alpha$ , PP1 $\beta$ , and PP1 $\gamma$ . The sequences of PP1c  $\beta$  from mouse, rat, and human are nearly 100% homologous. In 2004, a crystal structure of the complex between PP1c  $\beta$  and residues 1-299 of MYPT1 (Terrak, Kerff et al. 2004) isolated from chicken gizzard was published. From this structure, it was predicted that MYPT1 interacts with PP1c  $\beta$  at three separate regions: 1. the N-terminal arm, 2. the RVxF motif, and 3. the second group of ankyrin repeats, which interact mainly with PP1c  $\beta$  residues Tyr A305 and Tyr A307. From these data, it is also predicted that PP1c  $\beta$  interacts with MYPT1 through its C-terminal domain.

Based on our analysis of the sequence and structure, when aligning the three different isoforms of human PP1c three things are present: 1. a somewhat divergent region at the extreme N-terminus, 2. a highly conserved region in the center of the protein, and 3. the sequence diverges between the three isoforms approximately within the last 30 amino acids at the C-terminus. From these data, it was hypothesized that the specificity of MYPT1 for PP1c  $\beta$  lies within the sequence located at the C-terminus.

In order to address this question, PP1 hybrid constructs were made by swapping different regions of the C-terminal domain of PP1c  $\beta$  with the C-terminal domain of PP1c  $\gamma$  and vice versa. Two sets of constructs were made. In the first pair of constructs, PP1 protein was split right down the center and the corresponding C-terminal domains of PP1c  $\beta$  and PP1c  $\gamma$  were switched. This pair of constructs was made to address the role of the somewhat divergent region of PP1 at the N-terminus. In the second set of constructs, the extreme C-terminus (approximately the last 30 amino acids) was swapped between PP1c  $\beta$  and PP1c  $\gamma$ . These constructs would address the role of the C-terminus in the interaction of MYPT1 and PP1c  $\beta$ . As expected, the construct containing the C-terminal half of PP1c  $\beta$  was able to interact with MYPT1 as determined through



immunoprecipitation assays while the construct containing the C-terminal half of PP1c  $\gamma$  was unable to interact with MYPT1. Surprisingly, the construct containing the last 30 amino acids of PP1c  $\gamma$  (and not that containing the last 30 amino acids of PP1c  $\beta$ ) was able to interact with MYPT1. These data illustrate that the interaction between PP1c  $\beta$  and MYPT1 is not specific for the C-terminal domain of the protein, but instead specific for a small region upstream of the C-terminal domain. As expected, PP1c  $\beta(\gamma1)$  (**lane 6**) (**Figure II-9**) was not capable of binding MYPT1 while PP1c  $\gamma(\beta1)$  (**lane 8**) was able to interact with MYPT1. Surprisingly, PP1c  $\beta(\gamma2)$  (**lane 10**) was capable of binding MYPT1 while PP1c  $\gamma(\beta2)$  (**lane 12**) was not. Based on this information, we deduced that the specificity of MYPT1 and PP1c  $\beta$  interaction does not lie within the C-terminal domain of PP1c  $\beta$  but instead in a region further upstream. The site of interaction is most likely in the region between residues 121-303 for PP1c  $\beta$ .

From the data described above, it was concluded that the interaction between PP1c  $\beta$  and MYPT1 occurs in the region between residues 121-303 for PP1c  $\beta$ . To further investigate this interaction, two different approaches were utilized. First, protein chimeras were made in PP1c  $\beta$  switching this region with residues 199-301 for PP1c  $\gamma$ . As expected, the construct containing this “center” region of PP1c  $\beta$  was capable of interacting with MYPT1, while the construct containing this region of PP1c  $\gamma$  was not. As predicted, PP1c  $\beta\gamma\beta$  (**lane 4**) was not capable of binding MYPT1 while PP1c  $\gamma\beta\gamma$  (**lane 6**) was able to bind MYPT1 (**Figure II-10**). This indicates that the site of interaction between PP1c  $\beta$  and MYPT1 is most likely in the region between residues 121-303 of PP1c  $\beta$ . Therefore, I have identified a novel binding region for MYPT1 on PP1c  $\beta$ .

The second approach taken to investigate this interaction was mutation of the divergent residues between PP1c  $\beta$  and  $\gamma$  isoforms in this region to the corresponding residue in the other isoform. The effects of these mutations on MYPT1 interaction was then studied using immunoprecipitation assays. The mutations made in PP1c  $\beta$  isoform were; T197Q, S232A, N236H/R237K, and G280A. The mutations made in the PP1c  $\gamma$  isoform were; Q198T, A233S, H237N/K238R, and A281G. In this fashion, it was

thought that the exact site of interaction between PP1c  $\beta$  and MYPT1 could be uncovered.

To date it has been illustrated that only one of the mutations made in PP1c  $\beta$  shows an effect. Mutation of residue 197 from glutamine to threonine in PP1c  $\beta$  shows a decreased affinity for MYPT1 (**Figure II-11**). From these data, we can deduce that residue 197 of PP1c  $\beta$  enables the interaction between PP1c  $\beta$  and MYPT1. The other two PP1c  $\beta$  mutations (S232A, G280A) had no effect on MYPT1 binding. When analyzing the PP1c  $\gamma$  mutants, none of the mutants were able to rescue the capability of binding to MYPT1. To further address this point, double and triple mutants were made introducing the T197Q mutation into the PP1c  $\beta$  mutant plasmids S232A, N236H/R237K, and G280A. Plasmids were also made introducing the Q198T mutation into the PP1c  $\gamma$  mutants A233S, H237N/K238R, and A281G.

Interestingly, when expressing a PP1c  $\beta$  construct with mutations T197Q and S232A, the ability of PP1c  $\beta$  to interact with MYPT1 was rescued. The ability of this construct to bind MYPT1 was approximately twenty percent. Similarly, a PP1c  $\beta$  construct with mutations N236H and R237K ( $\beta$ 2x) was able to interact with MYPT1. This construct was able to bind MYPT1 with an affinity of approximately sixty percent. Conversely, a PP1c  $\beta$  construct with mutations T197Q and  $\beta$ 2x was unable to interact with MYPT1. Similarly, a PP1c  $\beta$  construct with mutation T197Q and G280A was also unable to interact with MYPT1. These data illustrate that residue 197 of PP1c  $\beta$  enables its interaction with MYPT1. In PP1c  $\beta$  the mutation of residue 232 from serine to the corresponding alanine found in PP1c  $\gamma$  rescues the ability of PP1c  $\beta$  to interact with MYPT1. Concurrently, the mutation of residues 236 and 237 in PP1c  $\beta$  to the corresponding residues in PP1c  $\gamma$  also rescues the ability of PP1c  $\beta$  to interact with MYPT1.

In analyzing the results from the PP1c  $\gamma$  mutants made, the only construct that rescues the binding affinity for PP1c  $\gamma$  is the construct in which residues 237 and 238 are mutated to the corresponding residues found in PP1c  $\beta$  (H237N/K238R,  $\gamma$ 2x). This construct was able to bind MYPT1 with an affinity of approximately five percent. The remainder of the PP1c  $\gamma$  mutant constructs failed to interact with MYPT1. Taking all of these data into

account, one can say that residue 197 of PP1c  $\beta$  is needed for its interaction with MYPT1. In addition, from the PP1c  $\gamma$  mutant data, it can be stated that mutation of residues 237 and 238 in PP1c  $\gamma$  to the corresponding residues of PP1c  $\beta$  236 and 237 enables the interaction between PP1c  $\beta$  and MYPT1. Therefore, residues 236 and 237 of PP1c  $\beta$  enable the interaction between PP1c  $\beta$  and MYPT1 (**Figure II-12**).

As mentioned, the crystal structure of the complex between PP1c  $\beta$  and residues 1-299 of MYPT1 (Terrak, Kerff et al. 2004) predicts that PP1c  $\beta$  interacts with MYPT1 through its C-terminal domain. In contrast, our data indicate that MYPT1 interacts with PP1c  $\beta$  through its residues 197, 232, 236 and 237 (**Figure II-13**).

In conclusion, I showed that the MYPT1 subunit of MP interacts with the PP1c  $\beta$  isoform of PP1c, that the specificity of MYPT1 and PP1c  $\beta$  interaction does not lay within the C-terminal domain of PP1c  $\beta$  but instead in a region upstream, that the site of interaction is located in the region between residues 121-303 for PP1c  $\beta$ , and that PP1c  $\beta$  residues 197, 232, 236, and 237 mediate the interaction of PP1c  $\beta$  with MYPT1.

The overall goal of this project was to determine the role of the MP signaling pathway in cellular morphology and migration in tumor cells as the initial step in developing a new approach for cancer therapeutics. Future implications of these data are to use this information to drive the development of chemotherapeutic agents such as Taxol<sup>®</sup>, which target components of the cell infrastructure particularly important for tumor cell metastasis. In addition to the development of Taxol-like compounds, our site-directed mutants of PP1c  $\beta$  can be used in chemical screens targeted against other anti-cancer agents.

## **FUTURE DIRECTIONS:**

In order to further study the effect of PP1c  $\beta$  and MYPT1 knockdown on cell shape, size, and morphology, we would like to use immunofluorescence to analyze the presence of focal adhesions, the integrity of gap junctions and therefore the integrity of the plasma membrane. To look at focal adhesions, I would like to stain cells with an anti-vinculin antibody. Connexin (Cx) 43 can be used to observe gap junctions and E-cadherin can be used to look at the integrity of the plasma membrane.

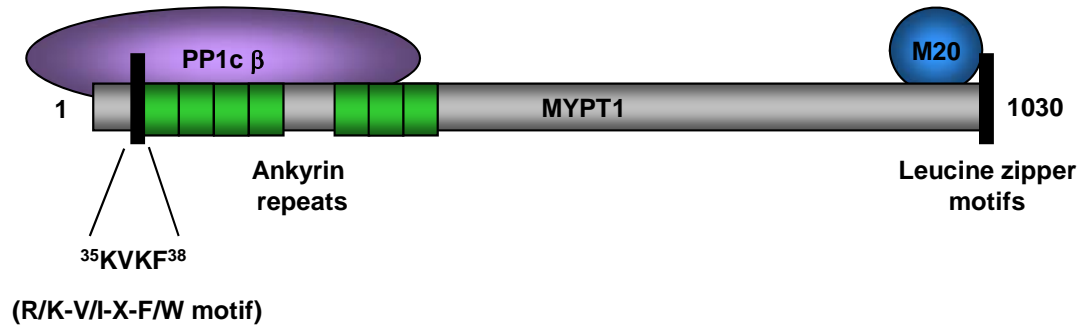
In order to further determine the consequence of using RNAi to knock down the myosin phosphatase (MP) subunits PP1c  $\beta$  and MYPT1 on the morphology and migration capability of cells we would like to use Transwell® migration assays and wound healing assays.

In order to ensure that our observations are not an artifact of our knockdown procedures, we would like to introduce wild type PP1c  $\beta$  or MYPT1 into knockdown cells to rescue phenotype. In order to bring this work to the next level, we would like to study the effect of expressing MYPT1 interaction deficient PP1c mutants in cells and studying the affect on cell morphology, localization and function. In this way, we may be able to make cells more susceptible to certain chemotherapeutic agents, such as those that target parts of the cell infrastructure like Taxol®. In addition to the development of Taxol-like compounds, our site-directed mutants of PP1c  $\beta$  can be used in chemical screens targeted against other anti-cancer agents. We would also like to use retroviral constructs expressing different size fragments of PP1c  $\beta$  to determine exact portion of protein required for proper localization and function.

Our RNAi data indicated a morphological change in the cell types studied. Some future directions of the project include looking at the effect of expressing MYPT1 interaction deficient PP1c mutants in cells and studying the affect on cell morphology, localization and function. In addition, we would like to use retroviral constructs expressing different size fragments of PP1c  $\beta$  to determine exact portion of protein required for proper localization and function. Finally, as described earlier, we would like to use our PP1c  $\beta$  mutant to screen for small molecular inhibitors to disrupt the MYPT1 and PP1c  $\beta$  interaction since the interaction is so tight.

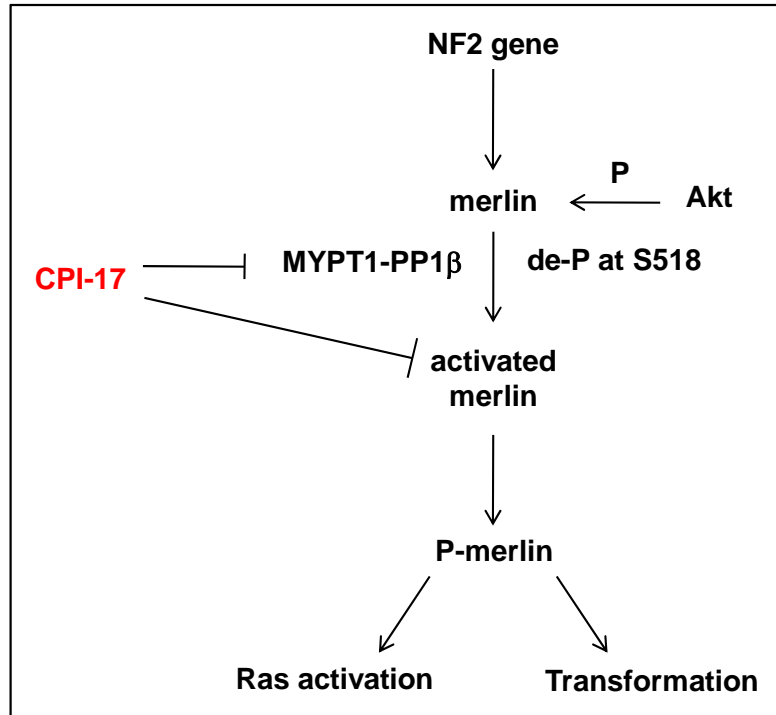
**FIGURES:**

**Figure 1: Myosin Phosphatase (MP)**



**Figure II-1: Myosin Phosphatase (MP). a. Representation of Myosin Phosphatase.** Myosin phosphatase is composed of three different subunits: 1. catalytic subunit (type 1 protein phosphatase, PP1c), 2. the myosin light chain (MLC) targeting subunit (MYPT), and 3. M20 (20 kDa subunit of unknown function). There are three different isoforms of PP1c:  $\alpha$ ,  $\beta$ , and  $\gamma$ . Figure adapted from Ito, M. *et al.*; *Mol. Cell. Biochem.* (2004); **259**: 197-209.

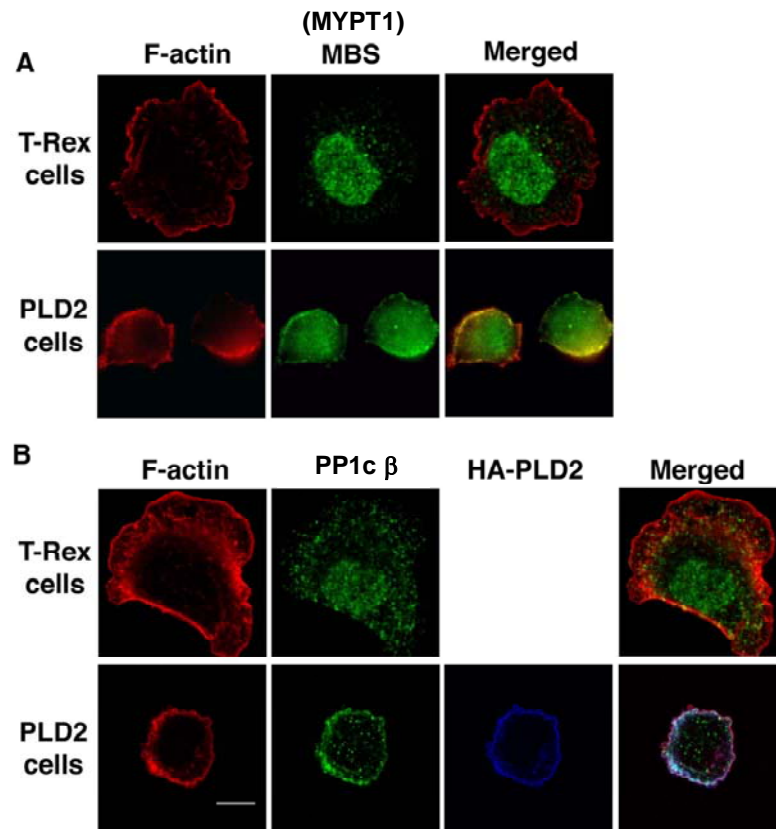
**Figure 2: Myosin Phosphatase and Merlin Signaling**



**Figure II-2: Myosin Phosphatase and Merlin Signaling.** Merlin is encoded by the NF2 gene and becomes phosphorylated (**P**) through the action of Akt kinase. Merlin becomes dephosphorylated at serine 518 through the action of MYPT1-PP1 $\beta$  myosin phosphatase. This allows for the activation of merlin. CPI-17, a negative regulator of myosin phosphatase, allows for the phosphorylation of merlin to occur. Phosphorylated merlin can allow for Ras activation and cellular transformation.

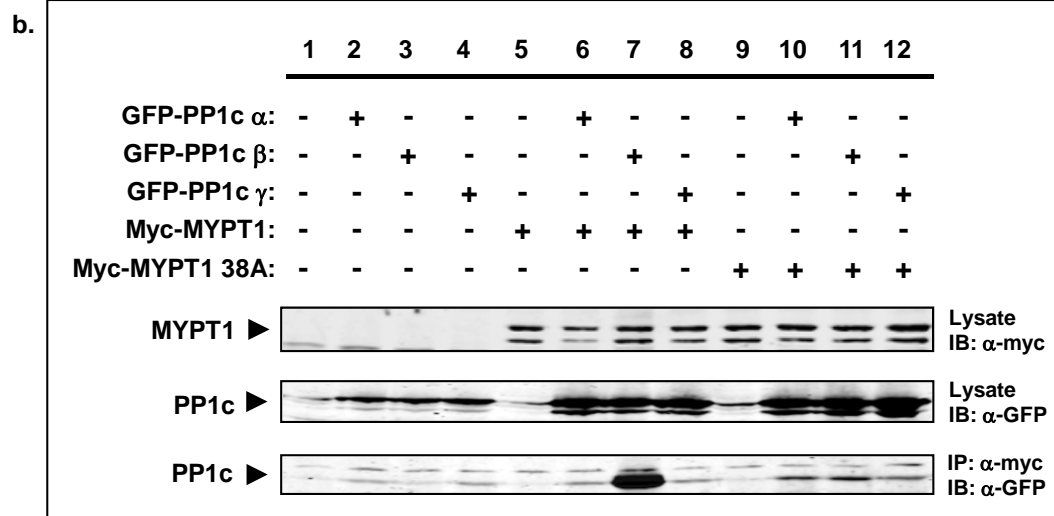
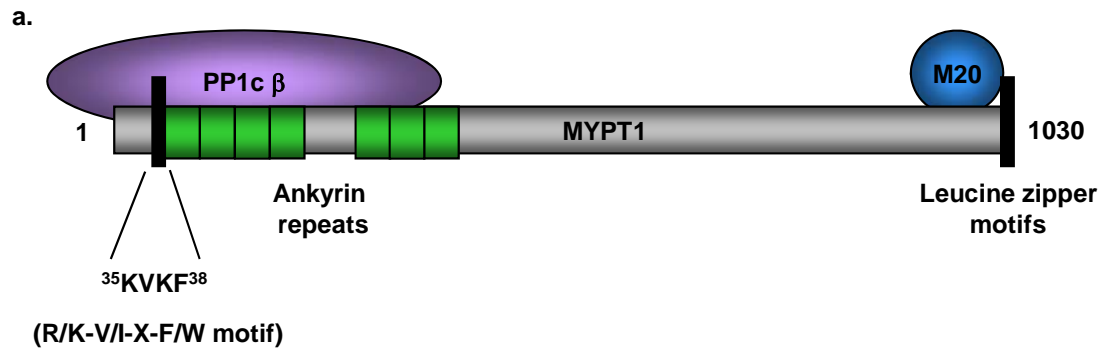


**Figure 3: Myosin Phosphatase and Lipid Signaling**



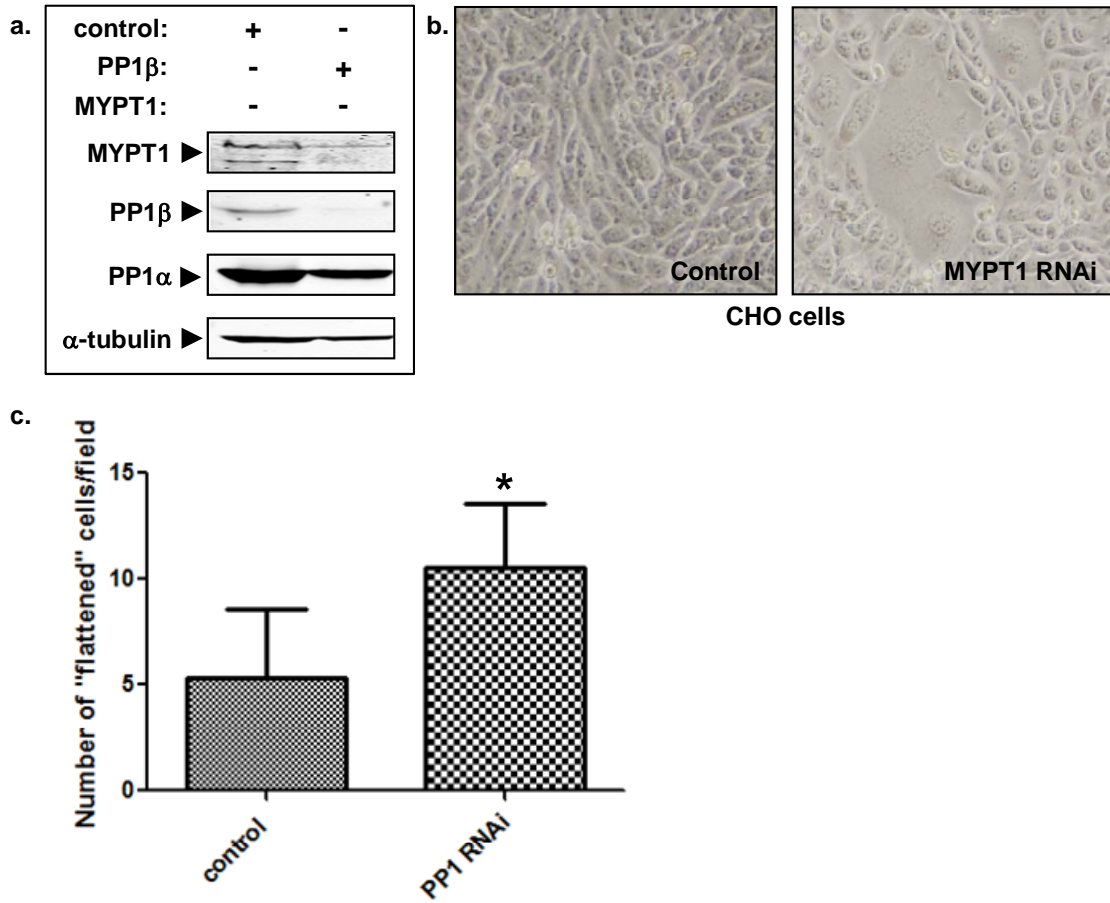
**Figure II-3: Myosin Phosphatase and Lipid Signaling a,b. PLD2 overexpression leads to accumulation of myosin phosphatase at the cell periphery.** Accumulation of the myosin phosphatase (MP) subunits MBS (MYPT1) and PP1c  $\beta$  at the cell periphery present upon PLD2 overexpression but not in control (T-Rex) cells. Upon PLD2 overexpression, cells also become rounded in appearance. Scale bar, 10  $\mu$ m. Figure adapted from (Du and Frohman 2008).

**Figure 4: Myosin Phosphatase (MP)**



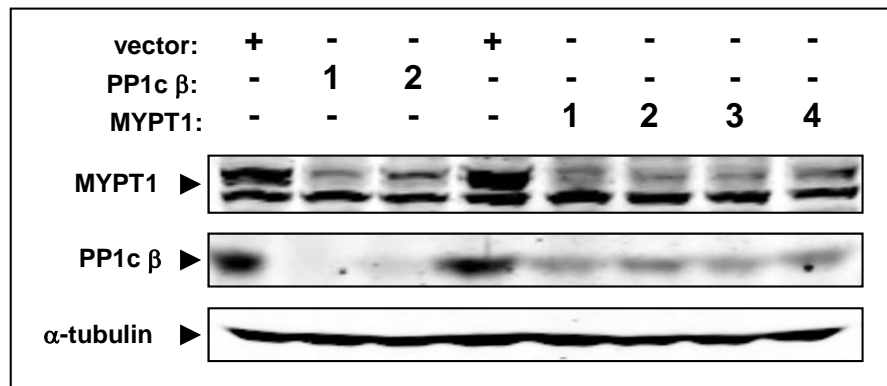
**Figure II-4: Myosin Phosphatase (MP). a. Representation of Myosin Phosphatase.** Myosin phosphatase is composed of three different subunits: 1. catalytic subunit (type 1 protein phosphatase, PP1c), 2. the myosin light chain (MLC) targeting subunit (MYPT), and 3. M20 (20 kDa subunit of unknown function). There are three different isoforms of PP1c:  $\alpha$ ,  $\beta$ , and  $\gamma$ . Figure adapted from Ito, M. *et al.*; *Mol. Cell. Biochem.* (2004); **259**: 197-209. **b. MYPT1 Specificity for PP1c  $\beta$  Isoform.** It has previously been published that MYPT1 interacts specifically with the beta form of PP1c (PP1c  $\beta$ ) (Eto, M. *et al.*; *Cell Motility and the Cytoskeleton* (2005); **62**:100–109.). In order to confirm this observation, we performed immunoprecipitation assays with an anti-myc antibody (Cell Signaling, Danvers, MA) on cell lysates from cells expressing myc-tagged MYPT1 and GFP-tagged PP1c constructs. Immunoprecipitate was then immunoblotted with anti-GFP antibody (abcam). As indicated, wild-type MYPT1 interacts specifically with the  $\beta$  isoform of PP1c (**lane 7**) and not the  $\alpha$  or  $\gamma$  isoforms. PP1c  $\beta$  does not interact with a MYPT1 construct that has a mutation in the PP1-binding site of MYPT1 (MYPT1 38A) (**lane 11**). The exact site of PP1c  $\beta$  required for MYPT1 binding has not been determined and was investigated in these studies.

**Figure 5: Interdependence of PP1c and MYPT1**



**Figure II-5: Interdependence of PP1c  $\beta$  and MYPT1.** **a.** CHO cells were transiently transfected with RNAi directed against either PP1c  $\beta$  or MYPT1. 48 hours following transfection, cells were lysed and western blots were performed against the corresponding proteins using the appropriate antibodies (see Materials and Methods). There are three independent RNAi oligonucleotides for each protein. An immunoblot representative of 2 experiments with similar outcomes is shown. **b. Morphological Changes Present Following MYPT1 Knockdown.** 48 hours following RNAi transfection, CHO cells were analyzed for changes in cellular morphology. Upon MYPT1 knockdown there are several morphological changes to the cells. The cells are larger, flattened and spread out. Cellular borders are less defined. There is also a decrease in cell number based on the density of cells and the number of dead cells present. **c. Quantitation of Morphological Changes Present Following PP1c  $\beta$  Knockdown.** The number of cells exhibiting the “flattened” phenotype were counted in 10 fields of vision. The average is displayed. Error bars represent the standard deviation (\*,  $P < 0.05$ ). The data shown is representative of 2 independent experiments.

**Figure 6:** MYPT1 and PP1c  $\beta$  are required for the stability of each other

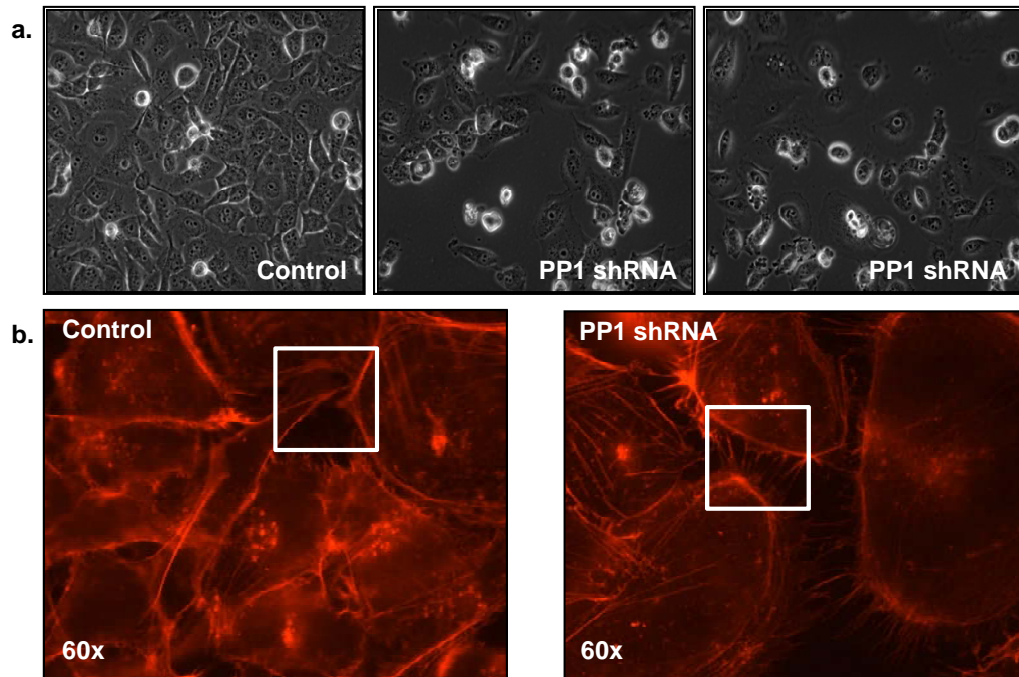


Guangwei Du

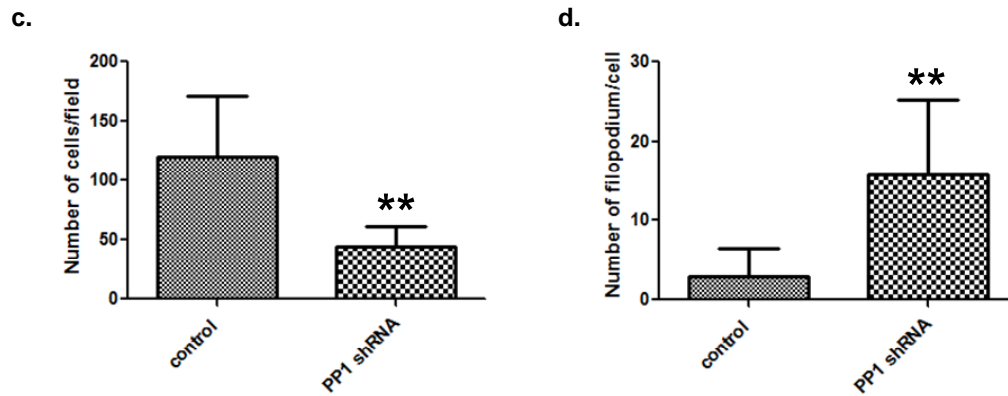
**Figure II-6: MYPT1 and PP1c  $\beta$  are required for the stability of each other.** CHO cells were infected with retrovirus expressing shRNAs for PP1c  $\beta$  and MYPT1 as indicated above. Cell lysates were collected and expression of MYPT1 and PP1c  $\beta$  was analyzed by western blot. Knockdown of either MYPT1 or PP1c  $\beta$  affects the expression level of the other, suggesting that formation of myosin phosphatase (MP) holoenzyme is required for stability of MYPT1 and PP1c  $\beta$ . **This data was generated by Guangwei Du, Ph.D., Department of Pharmacological Sciences, Stony Brook University.**



**Figure 7: Changes in Cell Number and Cell Shape Following PP1c Knockdown in MDA-MB-231 cells**

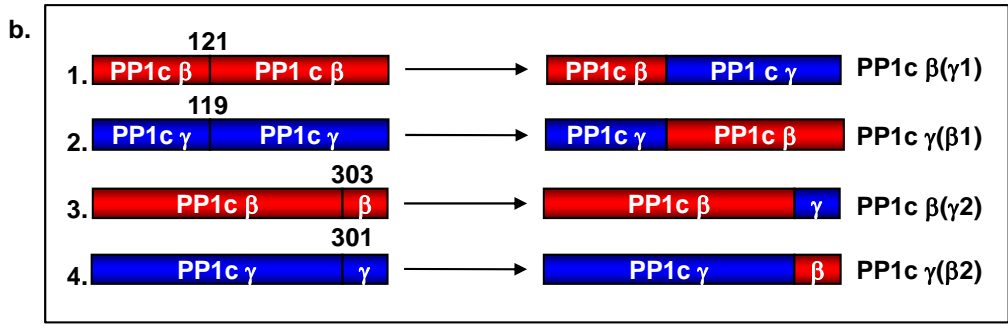
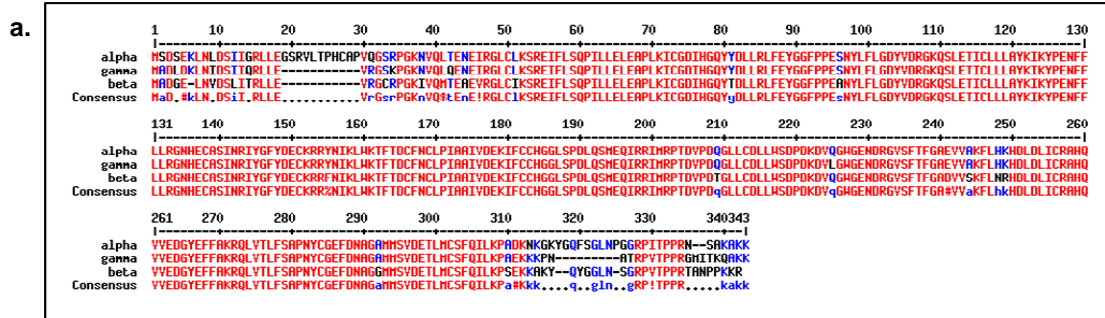


MDA-MB-231 cells



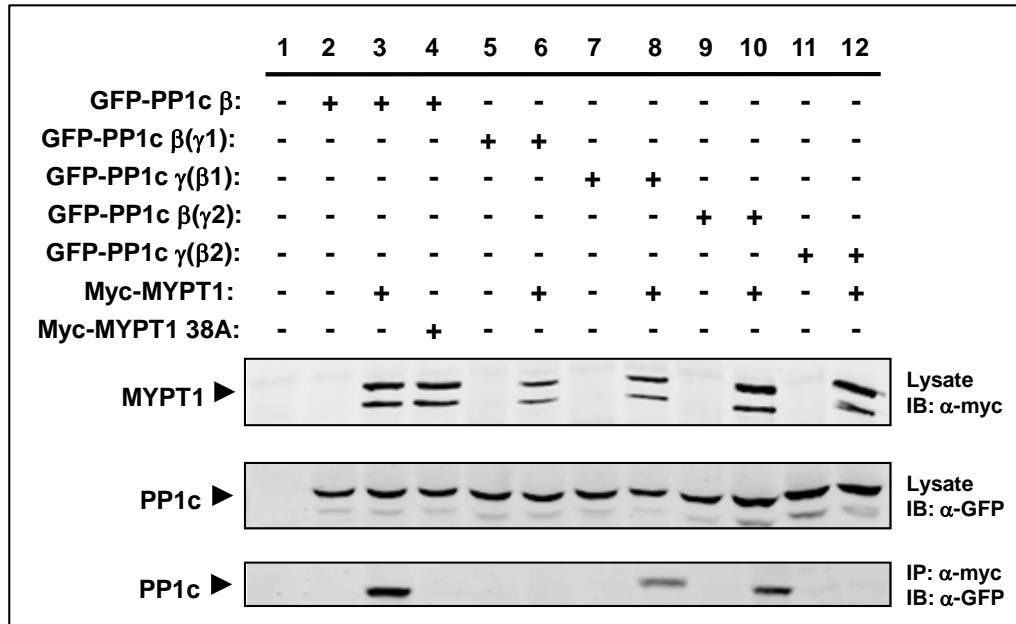
**Figure II-7: Changes in Cell Number and Cell Shape Following PP1c  $\beta$  Knockdown in MDA-MB-231 cells.** **a. Live Cell Analysis.** MDA-MB-231 breast cancer cells were infected with retrovirus against PP1c  $\beta$ . 48 hours following infection, live cell images were taken using Nikon Eclipse TS100 light microscope (Nikon Corporation, Melville, NY) and photographed using a Nikon Digital Sight camera (Nikon Corporation, Melville, NY). Images were analyzed using NIS-Elements F v2.30 Imaging Software (Nikon Instruments, Melville, NY) (see Materials and Methods). **b. Immunofluorescence Microscopy.** MDA-MB-231 breast cancer cells were infected with retrovirus against PP1c  $\beta$ . 48 hours following infection, cells were fixed in 3.7% paraformaldehyde and stained with an antibody against phalloidin (actin) conjugated to rhodamine (Invitrogen, Carlsbad, CA) (see Materials and Methods). Inset of the control panel represents the smooth edges observed in MDA-MB-231 cells prior to PP1c  $\beta$  knockdown. Inset of PP1 shRNA panel illustrates the increase in filopodia observed at the plasma membrane of MDA-MB-231 cells upon PP1c  $\beta$  knockdown. **c. Quantitation of decrease in cell number Following PP1c  $\beta$  Knockdown in MDA-MB-231 cells.** The number of cells per field of view for each condition were counted. Ten fields of view were counter per condition. The average was calculated and graphed. Error bars represent the standard deviation (SD) (\*\*,  $P < 0.01$ ). **d. Quantitation of increase in filopodia per cell Following PP1c  $\beta$  Knockdown in MDA-MB-231 cells.** The number of filopodia per cell were counted for ten cells per condition. The average was calculated and graphed. Error bars represent the standard deviation (SD) (\*\*,  $P < 0.01$ ).

**Figure 8: Schematic of PP1 Hybrid Constructs**



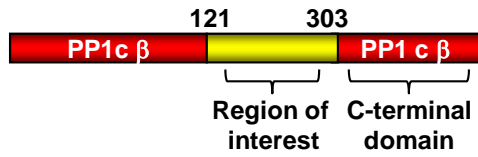
**Figure II-8: Schematic of PP1 Hybrid Constructs.** **a. Alignment of Human PP1 Isoforms.** A sequence alignment of the three isoforms of human PP1c was generated using the Network Protein Sequence Analysis: Multalin Alignment (Corpet 1988). As indicated, there is highly conserved sequence similarity (in red) between the three isoforms ( $\alpha$ ,  $\beta$ ,  $\gamma$ ) at the N-terminus. The sequences diverge between the three isoforms approximately within the last 30 amino acids at the C-terminus (in blue) and in a short sequence at the extreme N-terminus. Based on this information, it was proposed that the region in PP1c  $\beta$  that is responsible for its specific interaction with MYPT1 is located within the extreme C-terminus (last 30 amino acids). **b. Structure of PP1 Chimera Constructs.** Based on the alignment of the three human PP1c isoforms, it was proposed that C-terminus of PP1c  $\beta$  was the region responsible for the isoform specificity of MYPT1 interaction. In order to investigate this further, we made 2 sets of chimera constructs with PP1c  $\beta$  and PP1c  $\gamma$ . In the first set, PP1c was divided in half and the C-terminal halves of PP1c  $\beta$  and PP1c  $\gamma$  were exchanged. These constructs were named PP1c  $\beta(\gamma1)$  (1) and PP1c  $\gamma(\beta1)$  (2). For the second set of constructs, the extreme C-terminal (last 30 amino acids) of PP1c  $\beta$  and PP1c  $\gamma$  were exchanged. These constructs were named PP1c  $\beta(\gamma2)$  (3) and PP1c  $\gamma(\beta2)$  (4).





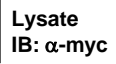


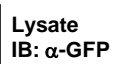
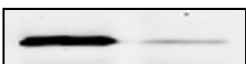

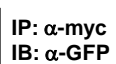
**Figure 9: Identification of the PP1c Domain Required for Interaction with MYPT1**



**Figure II-9: Identification of the PP1c Domain Required for Interaction with MYPT1. Immunoprecipitation Results.** CHO cells were transiently transfected with plasmids for the various GFP-tagged PP1c constructs and Myc-tagged MYPT1. 48 hours later, cells were lysed and western blots were performed against the corresponding proteins using the appropriate antibodies. Immunoprecipitation assays were performed with an anti-myc antibody (Cell Signaling, Danvers, MA). Immunoprecipitate was then immunoblotted with anti-GFP antibody (abcam, Cambridge, MA).

**Figure 10: Identification of the PP1c Domain Required for Interaction with MYPT1**



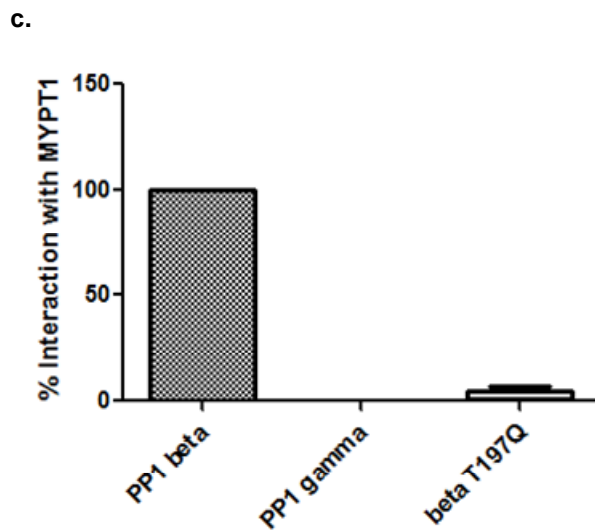
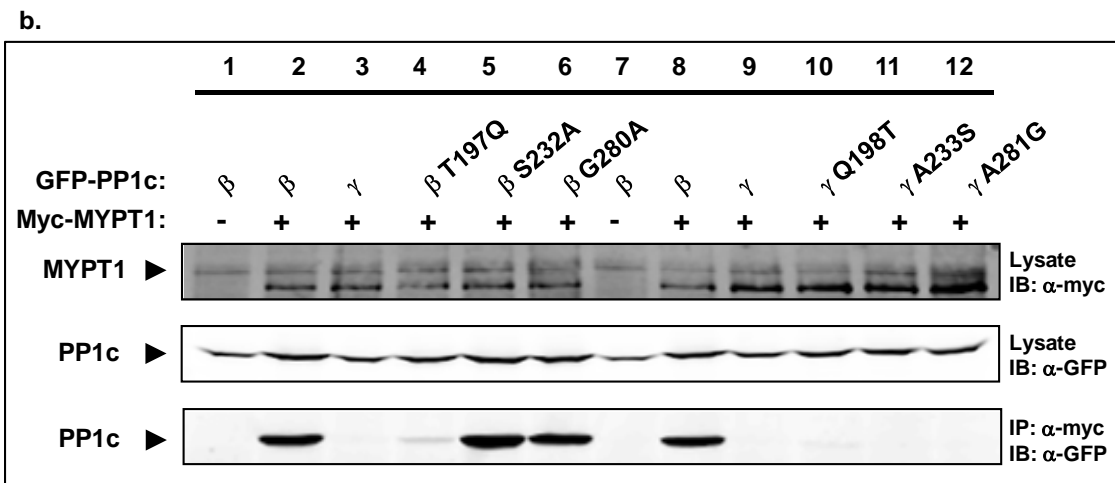
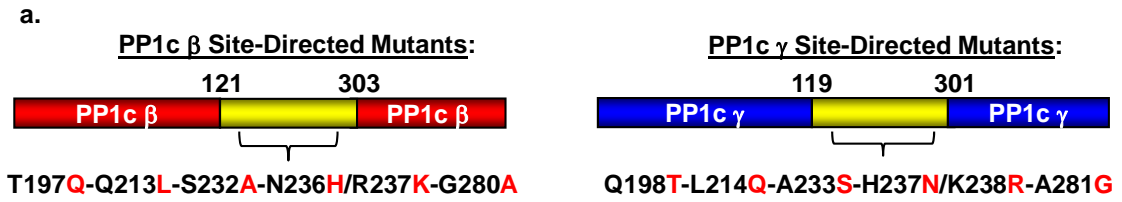
|   | 1   | 2 | 3  | 4 | 5   | 6 |                        |
|---|---|---|--|---|---|---|------------------------|
| GFP-PP1c β:   | +   | + | -  | - | -   | - |                        |
| GFP-PP1c βγβ:   | -   | - | +  | + | -   | - |                        |
|  |   |   |  |   |   |   |                        |
| GFP-PP1c γβγ:   | -   | - | -  | - | +   | + |                        |
|  |   |   |  |   |   |   |                        |
| Myc-MYPT1:  | +   | - | -  | + | -   | + |                        |
| Myc-MYPT1 38A:  | -   | + | -  | - | -   | - |                        |
| MYPT1 ▶   |   |   |   |   |   |   | Lysate<br>IB: α-myc    |
| PP1c ▶  |  |   |  |   |  |   | Lysate<br>IB: α-GFP    |
| PP1c ▶  |  |   |  |   |  |   | IP: α-myc<br>IB: α-GFP |

**Figure II-10: Identification of the PP1c Domain Required for Interaction with MYPT1. Schematic of PP1 Hybrid Constructs and Immunoprecipitation Results.**

Based on our data, we propose that the interaction between PP1c  $\beta$  and MYPT1 occurs in the region between residues 121-303 for PP1c  $\beta$ . To ensure that this was indeed the region required for the interaction we made chimeras of PP1c  $\beta$  (red) switching this region with residues 119-301 for PP1c  $\gamma$  (blue). These constructs were named PP1c  $\beta\gamma\beta$  and PP1c  $\gamma\beta\gamma$ . CHO cells were transiently transfected with plasmids for the various GFP-tagged PP1c constructs and Myc-tagged MYPT1. 48 hours later, cells were lysed and western blots were performed against the corresponding proteins using the appropriate antibodies. Immunoprecipitation assays were performed with an anti-myc antibody (Cell Signaling, Danvers, MA). Immunoprecipitate was then immunoblotted with anti-GFP antibody (abcam, Cambridge, MA).



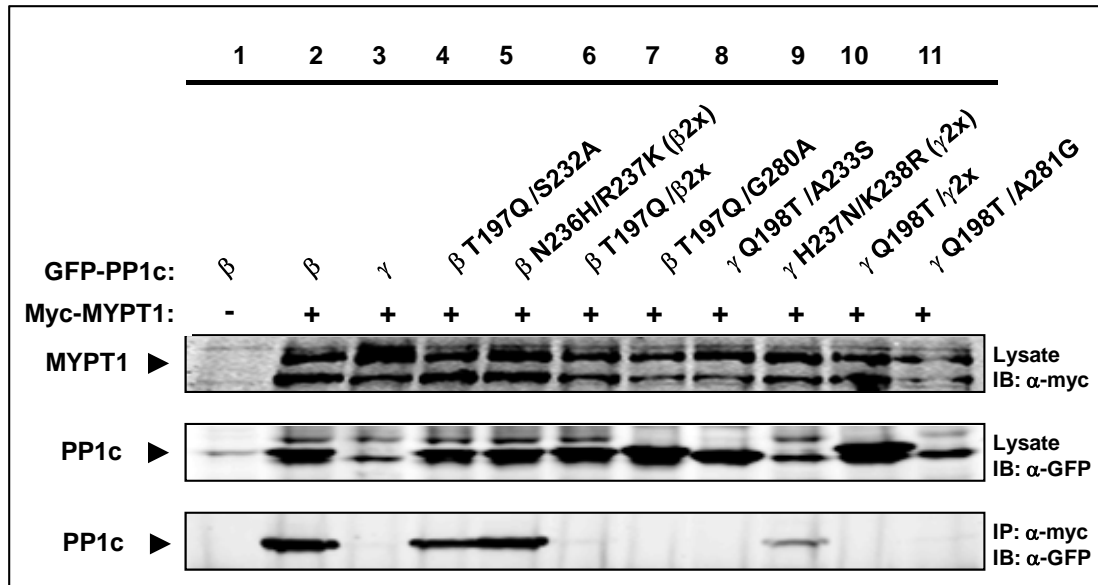
**Figure 11: Site-directed Mutagenesis of PP1c  $\beta$  and PP1c  $\gamma$**



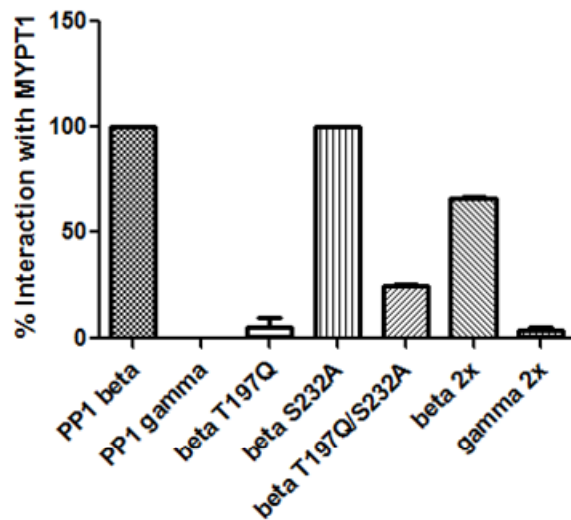
**Figure II-11: Site-directed Mutagenesis of PP1c  $\beta$  and PP1c  $\gamma$ .** **a. Schematic of PP1c  $\beta$  and PP1c  $\gamma$  site-directed mutants.** In an effort to determine the exact residues of PP1  $\beta$  required for its interaction with MYPT1, site-directed mutants were made at the residues that differed between PP1c  $\beta$  and PP1c  $\gamma$  in the region between residues 121-303 for PP1c  $\beta$ . The corresponding mutations were also made in PP1c  $\gamma$ . **b. Immunoprecipitation Results.** CHO cells were transiently transfected with plasmids for the various GFP-tagged PP1c constructs and Myc-tagged MYPT1. 48 hours later, cells were lysed and western blots were performed against the corresponding proteins using the appropriate antibodies. Immunoprecipitation assays were performed with an anti-myc antibody (Cell Signaling, Danvers, MA). Immunoprecipitate was then immunoblotted with anti-GFP antibody (abcam, Cambridge, MA). **c. Quantitation of PP1c  $\beta$  T197Q mutant MYPT1 binding.** Western blot band density was measured using the Odyssey Infrared Imaging System Software (LI-COR Biosciences, Lincoln, NE). The band density measurement for PP1c  $\beta$  plus MYPT1 (**PP1 beta**) was set at 100 percent. This represents the percentage of protein interacting with MYPT1. The percent interaction of PP1c  $\gamma$  (**PP1 gamma**) with MYPT1 was set at 0. Based on that measurement, the percentage of protein interacting with MYPT1 for PP1c  $\beta$  T197Q (**beta T197Q**) was calculated as a percentage of the control value for PP1c  $\beta$  plus MYPT1 of 100 percent. Represented here is the average of three experiments. Error bars represent the standard deviation.

**Figure 12: MYPT1 Binding Capability of Double and Triple PP1c Mutants**

a.

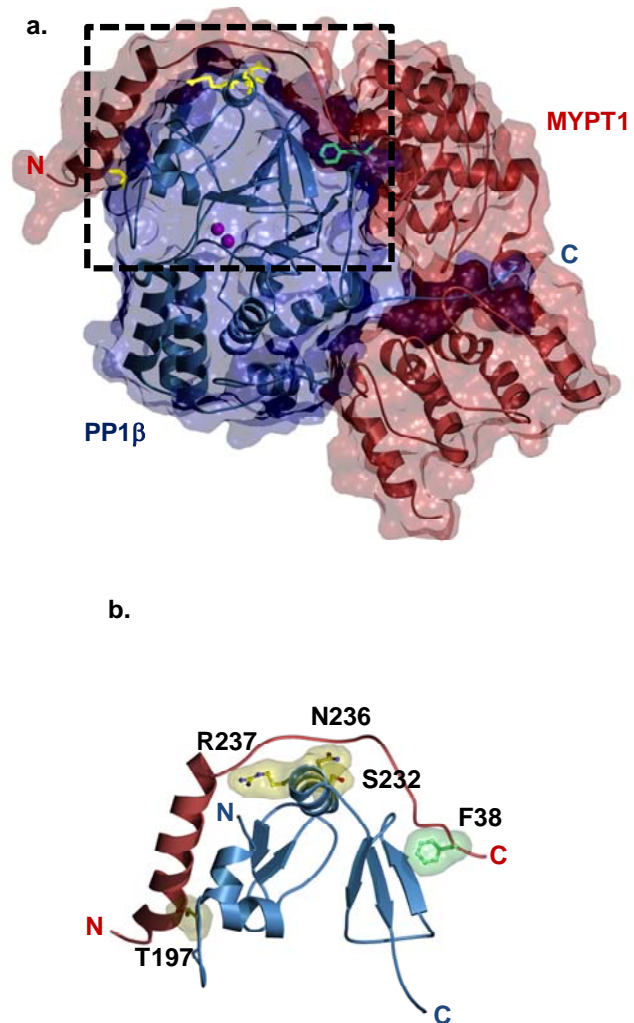


b.



**Figure II-12: MYPT1 Binding Capability of Double and Triple PP1c  $\beta$  and  $\gamma$  Mutants. a. Immunoprecipitation Results.** CHO cells were transiently transfected with plasmids for the various GFP-tagged PP1c constructs and Myc-tagged MYPT1. 48 hours later, cells were lysed and western blots were performed against the corresponding proteins using the appropriate antibodies. Immunoprecipitation assays were performed with an anti-myc antibody (Cell Signaling, Danvers, MA). Immunoprecipitate was then immunoblotted with anti-GFP antibody (abcam, Cambridge, MA). **b. Quantitation of PP1c  $\beta$  and PP1c  $\gamma$  Double and Triple Mutant MYPT1 binding.** Western blot band density was measured using the Odyssey Infrared Imaging System Software (LI-COR Biosciences, Lincoln, NE). The band density measurement for PP1c  $\beta$  plus MYPT1 (**PP1 beta**) was set at 100 percent. This represents the percentage of protein interacting with MYPT1. The percent interaction of PP1c  $\gamma$  (**PP1 gamma**) with MYPT1 was set at 0. Based on that measurement, the percentage of protein interacting with MYPT1 for the PP1c  $\beta$  and PP1c  $\gamma$  double and triple mutants was calculated as a percentage of the control value for PP1c  $\beta$  plus MYPT1 of 100 percent. Represented here is the average of at least two experiments for each construct. Error bars represent the standard deviation.

**Figure 13:** PP1c  $\beta$  Residues that Allow for Interaction with MYPT1



**Figure II-13: PP1c  $\beta$  residues that allow for interaction with MYPT1. a. Space-filling model of MYPT1 and PP1c  $\beta$  Interaction.** Residues 1-299 of MYPT1 are illustrated in red as previously published (Terrak, Kerff et al. 2004). Full-length PP1c  $\beta$  is shown in blue. Manganese ions are illustrated in magenta. The area of interest is indicated in the black box. Residues 197, 232, 236 and 237 are illustrated in yellow. Residue 38A of MYPT1 is shown in green. **b. PP1c  $\beta$  Residues 197, 232, 236 and 237 are necessary for MYPT1 binding.** Residues 197, 232, 236 and 237 are illustrated in yellow, as are the predicted van der Waal's interactions. **Molecular modeling was done in collaboration with Miguel Garcia-Diaz, Department of Pharmacological Sciences, Stony Brook University.**

### **Chapter 3: Investigation of the differential accumulation of H-Ras and K-Ras within the cell.**

#### **ABSTRACT:**

The signaling properties of H-Ras and K-Ras are redundant and currently fail to explain the preference for K-Ras mutation in cancer. Our hypothesis is that different C-terminal domains (HVRs) of H- and K-Ras are responsible for their different expression levels. Data from our lab presented here and others strongly indicates that at the protein level K-Ras is expressed at lower levels than H-Ras irrespective of the cell type, promoter or the activating mutation. I also show that differing patterns of K-Ras and H-Ras accumulation in the cell correlates with (or is dependent on) differing metabolic stability. My experimental plan included creating a mutant K-Ras in which the HVR was replaced by the HVR from H-Ras (K-Ras-H-tail, K-Ht). My data shows that this construct has a significantly higher half life when expressed within cells. Similarly, we constructed an H-Ras with the HVR region from K-Ras (H-Ras-K-tail, H-Kt) which was found to have a shorter half life when expressed in cells. Based on these data, it is concluded that the different C-terminal domains of H- and K-Ras are responsible for their different metabolic stabilities. Furthermore, I show using a retroviral infection system that K-Ras induces distinct morphological changes in when compared to H-Ras in mouse embryo fibroblasts (MEFs).

This work was done in collaboration with Natalia Jura, Bar-Sagi Lab, Stony Brook University.

## **INTRODUCTION:**

Ras proteins, which are represented by three isoforms: H-, N- and K-Ras, are small GTPases that cycle between active and inactive states. In its active, GTP-bound state, Ras mediates the signal from cell surface receptors to intracellular effector molecules. Ras proteins are critical regulators of signaling pathways that control cell proliferation and survival. In over 30% of human cancers, the activating mutation in Ras, glycine 12 to valine, has been detected. In the majority of cases, the mutation is in the splicing variant of K-Ras, K-Ras4B gene, referred to hereafter as K-Ras. The incidence of H-Ras mutation in cancer are not prevalent, however H-Ras is the most common isoform utilized in *in vitro* studies of cell transformation (Giehl 2005; Hancock and Parton 2005).

All Ras isoforms are nearly 90% homologous to one another and differ only in the hypervariable region (HVR) located at the C-terminus. At the N-terminus, there is a GTP-binding domain followed by an effector binding domain and a C-terminal tail ending in a CAAX box. The C-terminal domain of H-Ras contains two cysteine residues upstream of the CAAX box that becomes palmitoylated during processing. H-Ras is targeted to the plasma membrane through the Golgi. The C-terminal domain of K-Ras contains a polybasic region upstream of the CAAX box. K-Ras is targeted to the plasma membrane through an unknown mechanism. K-Ras is either mutated or absent in 90% of all pancreatic, colon and lung cancers. Here, I describe the targeting function for the HVR in RAS isoforms.

Additionally, I also investigated whether K-Ras and H-Ras exerted different biological functions dependent on the level of Ras signaling intensity. In primary mouse embryo fibroblasts (MEFs) high levels of oncogenic Ras have been shown to induce cell cycle arrest – senescence (Bringold and Serrano 2000). The role of K-Ras in MEFs has not been investigated in detail. Using a retroviral infection system, I have shown that K-Ras induces distinct morphological changes than H-Ras in MEFs.

Overall, the goals of these experiments included the investigation of the specific determinants of Ras stability, the determination if Ras stability is conferred within the hypervariable region (HVR), and to study the effects of oncogenic H- and K-Ras in mouse primary embryo fibroblasts (MEFs). These data will help us understand the role of Ras signaling and expression in primary cells.



## **MATERIALS AND METHODS:**

### **1. Mammalian tissue culture of CHOK1 and MEF cells.**

CHOK1 cells were cultured in Ham's F12 media supplemented with 10% fetal bovine serum (FBS) and maintained in a 5% CO<sub>2</sub> incubator. Primary mouse embryo fibroblast (MEF) cells were isolated and cultured according to standard protocol (Blat, Villaudy et al. 1994).

### **2. Transfection with Fugene Reagent.**

CHOK1 and COS-1 wells were transfected using Fugene 6 transfection reagent according to the manufacturer's protocols (Invitrogen, Carlsbad, CA).

### **3. Western Blotting techniques.**

Western Blot analysis of ectopic H-Ras (H) and K-Ras (K) expression in different cell lines was studied. Cells were transfected with equal amounts of DNA and the expression of the transgene was examined 48 hours post-transfection following standard western blotting techniques.

### **3. Pulse-Chase Analysis.**

Pulse-chase analysis of the stability of Ras proteins in COS-1 cells. COS-1 cells were transiently transfected with the H-RasV12 and K-RasV12-containing expression vectors. 24 hours post-transfection, cells were labeled with [S<sup>35</sup>]-methionine and chased for the indicated time points. The Storm Phospho Imager was used to quantitatively measure band intensity of western blots.

## **RESULTS AND DISCUSSION:**

In order to determine the expression levels of K-Ras compared to H-Ras, we conducted western blot analysis of ectopic RAS in different cell lines. In these experiments, we found that despite cell type, H-Ras is expressed at significantly higher levels than K-Ras in all cell lines tested (**Figure III-1A**).

It was then hypothesized that H-Ras had an enhanced stability compared to K-Ras which might explain this difference. To answer this question, I conducted several pulse chase experiments in COS-1 cells. Our results show that the half life of H-Ras is longer in comparison to K-Ras (**Figure III-1B**). Quantitative analysis of western blot band intensity shows curves displayed in **Figure III-1B**, which we used to determine half life of each protein. It was found that the half life of H-Ras is 36 hours whereas for K-Ras it was only 15 hours. Since one of the main differences in sequence homology between Ras isoforms lies in the hypervariable region localized at the C-terminus, we wanted to determine whether or not this region contributes to metabolic stability. A hybrid Ras protein was constructed in which the hypervariable region was swapped between H-Ras and K-Ras. These constructs were named H-Ras K-tail (H-Kt) and K-Ras H-tail (K-Ht). I expressed these isoforms in CHO-K1 cells and measured metabolic stability. These results show that when the H-Ras tail is present as is the case for K-Ras-Htail, metabolic stability is improved compared to when the K-Ras tail is present. This is shown by quantitation of western blots and time activity curves found in **Figure III-2**. From these hybrid experiments it was concluded that the HVR contains the determinants of Ras stability.

The next experiments were aimed at determining whether expression of different Ras isoforms in primary cells contributes to different morphological patterns. Different Ras isoforms were expressed in primary mouse embryo fibroblasts (MEFs) because they have been established representatives as proper examples of primary cells. Based on expression, it was found that K-Ras and H-Ras induce different morphological responses during early stages after infection. Compared to control MEFs, it was found that when H-RasV12 was expressed we observed aberrant proliferation (**Figure III-3**). These experiments show that this difference in morphology is conferred by the different intensity of Ras signaling.

Through these studies, it had been found that differential accumulation of K-Ras and H-Ras in the cell results from the difference in the metabolic stability between these two proteins. K-Ras had lower stability than H-Ras and accumulates to a significantly lower level in the cell than H-Ras.

Additionally, I discovered that the HVR region is most important for conferring metabolic stability of the two different Ras isoforms. Finally, I have shown that expression of the different Ras isoforms in primary cells caused a change in the morphological nature of the cells.

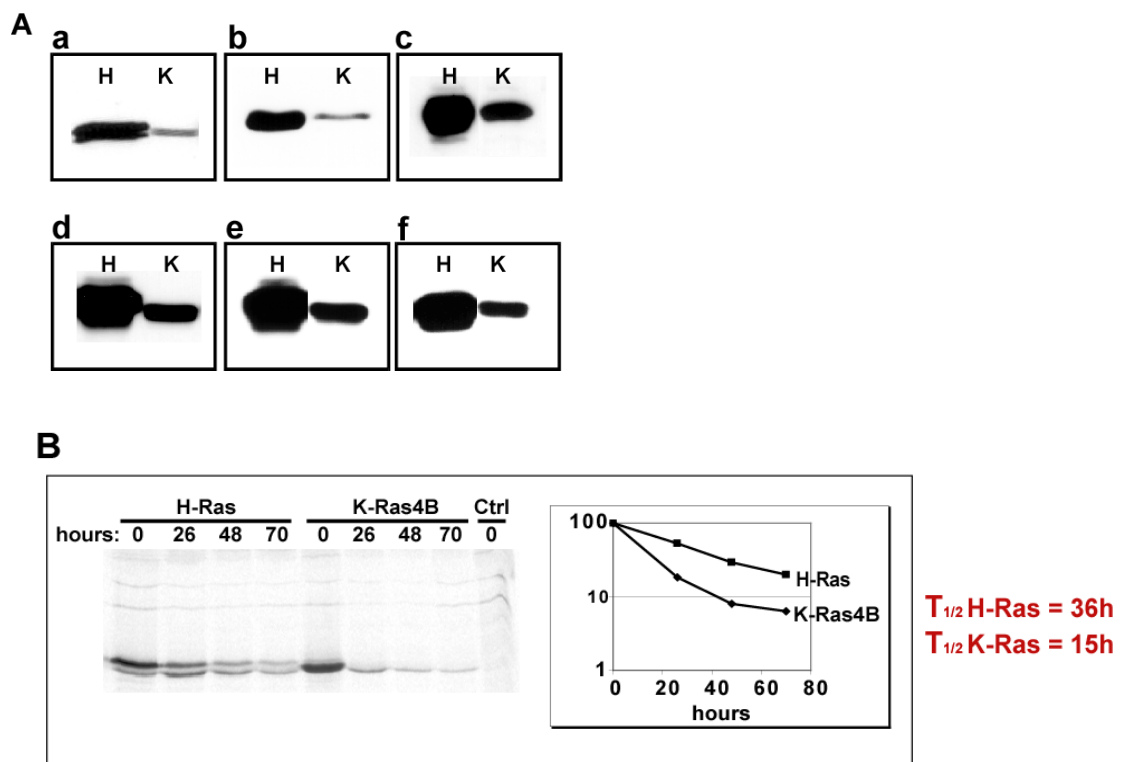
### **SUMMARY AND FUTURE DIRECTIONS:**

Only Ras protein at the plasma membrane is responsible for signaling from cell surface receptors. In order to look specifically at the membrane fraction of Ras, TritonX114 Membrane Partitioning protocol can be used. Data generated using TritonX114 partitioning has been unreliable, so other methods of membrane fractionation are being investigated.

It would also be interesting to determine the process through which H and K-Ras become differentially expressed and the biological outcomes of this difference. To address this, we would expand upon the MEF experiments by expressing different amounts of H-Ras and K-Ras and then looking at the effect on cell morphology and signaling properties.

**FIGURES:**

**Figure III-1: Expression Profiles and Metabolic Stability of H-Ras and K-Ras**



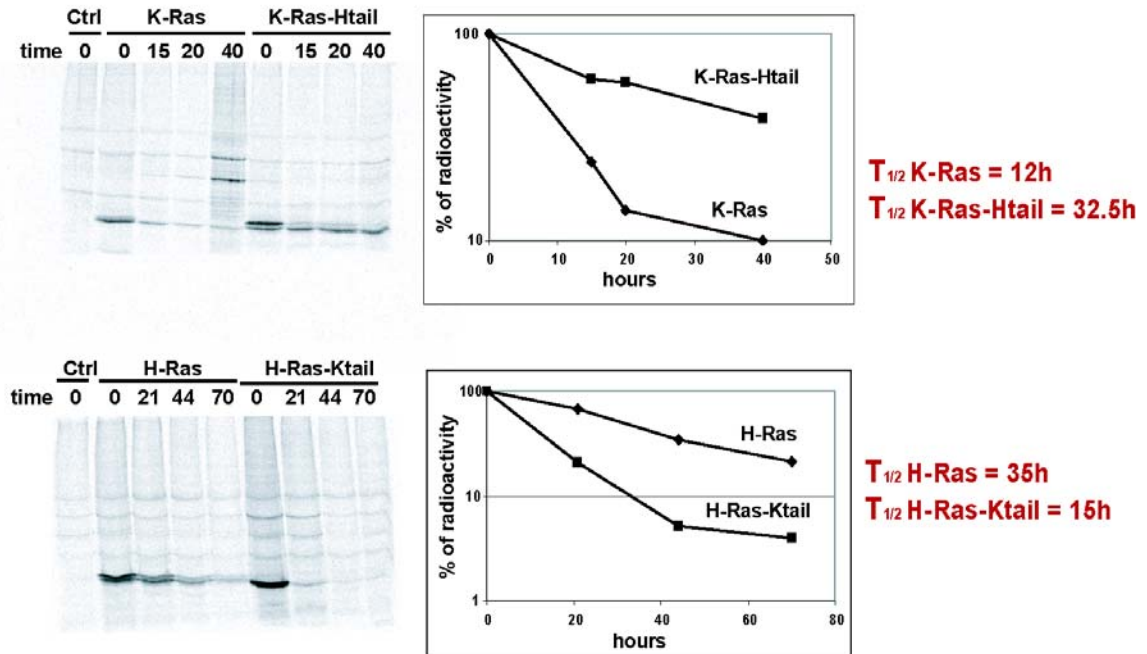
**Figure III-1: Expression Profiles and Metabolic Stability of H-Ras and K-Ras.**

**(A) K-Ras is expressed at significantly lower level than H-Ras irrespective of the cell-type, promoter or activating mutation.** Western Blot analysis of ectopic H-Ras (H) and K-Ras (K) expression in different cell lines. (a) MDA-MB-231 breast adenocarcinoma, Ras G12V mutants, CMV promoter; (b) Mouse embryonic fibroblasts p.6, Ras G12V mutants, CMV promoter; (c) HeLa cells, Ras G12V mutants, tetracycline-inducible CMV promoter; (d) CHOK1 cells, Ras G12V mutants, CMV promoter; (e) CHOK1 cells, wild-type Ras, CMV promoter; (f) Rat-1 cells, wild-type Ras, LTR promoter. Cells were transfected with equal amounts of DNA and the expression of the transgene was examined 48 hours post-transfection.

**(B) Differential accumulation of K-Ras and H-Ras in the cell is a result of the difference in their metabolic stability.** Pulse-chase analysis of the stability of Ras proteins in COS-1 cells. COS-1 cells were transiently transfected with the H-RasV12 and K-RasV12-containing expression vectors. 24 hours post-transfection, cells were labeled with [ $S^{35}$ ]-methionine and chased for the indicated time points. In the right panel – graphic representation of the data quantified with a Storm Phosphor Imager. The approximate half-life of K-Ras is 15 hours, the approximate half-life of H-Ras is 36 hours. This experiment is a representative of four independent experiments. The appearance of two bands on the pulse-chase gel reflects the presence of the processed (lower) and unprocessed (upper) form of Ras. In the case of the K-Ras isoform, separation between these two forms on the SDS-PAGE gel is less apparent than for H-Ras.

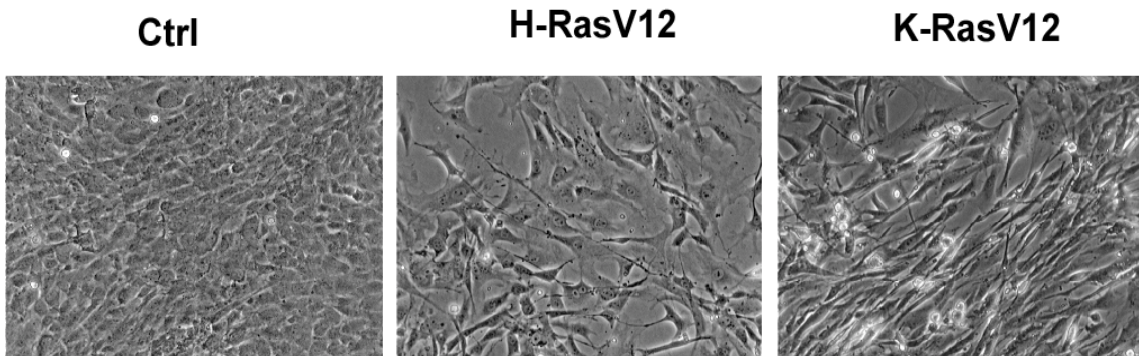
**Figure III-2: Hypervariable region contains determinants of Ras stability**

**Hypervariable region contains determinants of Ras stability**



**Figure III-2: Hypervariable region contains the determinants of Ras stability.** Pulse-chase analysis was performed to investigate whether the observed difference in expression between Ras proteins and their respective hybrids is due to the difference in their metabolic stability. CHOK-1 cells were transiently transfected with the H-RasV12, K-RasV12, H-Kt, and K-Ht-containing expression vectors. 24 hours post-transfection, cells were labeled with [<sup>35</sup>S]-methionine and chased for the indicated time points. In the panels on the right – graphic representation of the data quantified with a Storm Phosphor Imager. This experiment is representative of four independent experiments. In this experiment, the approximate half-life of K-Ras is 12 hours, and the approximate half-life of its hybrid, K-Ht is 33 hours. The approximate half-life of H-Ras is 35 hours, and the approximate half-life of its hybrid, H-Kt is 15 hours. These data strongly suggest that HVR region contains the determinants of Ras stability and by itself is sufficient to confer the metabolic stability of the protein.

**Figure III-3: Oncogenic H-Ras and K-Ras induce different morphological changes in mouse primary embryo fibroblasts (MEFs).**



**Figure III-3: Oncogenic H-Ras and K-Ras induce different morphological changes in mouse primary embryo fibroblasts (MEFs).** The initial effect of oncogenic Ras in primary cells is to induce proliferation, however this “aberrant” proliferation is not sustained and after few doublings, cells undergo permanent cell cycle arrest, termed premature senescence. We are interested in exploring whether the levels of oncogenic Ras signaling may be important for biological outcomes in primary cells. In order to check this hypothesis, MEFs passage 2, were infected with the replication-deficient retrovirus expressing vector alone (**Ctrl**) or vector encoding **H-RasV12** or **K-RasV12** together with the puromycin resistance gene. Cells were infected twice, and then selected for two days with puromycin. Our preliminary data shows that H-RasV12 induces a morphologically distinct phenotype in MEFs than K-RasV12. The pictures were captured two days after puromycin selection. This experiment is a representative of two independent experiments.



## **Chapter 4: Identification of Specific Determinants in the Cellular Localization and Regulation of Ras Ubiquitination.**

This work was based on a publication on which I was second author (Jura, Scotto-Lavino et al. 2006). My specific contributions were to Figures 1, 2 and 6.

### **INTRODUCTION:**

The Ras family of small GTPases play critical roles in several biological pathways. There are three different isoforms of Ras named HRas, NRas and KRas. Ras isoforms are nearly 90% homologous to one another, and differ only in the hypervariable region (HVR) at their C-terminus. The hypervariable region (HVR) is required for the proper trafficking and localization of Ras proteins to the plasma membrane. Ras proteins are preferentially mutated in 30% of all human cancers. H and KRas traffic and localize to different subdomains of the plasma membrane and also differentially activate downstream effector pathways of Ras (Chiu, Bivona et al. 2002; Roy, Wyse et al. 2002).

Ras proteins are essential components of signal transduction pathways that control cell proliferation, differentiation and survival. It is well recognized that the functional versatility of Ras proteins is accomplished through their differential compartmentalization, but the mechanisms that control their spatial segregation are not fully understood. Ubiquitination of membrane-associated proteins and receptors often serves to target proteins to the endocytic pathway (Finley, Sadis et al. 1994; Hicke 2001; Di Fiore, Polo et al. 2003). Recent studies in the lab have identified ubiquitination as a novel modification of HRas whose significance has not yet been determined. We have observed that HRas is subject to ubiquitin conjugation whereas KRas is not. Ubiquitin attachment to HRas modulates its ability to activate the Raf/MAPK signaling pathway. Therefore, differential ubiquitination of Ras proteins may control their location-specific signaling activities.

The overall purpose of these studies was to analyze the exact site of ubiquitin attachment to HRas, and to determine the subcellular location of HRas ubiquitination within the cell. The identity of the E3 ubiquitin ligase and the deubiquitinating enzyme (DUB) for Ras was also to be determined. In further characterizing the mechanism of Ras ubiquitination, it is our hope to understand the specific determinants in the regulation

of Ras ubiquitination, and the effects of Ras ubiquitination on the interaction of Ras with its downstream effectors and signaling.

## **BACKGROUND AND SIGNIFICANCE:**

### **The Ras family of small GTPases:**

The Ras family of small GTPases play critical roles in several biological pathways. Ras proteins cycle between an inactive GDP-bound and an active GTP-bound state. Ras proteins are essential components of signal transduction pathways that link extracellular stimuli with a diverse range of biological outcomes such as cell proliferation, differentiation and survival. Ras isoforms are nearly 90% homologous to one another, and differ only in a C-terminal domain termed the hypervariable region (HVR). The hypervariable region is composed of a membrane targeting domain and a linker domain. Both H and KRas contain a C-terminal CAAX motif that becomes farnesylated on the cysteine residue. HRas also contains two additional cysteine residues upstream of the CAAX box that become palmitoylated. This palmitoylation allows HRas to associate with the Golgi apparatus in route to the plasma membrane. KRas does not contain these cysteine residues but instead has a poly-lysine stretch upstream of the CAAX box. It is thought that this positively charged stretch of amino acids allows for electrostatic interactions of KRas with the negatively charged plasma membrane. Therefore, the hypervariable region (HVR) is required for the proper trafficking and localization of Ras proteins to the plasma membrane.

H and KRas also differentially activate downstream effector pathways of Ras. It has been shown that HRas can engage effectors on the endomembrane, not only on the plasma membrane (Chiu, Bivona et al. 2002). Inactive HRas associates with lipid rafts and caveolae, and upon activation, HRas is redistributed from rafts and caveolae to the disordered plasma membrane (Roy, Wyse et al. 2002). KRas, however, is predominantly localized to the disordered plasma membrane regardless of its activation state (Chiu, Bivona et al. 2002). It has been shown that HRas but not KRas requires endocytosis and endocytic recycling to signal through the Raf/MEK/MAPK cascade (Roy, Wyse et al. 2002). It is interesting to note that KRas is preferentially mutated in colon and pancreatic cancers, whereas HRas is infrequently mutated in human tumors. It is well recognized that the functional versatility of Ras proteins is accomplished through their differential compartmentalization, but the mechanisms that control their spatial segregation are not fully understood. Since the modification of proteins by the covalent attachment of

ubiquitin has been widely implicated in the regulation of protein trafficking (Di Fiore, Polo et al. 2003), we explored the role of ubiquitination in controlling the compartmentalization of Ras proteins.

#### **Post-translational Modification by Ubiquitination:**

Ubiquitin is a 76 amino acid protein that is conjugated to a substrate protein. Ubiquitin is attached to the lysine residue of a substrate protein through the action of three enzymatic reactions. The C-terminal glycine residue of ubiquitin is activated in an ATP-dependent manner by an ubiquitin-activating enzyme, E1. Activated ubiquitin is then transferred to an active site cysteine residue of an ubiquitin-conjugating enzyme, E2, through a thioester bond. Finally, the ubiquitin is linked to the epsilon amine group on the lysine residue of the substrate through an isopeptide bond by an ubiquitin-protein ligase, E3 enzyme.

There are three types of protein ubiquitination: monoubiquitination, multiubiquitination and polyubiquitination. Monoubiquitination is the addition of a single ubiquitin moiety to a single lysine residue on the substrate. Multiubiquitination is the addition of single ubiquitin moieties to several lysine residues on the substrate. Polyubiquitination is the addition of a polyubiquitin chain to a single lysine residue on the substrate. Polyubiquitination occurs through the addition of a ubiquitin moiety to the ubiquitin that has already been conjugated to its substrate. Polyubiquitin chains can form through three lysine residues on ubiquitin: Lys29 (K29), Lys48 (K48), and Lys63 (K63).

#### **Differential Modification of Ras Proteins by Ubiquitination:**

Ubiquitination of membrane-associated proteins and receptors often serves to target proteins to the endocytic pathway (Finley, Sadis et al. 1994; Hicke 2001; Roy, Wyse et al. 2002; Di Fiore, Polo et al. 2003). It has been shown in our lab that HRas was subject to ubiquitin conjugation whereas KRas is not ubiquitinated (**Figures IV-1 and IV-2**). Diubiquitination could arise from the conjugation of two ubiquitin moieties to a single lysine residue or through the addition of a single ubiquitin moiety to two lysines on HRas. I have shown that the diubiquitinated form of HRas is generated as a consequence of the addition of a diubiquitin chain to one lysine residue.

It is well established that the consequences of ubiquitination depend on the lysine residue that forms the isopeptide bond in the polyubiquitin chain. While K48-linked polyubiquitin chains serve as a signal for proteasome-dependent degradation, monoubiquitination is a signal for endocytosis or trafficking (Finley, Sadis et al. 1994; Hicke 2001). K63-linked polyubiquitin chains signal endocytosis, IKK activation, ribosome modification, or DNA repair (Finley, Sadis et al. 1994; Hicke 2001; Roy, Wyse et al. 2002; Di Fiore, Polo et al. 2003). A mutant form of ubiquitin, which lacks lysine 48, UbK48R, supported the formation of diubiquitinated HRas to the same extent as wild-type ubiquitin. Therefore, the diubiquitin chain on HRas is extended through lysine 63. To address this question directly, we have employed an UbK0 mutant in which lysine 63 was restored (UbK0R63K) (**Figure IV-3**). The ubiquitin mutant, UbK0, on which UbK0R63K is based, can support only monoubiquitination due to the substitution of all of its lysine residues with arginine residues (**Figure IV-3**). The extent of HRas diubiquitination in cells expressing UbK0R63K was identical to that observed in cells expressing wild-type Ub, indicating that HRas was modified by a lysine 63-linked diubiquitin chains (**Figure IV-3**).

It was proposed that the exact site of ubiquitin attachment to HRas, the subcellular location of HRas ubiquitination within the cell, and the enzymes involved in regulating Ras ubiquitination would be determined in these studies.

## **MATERIALS AND METHODS:**

### **1. Cloning of Ubiquitin and Ras Constructs**

The UbK0 mutant of ubiquitin was generated by replacing all lysines with arginines using PCR-based strategy with HA-tagged ubiquitin-containing mammalian expression vector (pCGN-Ub) as a template. The UbK0 R63K mutant of ubiquitin was generated using PCR-based strategy with pCGN-UbK0 as a template. HRas cDNA fused N-terminally to UbK48RΔG (Ub-HRas) constructs was generated by using standard polymerase chain (PCR) reaction. UbK48RΔG mutant of ubiquitin in which two C-terminal glycines were removed was used to avoid poly-ubiquitination of the fused ubiquitin and its removal by the deubiquitinating enzymes (Haglund, Sigismund et al. 2003). UbLIV-HRasV12 construct was generated by fusing N-terminally HRasV12 to UbK48RΔG mutant ubiquitin in which L8, I44 and V70 were mutated to alanines by PCR-based strategy. Fusion constructs were then subcloned into the T7-containing mammalian expression vector (pCGT). HRas8RK mutant was generated by replacing lysines 5, 42, 88, 101, 147, 167, 170 and 185 with arginines in HRasWT or HRasG12V using PCR-based strategy and subcloned into T7-tag containing expression vector (pCGT). All mutations and fusion constructs were confirmed by sequencing.

### **2. Ras immunoprecipitation and immunoblotting**

CHOK1 cells were cultured in Ham's F12 media supplemented with 10% fetal bovine serum (FBS). Cells were transiently transfected with the indicated plasmids using Fugene 6 (Roche, Basel, Switzerland). Cell lysis and immunoprecipitation of Ras with rat monoclonal anti-Ras antibody (Y13-259) was carried out as described (Corbalan-Garcia, Margarit et al. 1998). For precipitation of endogenous Ras, Y13-259 and control antibodies were cross-linked to protein A sepharose (Sigma, St. Louis, MO) precoupled to rabbit anti-rat IgG (Rockland Biosciences, Gilbertsville, PA) by using dimethyl pimelimidate\*2 HCl, DMP (Pierce) as previously described (Simanis and Lane 1985). The lysis buffer was supplemented with 3 mM N-ethylmaleimide, NEM (Sigma, St. Louis, MO) to inhibit deubiquitinating enzymes. Immunoblotting was performed using the following primary antibodies: anti-HA 12CA5 monoclonal (1:5000), anti-T7

monoclonal (Novagen, 1:10,000), anti-Ras monoclonal, clone Ras10 (Upstate 1:5000), anti-ubiquitin monoclonal, P4D1 (Santa Cruz Biotechnology, 1:1000), anti-EGFR polyclonal (Santa Cruz Biotechnology, 1:200), anti-total ERK monoclonal (Upstate, 1:1000) and anti-phosphoERK polyclonal (Cell Signaling, 1:1000). Secondary antibodies used were either goat anti-mouse (Cappel, 1:10,000) or goat anti-rabbit (Cappel, 1:5000) coupled to horseradish peroxidase.

### **3. Ras Targeting Constructs**

Ras targeting constructs were a kind gift from Chiu, V.K. et al.; *Nat. Cell Biol.* (2002); **4**: 343-350 (Chiu, Bivona et al. 2002) and Arozarena, I. et al.; *MCB* (2004); **24** (4): 1516-1530 (Arozarena, Matallanas et al. 2004).

### **4. Cellular Localization of Ras Targeting Constructs**

HTO cells were transfected with the appropriate constructs in the morning with Lipofectamine according to the manufacturer's instructions (Invitrogen, Carlsbad, CA). Approximately 6 hours following transfection, medium was changed and the cells were left overnight. In the morning of the following day, cells were fixed (3.7% formaldehyde) and stained. Immunofluorescence (IF) was performed using affinity purified anti-HA antibody.

## **RESULTS AND DISCUSSION:**

### **To determine where ubiquitination of Ras occurs within the cell:**

To determine where ubiquitination of HRas occurs within the cell, I proposed to selectively target Ras protein to cellular sites by using specific targeting motifs for certain subcellular compartments. It is important to decipher where HRas is ubiquitinated in the cell since HRas can engage effectors on both the plasma membrane and the endomembranes, including the endoplasmic reticulum (ER) and the Golgi (Chiu, Bivona et al. 2002). Ubiquitination of various proteins has been shown to take place on the plasma membrane, the Golgi apparatus, and the endoplasmic reticulum (ER) (**Figure IV-6**). It is therefore possible that ubiquitination of HRas can regulate its interaction with downstream effectors. These interactions can be dependent on the subcellular localization of ubiquitinated HRas.

The first construct to be generated is a palmitoylation-deficient HRas in which cysteines 181 and 184 will be mutated to serines (HRas C181/184S). This mutant is not retained at the plasma membrane and shuttles between the endoplasmic reticulum (ER) and cytoplasmic pools (Chiu, Bivona et al. 2002). The palmitoylation signal in HRas will then be substituted by alternative cues that would specifically direct HRas C181/184S to the desired locations. To deliver it to the ER, amino acids 1-66 of the avian infectious bronchitis virus M protein (M1) will be fused to the N-terminus of HRas C181/184S (M1-HRas C181/184S) (Swift and Machamer 1991). HRas C181/184S will be delivered to the Golgi complex by fusing it N-terminally to the KDEL receptor (KDELr) (Caloca, Zugaza et al. 2003). Due to the fact that the KDELr is a constantly moving protein that recycles back to the ER, an N193D mutation will be introduced which prevents the protein from redistributing to the ER and renders it a resident Golgi protein (KDELr-HRas C181/184S) (Cole, Smith et al. 1996). Please note that all of the above constructs will include an HA-tag to enable the detection of these proteins. Before use of these constructs, cellular localization must be confirmed using immunofluorescence and biochemical fractionation.

Once these constructs are generated, I planned to co-express them in CHOK1 cells with ubiquitin and test if these targeted Ras proteins become ubiquitinated using



immunoprecipitation assays. I also planned to target ubiquitination-deficient HRas to these cellular sites and compare its ability to become ubiquitinated with wild-type HRas. Expression of these constructs will be confirmed by western blot analysis as well as with immunofluorescence studies in which expression in the proper subcellular compartment will be tested with compartment markers. I plan to use the ER marker calreticulin (Calbiochem, San Diego, CA), the Golgi marker giantin (Calbiochem, San Diego, CA), and Rab5 (BD Biosciences Pharmingen, San Diego, CA) as a marker for endosomal compartments.

After thorough research of the literature, I started generating Ras targeting constructs based on the addition of short peptide sequences N-terminal to HRas that drive the targeting of the tagged protein to specific cellular locations (**Table 2**). This work proved unfruitful as the subcellular localization of these constructs was difficult to define in the COS-1 cell line under several different conditions. These short peptide targeting sequences were not efficient at targeting and trapping HRas within specific subcellular locations. The following constructs were requested and obtained from Dr Piero Crespo, Ph.D. (Instituto de Investigaciones Biomedicas, Consejo Superior de Investigaciones Cientificas (CSIC), Departamento de Biologia Molecular, Spain): M1-H-Ras SS (ER localized), KDELr-H-Ras SS (Golgi localized), and CD8-H-Ras SS (bulk plasma membrane localized) HA-tagged constructs (Table 3). Once received, the constructs were PEG prepped. I also looked at the subcellular localization of HRas V12 C181/184S (ER), HRas C181S (Golgi), HRas C184S (PM) (**Table 4**). These Ras constructs were also inefficient in targeting Ras to specific subcellular locations.

In July 2005, I started studying the effect of the E2 ubiquitin conjugating enzyme Ubc13 on Lysine63-linked Ras ubiquitination. Ubc13 has been identified as an E2 ubiquitin conjugating enzyme as part of a complex that is required for Lysine63-linked polyubiquitin chain assembly (Deng, Wang et al. 2000). It has been shown that TRAF6 (TNF receptor associated factor 6), a RING domain protein, functions together with Ubc13 to synthesize Lysine-63 linked polyubiquitin chains in the regulation of the NF- $\kappa$ B pathway (Deng, Wang et al. 2000). TRAF6 activates I $\kappa$ B kinase (IKK) in response to inflammatory cytokines through the assembly of Lys63-linked polyubiquitin chains (Deng, Wang et al. 2000).

In October 2005 the E2-enzyme UbcH7 and E3 Ub-ligase TRAF6 were shown to be required for the regulation of nerve growth factor (NGF) signaling through the stable formation of Lysine-63 linked polyubiquitin chains on the NGF receptor TrkA (Geetha, Jiang et al. 2005). In this instance, the formation of Lysine63-linked polyubiquitin chains on the TrkA receptor directs internalization of the activated receptor and subsequent signaling (Geetha, Jiang et al. 2005). During this time frame, I performed several experiments using Ubc13, dominant negative Ubc13 (Ubc13 C87A), UbcH7, and TRAF6. The co-expression of the Ubc13, Ubc13 C87A, or TRAF6 in CHOK1 with both HRas and ubiquitin had no effect on the ubiquitination status of HRas in immunoprecipitation assays with Y13-259 anti-Ras monoclonal antibody.

In early November, we received reviewer comments and revisions for our Molecular Cell manuscript entitled “*Differential Modification of Ras Proteins by Ubiquitination*” (Jura, Scotto-Lavino et al. 2006) which had been submitted in mid-October 2005. I mostly worked on revisions for the paper. The data presented in this paper was the Doctoral Dissertation work of a fellow lab mate, Natalia Jura, and was to be the basis of my work. In the paper, a Ub-HRas fusion protein was shown to trap HRas within endocytic vesicles (Jura, Scotto-Lavino et al. 2006). This Ub-HRas fusion protein was less efficient than wild type HRas in activating the ERK cascade and illustrated a decreased capacity to recruit Raf to the plasma membrane (Jura, Scotto-Lavino et al. 2006). It was suggested that the change in the signaling potential of Ub-HRas could be a result of the contortion of the HRas molecule by the fused ubiquitin moiety, and not a consequence of the targeting effect of ubiquitin. To address this question, I generated a fusion protein in which a ubiquitin moiety containing L8A, I44A and V70A substitutions was fused N-terminally to HRasV12 (UbLIV-HRasV12). These residues have been shown to be critical for the interactions of ubiquitin with ubiquitin-binding domains within proteins that control ubiquitin-dependent trafficking along the endocytic pathway (Swanson, Kang et al. 2003). The cloning of this construct proved difficult and required much time. Once the construct was made, I was able to show using IF studies that UbLIV-HRas escapes trapping in endocytic vesicles and regains the ability to activate ERK (Jura, Scotto-Lavino et al. 2006). This indicates that the change in signaling potential of Ub-HRas is not a result of the contortion of the HRas molecule by the fused

ubiquitin moiety, but rather a consequence of the targeting effect of ubiquitin. These data further support the idea that the signaling capacity of HRas can be regulated by ubiquitin-dependent trafficking.

Once the revised paper was submitted, I started indirect immunofluorescence (IF) experiments with the constructs acquired earlier. I first performed assays in CHOK1 and COS-1 cell lines. At this point, it was decided to focus on the Golgi-targeted HRas construct (KDELr-HA-HRas SS). As described in the paper, the ubiquitination-deficient HRas construct (HRas 8rk) had been shown to associate with the Golgi apparatus at an increased level when compared to wild type HRas and the ubiquitin HRas fusion construct (Ub-HRas) (Jura, Scotto-Lavino et al. 2006).

Thus far I have completed indirect immunofluorescence experiments in CHOK1, COS-1, HeLa, HTO and HEK 293 cell lines using both anti-Ras and affinity-purified anti-HA antibodies. From these studies, I decided to use affinity-purified anti-HA antibody for IF experiments since the anti-Ras antibody yielded a high level of background fluorescence. I have selected either HeLa or HTO cell lines to use in these assays due to high level of colocalization of the KDELr-HA-HRas SS construct with YFP- $\beta$ 1,4-galactosidase (trans-Golgi marker) in these cell lines (**Figure IV-7**). Using the KDEL-HA-HRas-SS construct, it is very clear that it colocalizes in the Golgi with the Golgi marker YFP- $\beta$ 1,4-galactosidase. In addition, immunoprecipitation assays with Y13-259 anti-Ras monoclonal antibody in CHOK1 cells yielded a strange polyubiquitination pattern of KDELr-HA-HRas SS (**Figure IV-8**). This could be due to high levels of expression of the protein, therefore I wanted to use lower expression levels in HeLa or HTO cells where co-localization of KDELr-HA-HRas and YFP- $\beta$ 1,4-galactosidase were very high.

I also tried to complete immunoprecipitation assays with Y13-259 anti-Ras monoclonal antibody in HTO cells. Unfortunately, when using lower levels of protein, I am unable to detect ubiquitination of wild-type HRas (positive control). These experiments were repeated using DNA concentrations that yielded acceptable levels of protein expression in CHOK1 cells. Additional controls in these experiments included: KDELr fused to pCGN to ensure that the receptor itself is not being ubiquitinated and, KDELr fused to HRas8rk C181/184S to examine the effect of targeting Ub-deficient Ras

to the Golgi on its ubiquitination capacity. I cloned these two additional controls. Once ubiquitination is established in these experiments, I planned to use Ub-HIS pulldown assays to confirm that these constructs were ubiquitinated. I planned to continue using these Ras targeting constructs to examine the effects of Ras localization on the activation of several downstream effectors of Ras.

## **SUMMARY AND FUTURE DIRECTIONS:**

### **I. To determine the site of Ras-ubiquitination:**

In order to further understand the molecular mechanism of Ras ubiquitination, it is necessary to determine the exact site of ubiquitin attachment to Ras. There are three lysine residues located in the hypervariable region (HVR) of HRas: lysine 167, 170 and 185. When all three lysine residues are mutated to arginine via site-directed mutagenesis (HRas 3R), this mutant is capable of being ubiquitinated in a pattern similar to wild-type HRas (**Figure IV-4**). In this series of experiments, the exact site of ubiquitin attachment to Ras will be determined using mass spectrometry (MS). Mass spectrometry based proteomics has allowed for the identification of ubiquitinated proteins, the elucidation of ubiquitin-modification sites, and the determination of polyubiquitin chain linkages (Kirkpatrick, Denison et al. 2005). The sites of ubiquitination can be identified using mass spectrometry, by the fact that isopeptide-linked ubiquitin can be cleaved by trypsin at the junction between Arg 74 and Gly 75, producing a –GG signature peptide (**Figure IV-3**) (Kirkpatrick, Denison et al. 2005). This signature peptide has a mass shift at the lysine residue of 114.1 Da as well as a missed proteolytic cleavage due to the fact that trypsin proteolysis cannot occur at the modified lysines (Peng, Schwartz et al. 2003). The site of ubiquitination on Ras will then be confirmed using site-directed mutagenesis and immunoprecipitation assays.

### **A. To determine the site of Ras ubiquitination using Mass Spectroscopy:**

Previous studies in our lab have shown that the di-ubiquitination of HRas occurs through a lysine 63 linked di-ubiquitin chain on HRas (**Figure IV-3**). We have been able to abolish this ubiquitination pattern by generating an ubiquitination deficient mutant of HRas (HRas8RK) (**Figure IV-5**) (Natalia Jura, Bar-Sagi Lab). All solvent exposed lysine residues as well as lysine residues found within the hypervariable region (HVR) of HRas were mutated to arginine via site-directed mutagenesis. Although deficient in its ability to become ubiquitinated, this mutant does not allow us to determine the exact site of ubiquitination on HRas. To perform this task, I propose to analyze ubiquitinated HRas protein by mass spectrometry (MS).

The protein of interest will be purified first for the purpose of analysis by mass spectrometry (MS). In order to purify ubiquitinated HRas I plan to use an affinity

purification approach. CHOK1 cells will be transfected using Fugene 6 Transfection Reagent (Roche Applied Science, Indianapolis, IN) with HA-tagged HRas (HA-HRas) and Flag-tagged ubiquitin (Flag-UbK0R63K) according to the manufacturer's protocol. Ras conjugates will then be purified by affinity chromatography. Cell lysates will be incubated with 12CA5 antibody-coupled protein A-Sepharose. Ras proteins will then be eluted by competition with HA-peptide. An aliquot of eluted Ras proteins will be analyzed for both HRas and ubiquitin expression via western blot analysis.

This sample will then be subjected to SDS-PAGE and visualized by silver staining. Prominent bands, including those migrating at approximately ~15 kDa and ~36 kDa (mono- and di-ubiquitinated forms of HRas), will be isolated. These bands will then be directly proteolyzed with trypsin and the sample will be sent to the mass spectrometry (MS) facility at the Stony Brook Proteomics Center for analysis.

Trypsin digestion will cleave proteins after every lysine (K) and arginine (R) residue. Since the minimum size protein fragment required for mass spectrometry (MS) is approximately eight residues long (Peng, Schwartz et al. 2003), this technique may not work for lysine residues K101 and K104 of HRas since they are only three residues apart. Therefore alternative enzymes can be used for digestion to generate longer signature peptides (Kirkpatrick, Denison et al. 2005).

**B. To mutate our ubiquitination deficient HRas back to a HRas protein that is capable of being ubiquitinated and function like wild-type HRas:**

Based on the mass spectrometry (MS) data attained, the lysine residue on which ubiquitin is attached to HRas will be mutated from an arginine back to a lysine residue in the ubiquitination deficient mutant of HRas (HRas8RK). This "reverse mutation" (arginine to lysine) will be made using a PCR-based site-directed mutagenesis approach. All mutations will be confirmed by DNA sequencing.

This construct (HRas7RK) will then be tested for ubiquitination capacity using an immunoprecipitation assay. CHOK1 cells will be plated onto 60 mm plates at 90% confluence, and transfected using Fugene 6 Transfection Reagent (Roche Applied Science, Indianapolis, IN) with each expression plasmid according to the manufacturer's protocol. Both T7-tagged HRas7RK (T7-HRas7RK) and HA-tagged ubiquitin (HA-Ub) will be expressed for 24 hours. After a 24 hour incubation period, the cells will be lysed

in immunoprecipitation lysis buffer and lysates will be immunoprecipitated with a monoclonal anti-Ras antibody (Y13-259). Immunoprecipitates will then be analyzed using western blot analysis. Ubiquitinated HRas protein will be detected using anti-HA monoclonal antibody.

There are some difficulties with using this approach. First, there is the possibility that restoring the single lysine residue at the site responsible for HRas ubiquitination will not restore the ubiquitination capacity of HRas8RK. If this is the case, individual mutations of each arginine residue in HRas8RK back to lysine will be made until ubiquitination capacity is restored.

Next, the functional capability of HRas7RK will be tested using ERK activation assays. Ubiquitination-deficient HRas protein activates the ERK cascade to a greater extent than wild-type HRas. Our HRas RL protein should activate ERK to a similar extent as wild-type HRas. CHOK1 cells will be cotransfected with Ras and ERK constructs and the activation of immunoprecipitated ERK will be assessed by immunoblotting with anti-phospho-ERK antibodies.

As an alternative approach to determine the site of Ras ubiquitination I would take the following approach: to mutate the arginine residues in the ubiquitination-deficient HRas (HRas8rk) back to lysine residues and test these constructs for their ability to become ubiquitinated. Once the site of Ras ubiquitination is identified, I suggested to compare the effects of wild-type and mutated Ras on the activation of the downstream effector of Ras, ERK. Suggestions were made to work at the endogenous protein level and to assay the activation of several downstream Ras effectors as a read out for Ras activity when it is ubiquitinated. To test that, I plan to look at both PI3K and p38 activation.

## **II. To determine where ubiquitination of Ras occurs within the cell:**

Ubiquitination of membrane proteins and receptors has been shown to occur at the plasma membrane (Finley, Sadis et al. 1994; Hicke 2001; Di Fiore, Polo et al. 2003), Golgi apparatus (Hicke and Dunn 2003), and the endoplasmic reticulum (ER) (Hicke and Dunn 2003). This ubiquitination serves an important role in the internalization and targeting of these proteins to the endocytic pathway (Finley, Sadis et al. 1994; Hicke 2001; Di Fiore, Polo et al. 2003). The subcellular location of Ras ubiquitination within the cell has yet to be determined. In these series of experiments, Ras will be tethered to

different subcellular compartments using different targeting motifs. Dependent upon the ability of HRas to become ubiquitinated at the Golgi or endoplasmic reticulum (ER), sucrose flotation gradient experiments will be performed to further characterize the subcellular site of Ras ubiquitination. The ability of HRas at different subcellular compartments to be ubiquitinated will be analyzed using both biochemical and immunofluorescence approaches including ubiquitin-mediated fluorescence complementation (UbFC) assays.

**A. Biochemical fractionation using sucrose flotation gradients:**

If ubiquitination does not occur to HRas that has been selectively tethered to the Golgi or to the ER, then one can propose that Ras ubiquitination occurs at the plasma membrane. To determine the fraction of the plasma membrane where HRas ubiquitination occurs, sucrose flotation gradients of lysates from cells expressing both HRas and ubiquitin can be used. Since inactive HRas associates with lipid rafts and caveolae, and upon activation, HRas is redistributed to the disordered plasma membrane, it is important to differentiate between these components of the plasma membrane (Roy, Wyse et al. 2002). If HRas ubiquitination occurs within the disordered plasma membrane where active HRas resides, it is possible that ubiquitination is a novel mechanism for regulating the activation of downstream effector pathways of Ras. BHK cells will be plated onto 10 cm plates at 50% confluence, and transfected using Lipofectamine (Invitrogen Corporation, Carlsbad, CA) with 2-15  $\mu\text{g}$  of each expression plasmid according to the manufacturer's protocol. I planned to use three 10 cm plates per experimental condition. After overnight incubation, cells will be processed for biochemical analysis using sucrose flotation gradients.

Sucrose flotation gradients will be performed as described in Prior, I.A. et al. (Prior, Harding et al. 2001). For sucrose flotation gradients, BHK cells will be gathered in PBS, centrifuged and resuspended in 0.5 M  $\text{Na}_2\text{CO}_3$ . After homogenization through a 23-gauge needle and sonication, lysates were mixed with an equal volume of 90% sucrose in MES-buffered saline (MBS; 25 mM MES, pH 6.5, 150 mM NaCl). Next, 1 mL of 45% sucrose/lysates will be sequentially overlaid with 1.2 mL of 35% sucrose, 1 mL 30% sucrose, 1 mL 25% sucrose, and 1 mL 5% sucrose. The gradient will then be centrifuged in a Beckman SW-55 rotor for 16 hours at 48,000 rpm. Following centrifugation, 10 0.4



mL fractions will be collected from the top of the gradient and diluted into 1 mL MBS. Protein content will then be measured using the Bradford reaction, and the diluted fractions will be re-centrifuged at 100,000 g for 30 minutes. Membrane pellets will then be resuspended directly into SDS-PAGE sample buffer for western blot analysis.

In order to confirm that the sucrose gradient is separating cellular compartments properly, gradient fractions will be immunoblotted with HRas isoform-specific antisera (Santa Cruz Biotechnology, Santa Cruz, CA) and the following membrane markers. As a lipid raft marker, I plan to use glycosyl phosphatidyl (GPI)-anchored placental alkaline phosphatase (PLAP) (Dako Corporation, Carpinteria, CA), a protein which is localized to lipid rafts. Caveolin will be used as a marker for caveolae (BD Biosciences Pharmingen, San Diego, CA). As a non-raft plasma membrane marker, I plan to use an antibody against Na<sup>+</sup>/K<sup>+</sup>-ATPase (BD Biosciences Pharmingen, San Diego, CA).

**B. To determine the site of Ras ubiquitination in the cell using ubiquitin-mediated fluorescence complementation (UbFC):**

In addition to the above experiments, ubiquitin-mediated fluorescence complementation (UbFC) assays was planned. This approach is based upon the complementation of two nonfluorescent fragments of the yellow fluorescent protein (YFP) when they are brought together by interactions between ubiquitin and a substrate protein (in this case, HRas) fused to each fragment (Fang and Kerppola 2004). The UbFC strategy enables simultaneous visualization of proteins modified by ubiquitin peptides and comparison of their effects on protein localization. In order to proceed with this approach, several constructs will need to be developed. The N-terminal fragment of the yellow fluorescent protein (YFP) and a linker region will be fused to the N-terminus of ubiquitin. This linker region will allow complementation with the other portion of YFP. The complementary fragment of YFP will be fused separately to the N-terminus of HRas and HRas 8rk. During observation by fluorescence, only Ras protein that has become ubiquitinated will be visualized using the YFP channel due to complementation of the two fragments of YFP. All constructs will be confirmed by DNA sequencing.

COS-1 cells will be plated onto glass coverslips at 80% confluence, and transfected using Fugene 6 Transfection Reagent (Roche Applied Science, Indianapolis, IN) with expression plasmids encoding the indicated combinations of fusion proteins according to

the manufacturer's protocol. Fluorescence images will be collected by confocal microscopy. Subcellular localization of ubiquitinated HRas protein will be confirmed with the subcellular compartment markers used in Specific Aim 2A. In addition, anti-EEA1 antibody (BD Biosciences Pharmingen, San Diego, CA) will be used as a marker for early endosomal compartments.

As an alternative to ubiquitin-mediated fluorescence conjugation (UbFC), I proposed to use fluorescence resonance energy transfer (FRET). Interactions between two proteins can be imaged by detecting fluorescence resonance energy transfer (FRET) between donor and acceptor fluorophores. FRET involves the transfer of energy from a fluorescent donor in its excited state to another excitable moiety, the acceptor, by a nonradiative dipole-dipole interaction (Gordon, Berry et al. 1998). FRET requires that the donor be fluorescent and have a long half-life, the transfer does not involve the actual resorption of light by the acceptor, the donor molecule's fluorescence emission spectrum overlaps the excitation spectrum of the acceptor molecule, and the distance between the donor and acceptor molecules is small (1-10 nm) (Gordon, Berry et al. 1998). The dependence of the energy transfer efficiency on the distance between donor and acceptor provides the basis for the use of this technique in the study of sub-cellular protein interactions.

COS-1 cells will be plated onto glass bottom culture plates at 80% confluence and transiently transfected with CFP fused N-terminal to HRas (CFP-HRas) and YFP fused N-terminal to ubiquitin (YFP-Ub) using Fugene 6 Transfection Reagent (Roche Applied Science, Indianapolis, IN). Expression of CFP- and YFP-fused proteins will be confirmed by western blotting. FRET will be detected by exciting CFP-HRas with a light of wavelength corresponding to the absorption spectrum of the donor (CFP) and detecting light emitted at the wavelengths corresponding to the emission spectrum of the acceptor (YFP-Ub) (Gordon, Berry et al. 1998). After 24 hours, FRET measurements and imaging will be acquired sequentially using YFP and CFP settings. FRET will be analyzed as sensitized acceptor emission by excitation at 458 nm with an Argon laser and the detection of emissions, limited by a 560 nm filter (Chiu, Bivona et al. 2002). FRET will be quantified by excitation at 458 nm and then by determining the ratio of sensitized

acceptor emission (>560 nm) over quenched donor emission (<475) (Gordon, Berry et al. 1998; Chiu, Bivona et al. 2002).

### **III. To identify the ubiquitination machinery required for the ubiquitination of HRas:**

In order to understand the mechanism by which Ras is ubiquitinated, the fate of ubiquitinated Ras, and the regulation of Ras ubiquitination, it is essential to know what enzymes are involved. In this series of experiments, the E3 ubiquitin ligase and deubiquitinating enzyme (DUB) for Ras will be identified. Similar to Ras, E3 ubiquitin ligases have been shown to be key mediators of tumorigenesis (Ohta and Fukuda 2004; Beckmann, Maurer et al. 2005). Correlations between alterations in ubiquitination processes and oncogenesis have also been documented (Yang, Li et al. 2004; Zhang, Wang et al. 2004). Due to the large number of E3 ubiquitin ligases, their enzymatic nature, and their specific substrate recognition, E3 ubiquitin ligases can be used as possible therapeutic targets (Burger and Seth 2004). E3 ubiquitin ligases could also serve as baits for the identification of additional cancer genes through their interactions. Therefore, E3 ubiquitin ligase genes can serve as targets for the design of novel therapies (Weissman 2001; Ohta and Fukuda 2004). It is our hope that in understanding the enzymes that regulate the ubiquitination of Ras, we will be able to further understand this newly discovered mechanism of Ras regulation within the cell.

#### **A. To identify the E3 ubiquitin ligase for HRas:**

The enzyme family of E3 ubiquitin ligases can be divided into two separate classes: HECT-type and RING-type families. HECT domain E3s form thiolester intermediates with ubiquitin as part of the process, leading to ubiquitination of substrates (HECT domain stands for homologous to E6-AP carboxyl terminus, E6-AP being the founding member of this family) (Weissman 2001). Members of the other class, RING FINGER E3s, are now believed to mediate the direct transfer of ubiquitin from E2 to substrate.

In order to identify the E3 ubiquitin ligase for Ras, we currently plan to study several previously identified E3 ubiquitin ligases. The ligases to be analyzed include IMP, Smurf-1 and Ubc13. The protein IMP (Impedes Mitogenic signal Propagation), is an E3 ubiquitin ligase that binds Ras and modulates MAP kinase signaling (Matheny, Chen et al. 2004). Smurf-1 is a Smad1 ubiquitin ligase that has been shown to suppress the

osteogenic activity of osteoblasts through MEKK2 degradation (Yamashita, Ying et al. 2005). We will also study the E2 ubiquitin conjugating enzyme Ubc13, which has been shown to catalyze the formation of lysine63-linked polyubiquitin chains (Hofmann and Pickart 1999).

To identify the E3 ubiquitin ligase for Ras, I propose to perform a biochemical reconstitution assay to isolate Ras-containing protein complexes from human cells (Chen, Kon et al. 2005; Zhong, Gao et al. 2005). This method has been used successfully for the identification of the E3 ubiquitin ligase Mule, required for the degradation of Mcl-1, an anti-apoptotic Bcl-2 family member (Chen, Kon et al. 2005). Cell lysates from HeLa cells stably expressing HRas or HRas8RK (Specific Aim 3A) will be fractionated through an ion exchange Q-Sepharose column into four fractions: Flow through (QFT), proteins bound to the column and eluted at 150 mM NaCl (Q15), 300 mM NaCl (Q30), and 1 M NaCl (Q100) (Chen, Kon et al. 2005). Aliquots from all four fractions, or without QFT, Q30, or Q100 will be incubated with an aliquot of methyl-ubiquitin in the presence of HA-HRas at 37°C for one hour (Chen, Kon et al. 2005). After terminating the reactions with SDS sample buffer, reaction products will be fractionated by SDS-PAGE and analyzed by western blotting with anti-HA antibody. The fraction that contains the E3 ubiquitin ligase for Ras will not promote HRas ubiquitination when removed from the reaction mixture. This method is based on a similar reconstitution approach showing that the majority of E2 activity is present in the QFT, while the E1 resides in the Q30 fraction (Hershko, Heller et al. 1983). Therefore, the E3 ubiquitin ligase will be should be in the Q100 fraction. When added back to the reaction mixture, an aliquot of the Q100 fraction should restore HRas ubiquitination capacity (Zhong, Gao et al. 2005). The Q100 fraction will be fractionated by SDS-PAGE and visualized by silver staining. Prominent bands will then be isolated from the gel and identified via peptide sequencing by mass spectrometry (MS). Sequence analysis will then be performed and homology to E3 ubiquitin ligase domains similar to HECT-domain or RING finger-domain motifs (C2, WW, or HECT domains etc.) will be analyzed. The HECT domain (~350 amino acids) contains a cysteine residue that forms a catalytic thiolester with ubiquitin and is essential for the enzymatic activity of HECT proteins.

Any E3 ubiquitin ligase-like proteins that are identified from the above assays will be subjected to *in vitro* assays to confirm that these E3 ubiquitin ligase like proteins interact with HRas. *In vitro* assays will include immunoprecipitation assays with anti-Ras monoclonal antibody (Y13-259) as described. In addition, *in vitro* ubiquitination assays (Chen, Kon et al. 2005) will be performed. In a fifteen  $\mu\text{L}$  reaction, 200 ng of recombinant HA-HRas will be incubated with ATP regenerating system (50 mM Tris [pH 7.6], 5 mM  $\text{MgCl}_2$ , 2 mM ATP, 10 mM creatinine phosphate, 3.5 U/mL creatinine kinase), 10  $\mu\text{g}$  of methyl-ubiquitin, 10 ng human E1, 100 ng recombinant E2, 2  $\mu\text{M}$  ubiquitin aldehyde, and 10  $\mu\text{g}$  of the potential E3 ubiquitin ligase at 37°C for one hour. After terminating the reactions with SDS sample buffer, reaction products will be fractionated by SDS-PAGE and analyzed by western blotting with anti-HA antibody.

**B. To identify the deubiquitinating enzyme (DUB) for Ras:**

To identify the deubiquitinating enzyme for Ras, I plan to use an RNA interference (RNAi) library for 55 human deubiquitinating enzymes that recently became available (Brummelkamp, Nijman et al. 2003; Nijman, Huang et al. 2005). This RNA interference library was originally generated to study and identify deubiquitinating enzymes in cancer-relevant pathways (Hershko, Heller et al. 1983). The library consists of four independent shRNA (short hairpin RNA)-encoding plasmids targeting each of fifty-five DUBs for suppression by RNA interference (Brummelkamp, Nijman et al. 2003). In essence, we would like to find an enzyme that causes a decrease in Ras monoubiquitination or an enzyme that through its knockdown causes an increase in Ras ubiquitination.

Each pool of DUB knockdown vectors will be separately electroporated into a tetracycline-inducible HeLa stable cell line that has been induced to overexpress HA-HRas. Cells will then be selected for shRNA expression with puromycin (Hershko, Heller et al. 1983). Seventy-two hours after transfection, whole-cell lysates will be prepared and analyzed by western blotting with a monoclonal anti-HA antibody for HRas detection.

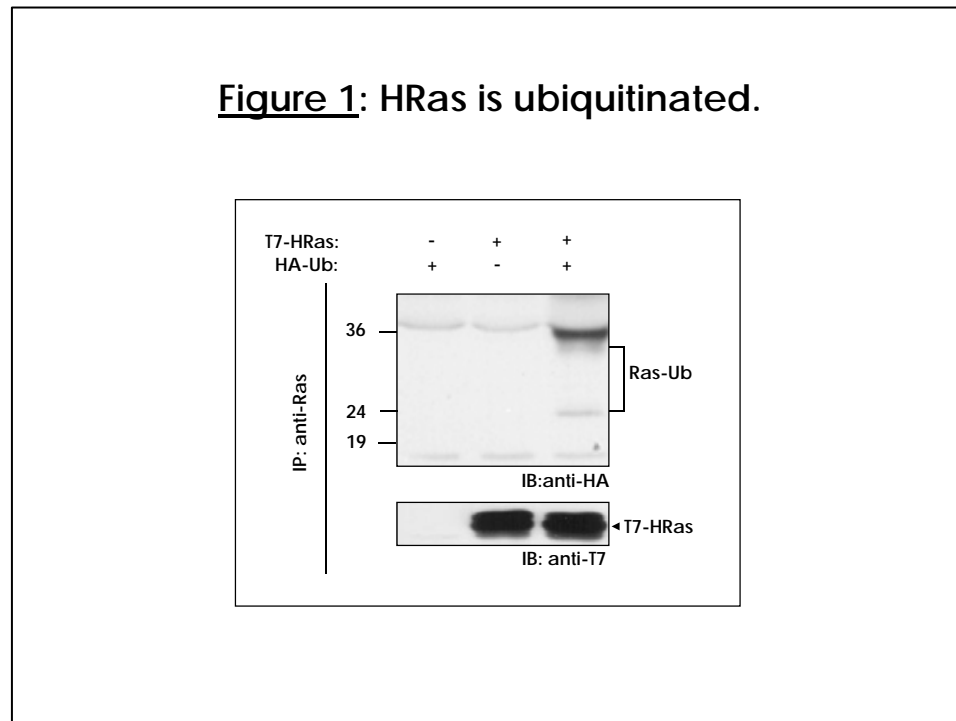
Any deubiquitination enzyme (DUB) identified through this initial screen will be further characterized as indicated below. First, the four independent shRNA vectors present in the original pool will be tested for their ability to induce accumulation of

ubiquitinated HRas (Brummelkamp, Nijman et al. 2003). This will indicate the potency of the vectors to induce accumulation of ubiquitinated HRas. Secondly, to ensure that the deubiquitination enzyme for Ras is indeed inhibited by the knockdown vectors, CHOK1 cells will be cotransfected with the four shRNA vectors and an expression vector containing a green fluorescent protein (GFP) tagged version of the identified deubiquitination enzyme for HRas (Brummelkamp, Nijman et al. 2003).

Upon identification, the deubiquitination enzyme for Ras will be isolated, cloned by RT-PCR and inserted into the pCGN vector. To confirm the function of the deubiquitination enzyme identified, this construct will then be overexpressed in CHOK1 cells with T7-tagged HRas (T7-HRas) and HA-tagged ubiquitin (HA-Ub). After a 24 hour incubation period, the cells will be lysed in an immunoprecipitation lysis buffer and lysates will be immunoprecipitated with a monoclonal anti-Ras antibody (Y13-259). Immunoprecipitates will then be analyzed using western blot analysis. Ubiquitinated HRas protein will be detected using anti-HA monoclonal antibody. Upon expression of the identified deubiquitination enzyme in cells with HRas, one would predict to see a decrease in ubiquitinated HRas protein.

Once deubiquitination activity has been confirmed, I will test the effects of deubiquitination on Ras signaling. The signaling capacity of deubiquitinated HRas will be tested using ERK activation assays. CHOK1 cells will be cotransfected with HRas, the deubiquitination enzyme, and ERK constructs and the activation of immunoprecipitated ERK will be assessed by immunoblotting with anti-phospho-ERK antibodies.

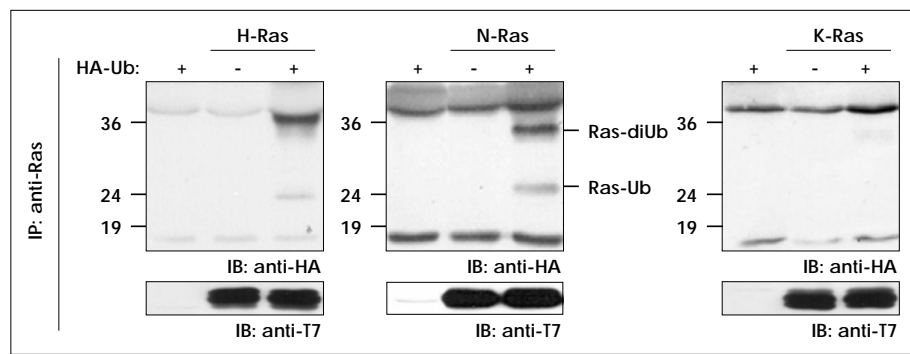
**FIGURES:**



**Figure IV-1: HRas is ubiquitinated.**

HRas undergoes mono- and diubiquitination *in vivo*. Lysates from CHOK1 cells expressing T7-HRas and HA-ubiquitin (HA-Ub) alone or in combination were subjected to Ras immunoprecipitation (IP) followed by immunoblotting (IB) with the indicated antibodies. The ubiquitinated forms of T7-HRas migrated ~ 5 kDa and 15 kDa above the unmodified T7-HRas. Considering that a single ubiquitin molecule is approximately 8 kDa, the slower migrating form of ubiquitin-conjugated Ras (~ 36 kDa) most likely corresponds to a diubiquitinated form of the protein.

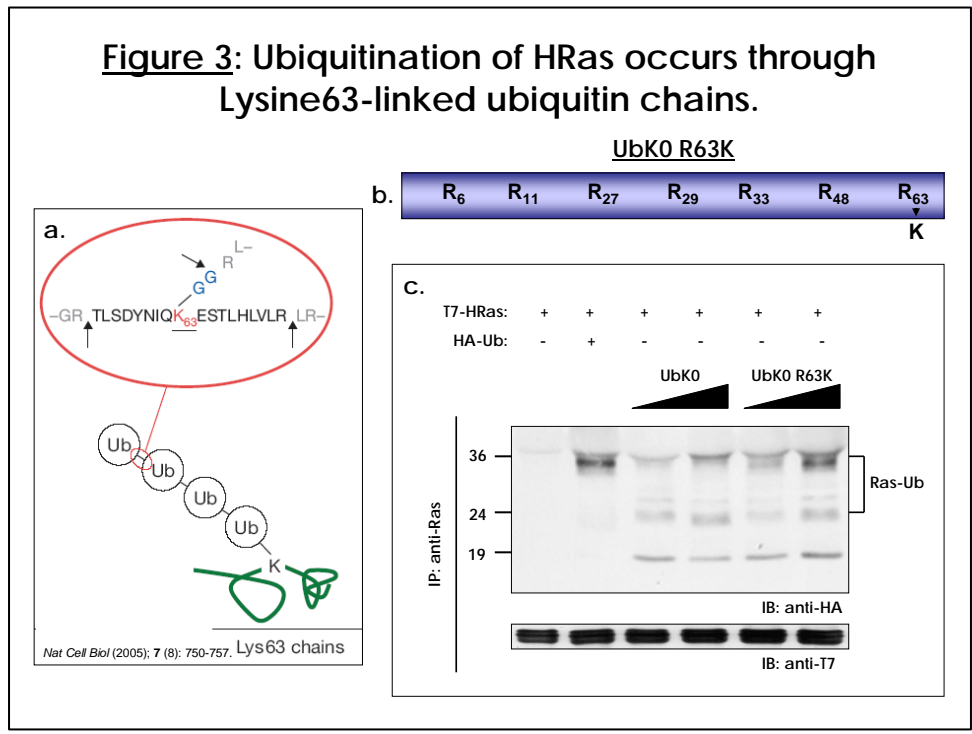
**Figure 2: H and NRas but not KRas is ubiquitinated.**



**Figure IV-2: H and NRas but not KRas is ubiquitinated.**

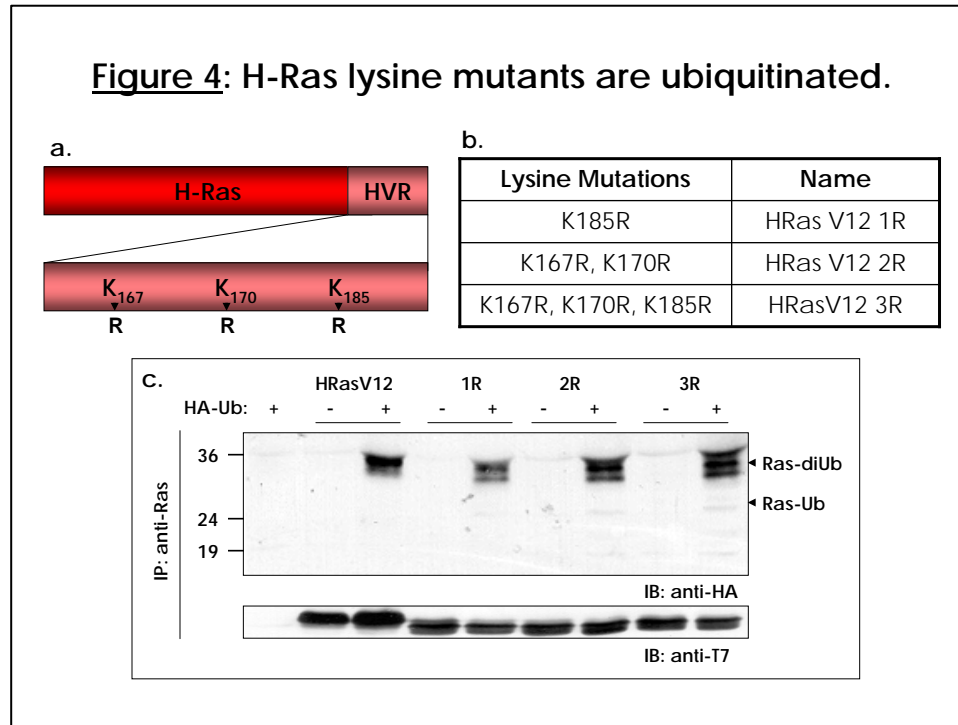
HRas and NRas undergo mono- and diubiquitination *in vivo*. KRas is not ubiquitinated. Lysates from CHOK1 cells expressing H, N, or KRas and HA-ubiquitin (HA-Ub) alone or in combination were subjected to Ras immunoprecipitation (IP) followed by immunoblotting (IB) with the indicated antibodies.





**Figure IV-3: Ubiquitination of HRas occurs through Lys63-linked ubiquitin chains.**  
**(a)** Schematic diagram of unique diglycine (-GG) signature peptides for Lys63-linked polyubiquitin chains.  
**(b)** Schematic representation of arginine to lysine mutation at position 63 in UbK0 R63K.  
**(c)** Immunoprecipitation of Ras from CHOK1 cells expressing T7-HRas with HA-Ub, lysine deficient HA-Ub (HA-UbK0) or HA-UbK0 with lysine 63 single knock-in (HA-UbK0R63K).  
 Adapted from (Jura, Scotto-Lavino et al. 2006).

**Figure 4: H-Ras lysine mutants are ubiquitinated.**



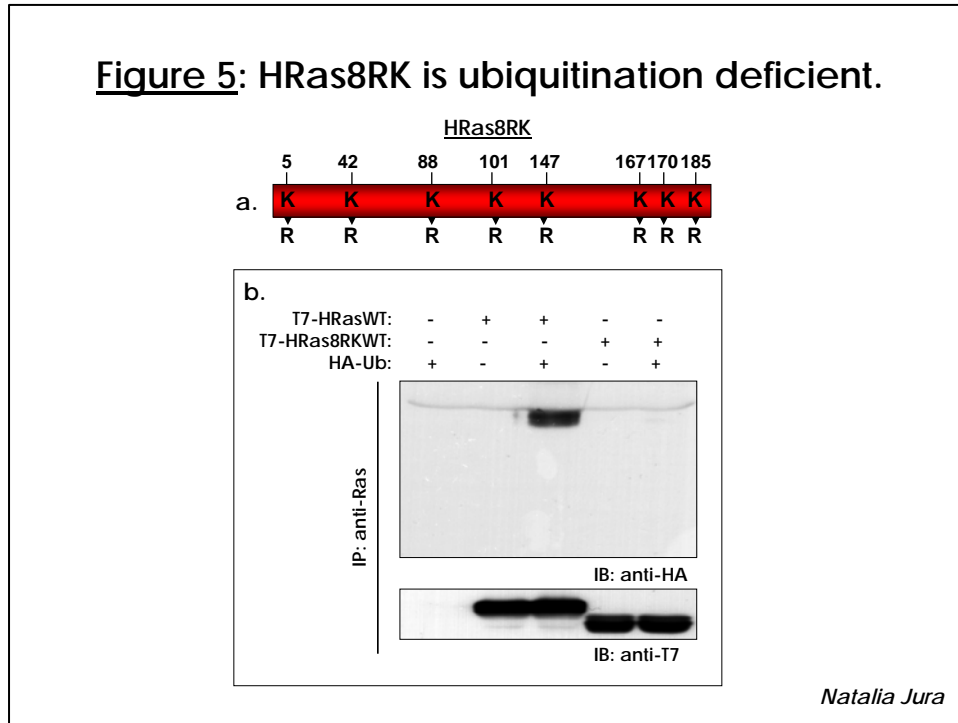
**Figure IV-4: H-Ras hypervariable region (HVR) lysine mutants are ubiquitinated.**

(a) The hypervariable region (HVR) of HRas contains three lysines (K167, K170, K185) which in principal could serve as acceptor sites for ubiquitin.

(b) Table of the HVR lysine mutants constructed.

(c) CHOK1 cells were transiently transfected with Fugene 6 Transfection Reagent. Forty-eight hours after transfection, cells were lysed and immunoprecipitated with an anti-Ras monoclonal antibody (Y13-259). The replacement of these lysines with arginines, individually or in combination, had no effect on the ubiquitination of H-Ras.

**Figure 5: HRas8RK is ubiquitination deficient.**



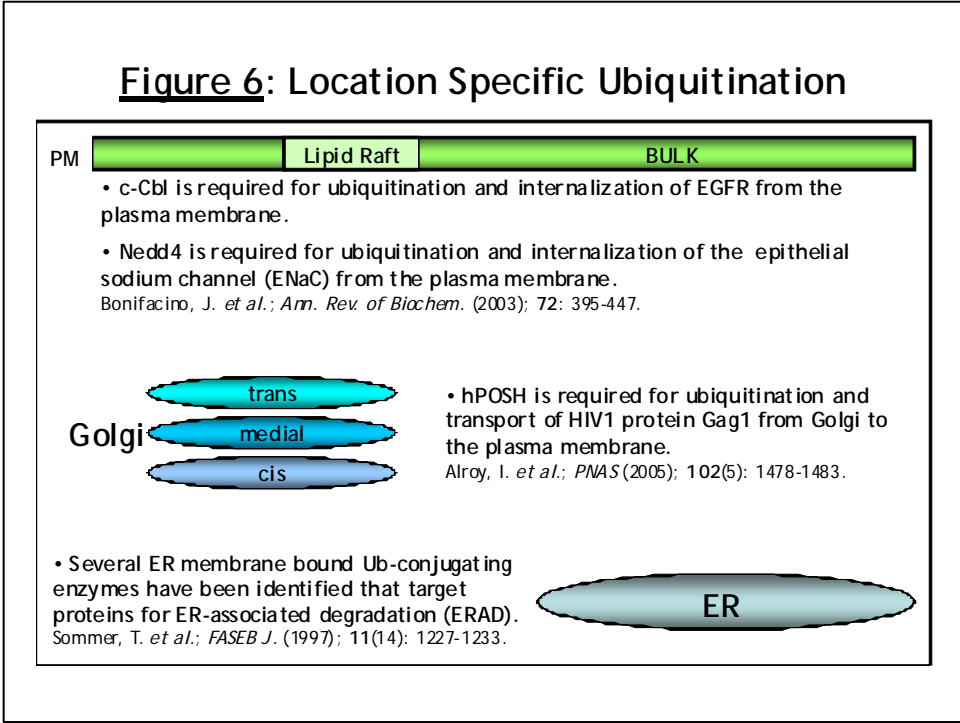
**Figure IV-5: Ubiquitination deficient HRas 8RK.**

(a) Schematic representation of lysine mutations in HRas8RK.

(b) The ubiquitination status of HRas and HRas8RK mutants was examined as described in the legend for **Figure 1**.

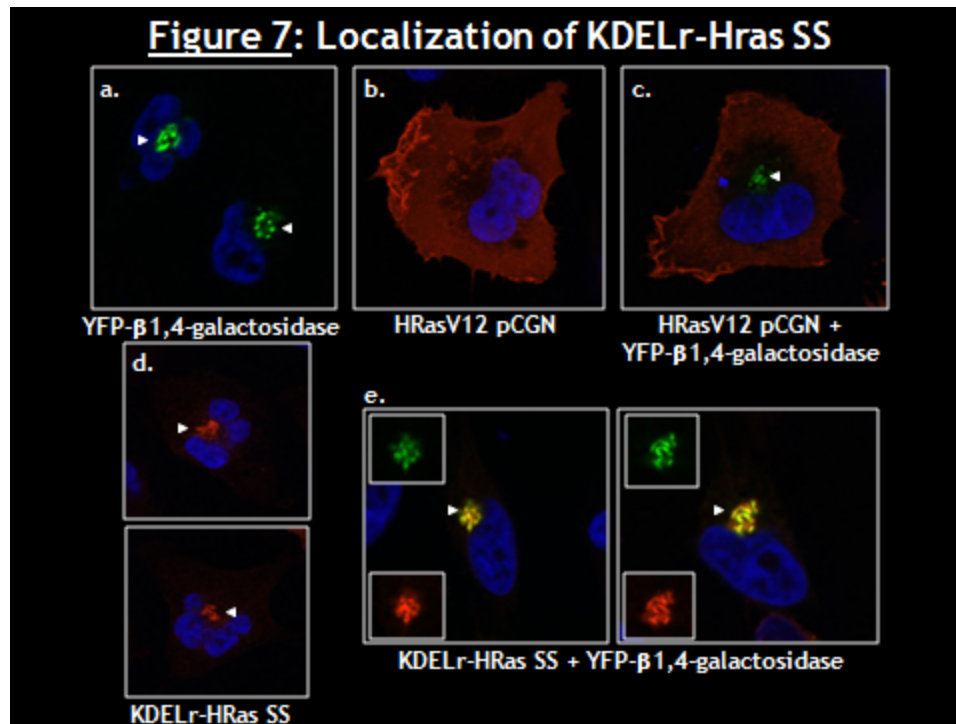
**This construct and data were generated by Natalia Jura, Bar-Sagi Lab.**

Adapted from (Jura, Scotto-Lavino et al. 2006).



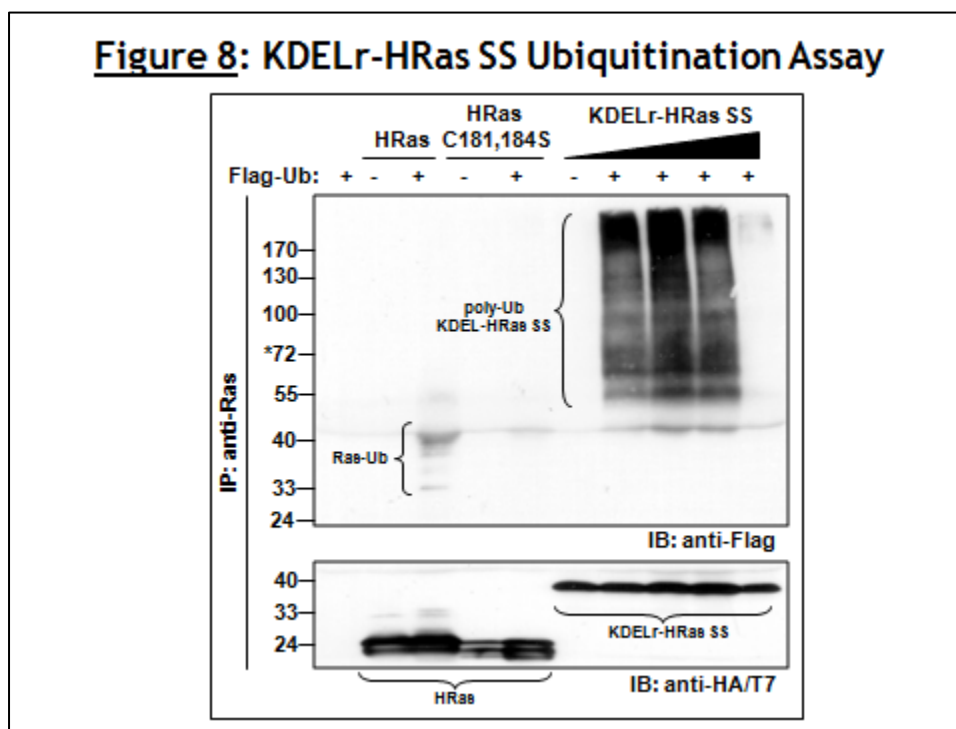
**Figure IV-6: Location Specific Ubiquitination within the Cell.**

Ubiquitination can occur at many different sites within the cell. Represented are examples of proteins ubiquitinated at the plasma membrane (PM), Golgi apparatus, and the endoplasmic reticulum (ER).



**Figure IV-7: Localization of KDELr-HRas SS.**

HTO cells were transfected with the appropriate constructs in the morning with Lipofectamine according to the manufacturer's instructions (Invitrogen, Carlsbad, CA). Approximately 6 hours following transfection, medium was changed and the cells were left overnight. In the morning of the following day, cells were fixed (3.7% formaldehyde) and stained. Immunofluorescence (IF) was performed using affinity purified anti-HA antibody. **(a)** Localization of YFP-β1,4-galactosidase to the Golgi illustrated in green. Nuclei are stained with DAPI in blue. **(b)** Localization of HRasV12 (red) in HTO cells. **(c)** Localization of HRasV12 (red) and YFP-β1,4-galactosidase (green). **(d)** Localization of Golgi-localized KDELr-HRas SS (green). **(e)** Co-localization of KDEL-HRas-SS and YFP-β1,4-galactosidase is indicated by arrows (yellow).



**Figure IV-8: KDELr-HRas SS Ubiquitination Assay.**

CHOK1 cells were cultured in Ham's F12 media supplemented with 10% fetal bovine serum (FBS). Cells were transiently transfected with the indicated plasmids using Fugene 6 (Roche). Cell lysis and immunoprecipitation of Ras with rat monoclonal anti-Ras antibody (Y13-259) was carried out as described (Corbalan-Garcia, Margarit et al. 1998). For precipitation of endogenous Ras, Y13-259 and control antibodies were cross-linked to protein A sepharose (Sigma) precoupled to rabbit anti-rat IgG (Rockland) by using dimethyl pimelimidate\*2 HCl, DMP (Pierce) as previously described (Simanis and Lane 1985). The lysis buffer was supplemented with 3 mM N-ethylmaleimide, NEM (Sigma) to inhibit deubiquitinating enzymes. Immunoblotting was performed using the following primary antibodies: anti-HA 12CA5 monoclonal (1:5000), anti-T7 monoclonal (Novagen, 1:10,000), anti-Ras monoclonal, clone Ras10 (Upstate 1:5000), anti-ubiquitin monoclonal, P4D1 (Santa Cruz Biotechnology, 1:1000), anti-EGFR polyclonal (Santa Cruz Biotechnology, 1:200), anti-total ERK monoclonal (Upstate, 1:1000) and anti-phosphoERK polyclonal (Cell Signaling, 1:1000). Secondary antibodies used were either goat anti-mouse (Cappel, 1:10,000) or goat anti-rabbit (Cappel, 1:5000) coupled to horseradish peroxidase.

**TABLES: Ras Targeting Constructs**

**Table 1: Constructs proposed in Thesis Proposal (August 2005)**

Chiu, V.K. et al.; *Nat. Cell Biol.* (2002); **4**: 343-350.

Arozarena, I. et al.; *MCB* (2004); **24** (4): 1516-1530.

| Title of Construct  | Subcellular Localization  | Characteristics   |
|---|---|---|
| <b>HRas C181/184S</b>   | <ul style="list-style-type: none"> <li>• Shuttles between ER and cytoplasm</li> <li>• Not retained at PM</li> </ul> | <ul style="list-style-type: none"> <li>• Palmitoylation deficient</li> <li>• HA-tag</li> </ul>  |
| <b>M1-HRas C181/184S</b><br>(avian infectious bronchitis virus M protein) | <b>ER</b>   | <ul style="list-style-type: none"> <li>• Residues 1-66</li> <li>• N-terminal fusion</li> <li>• HA-tag</li> </ul>                            |
| <b>KDELr-HRas C181/184S</b><br>(KDEL receptor)                            | <b>Golgi</b>  | <ul style="list-style-type: none"> <li>• N193D mutation so does not recycle to ER</li> <li>• N-terminal fusion</li> <li>• HA-tag</li> </ul> |

**Table 2: Peptide sequences used to target Ras to specific subcellular locations.**

| Peptide Sequence | Subcellular Localization         | Purpose  | Original Publication   |
|------------------|----------------------------------|--|--|
| <b>KDEL</b>      | <b>ER</b>                        | Used to target the fluorophore BODIPY <sup>581/591</sup> to the ER.  | Pap, E.H.W. et al.; <i>Experimental Cell Research</i> (2001); <b>265</b> : 288-293.      |
| <b>YQRL</b>      | <b>Trans-Golgi network (TGN)</b> | Used to target the ricin A chain to the TGN.                         | Zhan, J. et al.; <i>Biochem &amp; Biophys Res Commun</i> (2004); <b>313</b> : 1053-1057. |
| <b>SQYQRL</b>    | <b>Trans-Golgi network (TGN)</b> | Used to target the fluorophore BODIPY <sup>581/591</sup> to the TGN. | Pap, E.H.W. et al.; <i>Experimental Cell Research</i> (2001); <b>265</b> : 288-293.      |

**Table 3: All Ras targeting constructs used by Piero Crespo**Arozarena, I. et al.; *MCB* (2004); **24** (4): 1516-1530.Matallanas D. et al.; *MCB* (2006); **26** (1): 100-16.

| <b>Title of Construct</b>  | <b>Subcellular Localization</b>   | <b>Characteristics</b>  | <b>Original Publication</b>   |
|--|---|---|---|
| <b>HV12 SS (C181/184S)</b>   | <ul style="list-style-type: none"> <li>• <b>Shuttles between ER and cytoplasm</b></li> <li>• <b>not retained at PM</b></li> </ul> | <ul style="list-style-type: none"> <li>• Palmitoylation deficient</li> <li>• HA-tag</li> </ul>  | Chiu, V.K. et al.; <i>Nat. Cell Biol.</i> (2002); <b>4</b> : 343-350. |
| <b>M1-V12</b><br>(avian infectious bronchitis virus M protein)   | <b>ER</b>   | <ul style="list-style-type: none"> <li>• Residues 1-66</li> <li>• N-terminal fusion</li> <li>• HA-tag</li> </ul>                            | Arozarena, I. et al.; <i>MCB</i> (2004); <b>24</b> (4): 1516-1530.    |
| <b>KDELr-V12</b><br>(KDEL receptor)  | <b>Golgi</b>  | <ul style="list-style-type: none"> <li>• N193D mutation so does not recycle to ER</li> <li>• N-terminal fusion</li> <li>• HA-tag</li> </ul> | Arozarena, I. et al.; <i>MCB</i> (2004); <b>24</b> (4): 1516-1530.    |
| <b>CD8-V12</b><br>(CD $\alpha$ receptor)   | <b>Bulk membrane</b>  | <ul style="list-style-type: none"> <li>• N-terminus of the TM domain</li> <li>• N-terminal fusion</li> <li>• HA-tag</li> </ul>              | Arozarena, I. et al.; <i>MCB</i> (2004); <b>24</b> (4): 1516-1530.    |
| <b>LCK-V12</b><br>(protein kinase enriched in lipid rafts of T-cells; Tyr-phosphorylated upon T cell activation) | <b>Lipid rafts</b>  | <ul style="list-style-type: none"> <li>• N-terminal myristoylation signal of LCK (1-14)</li> <li>• HA-tag</li> </ul>                        | Su, M. et al.; <i>J. Immunology</i> (2001); <b>166</b> : 3975-3982.   |



**Table 4: Additional published Ras targeting constructs**

| <b>Title of Construct</b>      | <b>Subcellular Localization</b> | <b>Publication</b>  |
|--------------------------------|---------------------------------|---|
| <b>HRas V12 SS (C181/184S)</b> | <b>ER</b>                       | Chiu, V.K. et al.; <i>Nat. Cell Biol.</i> (2002); <b>4</b> : 343-350.   |
| <b>HRas C181S</b>              | <b>Golgi</b>                    | Roy, S. et al.; <i>Mol Cell Biol</i> (2005); <b>25</b> (15): 6722-6733. |
| <b>HRas C184S</b>              | <b>PM</b>                       | Roy, S. et al.; <i>Mol Cell Biol</i> (2005); <b>25</b> (15): 6722-6733. |

## **REFERENCES:**

- Andersen, J. S., C. E. Lyon, et al. (2002). "Directed proteomic analysis of the human nucleolus." Curr Biol **12**(1): 1-11.
- Andreassen, P. R., F. B. Lacroix, et al. (1998). "Differential subcellular localization of protein phosphatase-1 alpha, gamma1, and delta isoforms during both interphase and mitosis in mammalian cells." J Cell Biol **141**(5): 1207-15.
- Arozarena, I., D. Matallanas, et al. (2004). "Activation of H-Ras in the endoplasmic reticulum by the RasGRF family guanine nucleotide exchange factors." Mol Cell Biol **24**(4): 1516-30.
- Beckmann, J. S., F. Maurer, et al. (2005). "On ubiquitin ligases and cancer." Hum Mutat **25**(6): 507-12.
- Blat, C., J. Villaudy, et al. (1994). "Density-dependent inhibition of mouse embryo fibroblast growth: involvement of IGFBP-3." Exp Cell Res **215**(1): 114-8.
- Bringold, F. and M. Serrano (2000). "Tumor suppressors and oncogenes in cellular senescence." Exp Gerontol **35**(3): 317-29.
- Brummelkamp, T. R., S. M. Nijman, et al. (2003). "Loss of the cylindromatosis tumour suppressor inhibits apoptosis by activating NF-kappaB." Nature **424**(6950): 797-801.
- Burger, A. M. and A. K. Seth (2004). "The ubiquitin-mediated protein degradation pathway in cancer: therapeutic implications." Eur J Cancer **40**(15): 2217-29.
- Caloca, M. J., J. L. Zugaza, et al. (2003). "Exchange factors of the RasGRP family mediate Ras activation in the Golgi." J Biol Chem **278**(35): 33465-73.
- Chen, D., N. Kon, et al. (2005). "ARF-BP1/Mule is a critical mediator of the ARF tumor suppressor." Cell **121**(7): 1071-83.
- Chiu, V. K., T. Bivona, et al. (2002). "Ras signalling on the endoplasmic reticulum and the Golgi." Nat Cell Biol **4**(5): 343-50.

- Cohen, P. T. (1988). "Two isoforms of protein phosphatase 1 may be produced from the same gene." FEBS Lett **232**(1): 17-23.
- Colbran, R. J., M. A. Bass, et al. (1997). "Association of brain protein phosphatase 1 with cytoskeletal targeting/regulatory subunits." J Neurochem **69**(3): 920-9.
- Cole, N. B., C. L. Smith, et al. (1996). "Diffusional mobility of Golgi proteins in membranes of living cells." Science **273**(5276): 797-801.
- Corbalan-Garcia, S., S. M. Margarit, et al. (1998). "Regulation of Sos activity by intramolecular interactions." Mol Cell Biol **18**(2): 880-6.
- Corpet, F. (1988). "Multiple sequence alignment with hierarchical clustering." Nucleic Acids Res **16**(22): 10881-90.
- Croft, D. R., M. L. Coleman, et al. (2005). "Actin-myosin-based contraction is responsible for apoptotic nuclear disintegration." J Cell Biol **168**(2): 245-55.
- Dakshinamurti, S. (2005). "Regulation of myosin light chain phosphatase and pulmonary arterial relaxation." Can J Physiol Pharmacol **83**(10): 893-8.
- Deng, L., C. Wang, et al. (2000). "Activation of the I $\kappa$ B kinase complex by TRAF6 requires a dimeric ubiquitin-conjugating enzyme complex and a unique polyubiquitin chain." Cell **103**(2): 351-61.
- Di Fiore, P. P., S. Polo, et al. (2003). "When ubiquitin meets ubiquitin receptors: a signalling connection." Nat Rev Mol Cell Biol **4**(6): 491-7.
- Dimopoulos, G. J., S. Semba, et al. (2007). "Ca<sup>2+</sup>-dependent rapid Ca<sup>2+</sup> sensitization of contraction in arterial smooth muscle." Circ Res **100**(1): 121-9.
- Du, G. and M. A. Frohman (2008). "A Lipid-sigaled Myosin Phosphatase Surge Disperses Cortical Contractile Force Early in Cell Spreading." Mol Biol Cell.

- Durfee, T., K. Becherer, et al. (1993). "The retinoblastoma protein associates with the protein phosphatase type 1 catalytic subunit." Genes Dev **7**(4): 555-69.
- Egloff, M. P., P. T. Cohen, et al. (1995). "Crystal structure of the catalytic subunit of human protein phosphatase 1 and its complex with tungstate." J Mol Biol **254**(5): 942-59.
- Eto, M., J. A. Kirkbride, et al. (2005). "Assembly of MYPT1 with protein phosphatase-1 in fibroblasts redirects localization and reorganizes the actin cytoskeleton." Cell Motil Cytoskeleton **62**(2): 100-9.
- Fang, D. and T. K. Kerppola (2004). "Ubiquitin-mediated fluorescence complementation reveals that Jun ubiquitinated by Itch/AIP4 is localized to lysosomes." Proc Natl Acad Sci U S A **101**(41): 14782-7.
- Finley, D., S. Sadis, et al. (1994). "Inhibition of proteolysis and cell cycle progression in a multiubiquitination-deficient yeast mutant." Mol Cell Biol **14**(8): 5501-9.
- Geetha, T., J. Jiang, et al. (2005). "Lysine 63 polyubiquitination of the nerve growth factor receptor TrkA directs internalization and signaling." Mol Cell **20**(2): 301-12.
- Giehl, K. (2005). "Oncogenic Ras in tumour progression and metastasis." Biol Chem **386**(3): 193-205.
- Goldberg, J., H. B. Huang, et al. (1995). "Three-dimensional structure of the catalytic subunit of protein serine/threonine phosphatase-1." Nature **376**(6543): 745-53.
- Gordon, G. W., G. Berry, et al. (1998). "Quantitative fluorescence resonance energy transfer measurements using fluorescence microscopy." Biophys J **74**(5): 2702-13.
- Haglund, K., S. Sigismund, et al. (2003). "Multiple monoubiquitination of RTKs is sufficient for their endocytosis and degradation." Nat Cell Biol **5**(5): 461-6.

- Hancock, J. F. and R. G. Parton (2005). "Ras plasma membrane signalling platforms." Biochem J **389**(Pt 1): 1-11.
- Hartshorne, D. J. and K. Hirano (1999). "Interactions of protein phosphatase type 1, with a focus on myosin phosphatase." Mol Cell Biochem **190**(1-2): 79-84.
- Hartshorne, D. J., M. Ito, et al. (1998). "Myosin light chain phosphatase: subunit composition, interactions and regulation." J Muscle Res Cell Motil **19**(4): 325-41.
- Hershko, A., H. Heller, et al. (1983). "Components of ubiquitin-protein ligase system. Resolution, affinity purification, and role in protein breakdown." J Biol Chem **258**(13): 8206-14.
- Hicke, L. (2001). "Protein regulation by monoubiquitin." Nat Rev Mol Cell Biol **2**(3): 195-201.
- Hicke, L. and R. Dunn (2003). "Regulation of membrane protein transport by ubiquitin and ubiquitin-binding proteins." Annu Rev Cell Dev Biol **19**: 141-72.
- Hofmann, R. M. and C. M. Pickart (1999). "Noncanonical MMS2-encoded ubiquitin-conjugating enzyme functions in assembly of novel polyubiquitin chains for DNA repair." Cell **96**(5): 645-53.
- Hrabchak, C., H. Henderson, et al. (2007). "A testis specific isoform of endophilin B1, endophilin B1t, interacts specifically with protein phosphatase-1c gamma2 in mouse testis and is abnormally expressed in PP1c gamma null mice." Biochemistry **46**(15): 4635-44.
- Ito, M., T. Nakano, et al. (2004). "Myosin phosphatase: structure, regulation and function." Mol Cell Biochem **259**(1-2): 197-209.
- Jin, H., T. Sperka, et al. (2006). "Tumorigenic transformation by CPI-17 through inhibition of a merlin phosphatase." Nature **442**(7102): 576-9.
- Jung, J. R., H. Kim, et al. (2005). "The Phosphorylation status of merlin is important for regulating the Ras-ERK pathway." Mol Cells **20**(2): 196-200.

- Jura, N., E. Scotto-Lavino, et al. (2006). "Differential modification of Ras proteins by ubiquitination." Mol Cell **21**(5): 679-87.
- Kaneko, K., K. Satoh, et al. (2002). "Myosin light chain kinase inhibitors can block invasion and adhesion of human pancreatic cancer cell lines." Pancreas **24**(1): 34-41.
- Kirkpatrick, D. S., C. Denison, et al. (2005). "Weighing in on ubiquitin: the expanding role of mass-spectrometry-based proteomics." Nat Cell Biol **7**(8): 750-7.
- Kita, A., S. Matsunaga, et al. (2002). "Crystal structure of the complex between calyculin A and the catalytic subunit of protein phosphatase 1." Structure **10**(5): 715-24.
- Matheny, S. A., C. Chen, et al. (2004). "Ras regulates assembly of mitogenic signalling complexes through the effector protein IMP." Nature **427**(6971): 256-60.
- Matsumura, F. and D. J. Hartshorne (2008). "Myosin phosphatase target subunit: Many roles in cell function." Biochem Biophys Res Commun **369**(1): 149-56.
- Maynes, J. T., K. S. Bateman, et al. (2001). "Crystal structure of the tumor-promoter okadaic acid bound to protein phosphatase-1." J Biol Chem **276**(47): 44078-82.
- Mills, J. C., N. L. Stone, et al. (1998). "Apoptotic membrane blebbing is regulated by myosin light chain phosphorylation." J Cell Biol **140**(3): 627-36.
- Nijman, S. M., T. T. Huang, et al. (2005). "The deubiquitinating enzyme USP1 regulates the Fanconi anemia pathway." Mol Cell **17**(3): 331-9.
- Ohta, T. and M. Fukuda (2004). "Ubiquitin and breast cancer." Oncogene **23**(11): 2079-88.
- Okubo, S., M. Ito, et al. (1994). "A regulatory subunit of smooth muscle myosin bound phosphatase." Biochem Biophys Res Commun **200**(1): 429-34.

- Parra, M., T. Mahmoudi, et al. (2007). "Myosin phosphatase dephosphorylates HDAC7, controls its nucleocytoplasmic shuttling, and inhibits apoptosis in thymocytes." Genes Dev **21**(6): 638-43.
- Peng, J., D. Schwartz, et al. (2003). "A proteomics approach to understanding protein ubiquitination." Nat Biotechnol **21**(8): 921-6.
- Prior, I. A., A. Harding, et al. (2001). "GTP-dependent segregation of H-ras from lipid rafts is required for biological activity." Nat Cell Biol **3**(4): 368-75.
- Roy, S., B. Wyse, et al. (2002). "H-Ras signaling and K-Ras signaling are differentially dependent on endocytosis." Mol Cell Biol **22**(14): 5128-40.
- Schlabach, M. R., J. Luo, et al. (2008). "Cancer proliferation gene discovery through functional genomics." Science **319**(5863): 620-4.
- Scotto-Lavino, E., G. Du, et al. (2006). "3' end cDNA amplification using classic RACE." Nat Protoc **1**(6): 2742-5.
- Scotto-Lavino, E., G. Du, et al. (2006). "5' end cDNA amplification using classic RACE." Nat Protoc **1**(6): 2555-62.
- Scotto-Lavino, E., G. Du, et al. (2006). "Amplification of 5' end cDNA with 'new RACE'." Nat Protoc **1**(6): 3056-61.
- Shima, H., Y. Hatano, et al. (1993). "Identification of PP1 catalytic subunit isotypes PP1 gamma 1, PP1 delta and PP1 alpha in various rat tissues." Biochem Biophys Res Commun **192**(3): 1289-96.
- Simanis, V. and D. P. Lane (1985). "An immunaffinity purification procedure for SV40 large T antigen." Virology **144**(1): 88-100.
- Simpson, K. J., L. M. Selfors, et al. (2008). "Identification of genes that regulate epithelial cell migration using an siRNA screening approach." Nat Cell Biol.

- Swanson, K. A., R. S. Kang, et al. (2003). "Solution structure of Vps27 UIM-ubiquitin complex important for endosomal sorting and receptor downregulation." Embo J **22**(18): 4597-606.
- Swift, A. M. and C. E. Machamer (1991). "A Golgi retention signal in a membrane-spanning domain of coronavirus E1 protein." J Cell Biol **115**(1): 19-30.
- Terrak, M., F. Kerff, et al. (2004). "Structural basis of protein phosphatase 1 regulation." Nature **429**(6993): 780-4.
- Vale, R. D. and R. A. Milligan (2000). "The way things move: looking under the hood of molecular motor proteins." Science **288**(5463): 88-95.
- Weissman, A. M. (2001). "Themes and variations on ubiquitylation." Nat Rev Mol Cell Biol **2**(3): 169-78.
- Xia, D., J. T. Stull, et al. (2005). "Myosin phosphatase targeting subunit 1 affects cell migration by regulating myosin phosphorylation and actin assembly." Exp Cell Res **304**(2): 506-17.
- Yamashita, M., S. X. Ying, et al. (2005). "Ubiquitin ligase Smurf1 controls osteoblast activity and bone homeostasis by targeting MEKK2 for degradation." Cell **121**(1): 101-13.
- Yang, Y., C. C. Li, et al. (2004). "Regulating the p53 system through ubiquitination." Oncogene **23**(11): 2096-106.
- Yoshida, K., M. Watanabe, et al. (1999). "BH-protocadherin-c, a member of the cadherin superfamily, interacts with protein phosphatase 1 alpha through its intracellular domain." FEBS Lett **460**(1): 93-8.
- Zhang, H. G., J. Wang, et al. (2004). "Regulation of apoptosis proteins in cancer cells by ubiquitin." Oncogene **23**(11): 2009-15.



Zhong, Q., W. Gao, et al. (2005). "Mule/ARF-BP1, a BH3-only E3 ubiquitin ligase, catalyzes the polyubiquitination of Mcl-1 and regulates apoptosis." Cell **121**(7): 1085-95.

## **APPENDIX:**

### **Rapid Amplification of cDNA ends (RACE) Methods.**

During my time in the Frohman Lab, I was privileged to publish three method papers on rapid amplification of cDNA ends (RACE). Presented below are the abstracts from these papers.

#### **A. 5' RACE**

The 5' ends of transcripts provide important information about transcription initiation sites and the approximate locations of local cis-acting enhancer elements; it is therefore important to establish the 5' ends with some precision. RACE (rapid amplification of cDNA ends) PCR is useful for quickly obtaining full length cDNAs for mRNAs for which only part of the sequence is known and to identify alternative 5' or 3' ends of fully sequenced genes. The method consists of using PCR to amplify, from complex mixtures of cellular mRNA, the regions between the known parts of the sequence and non-specific tags appended to the ends of the cDNA. Whereas the poly(A) tail serves to provide such a tag at the 3' end of the mRNA, an artificial one needs to be generated at the 5' end, and various approaches have been described to address this step. The classical scheme for 5' RACE described here is simple, suffices in many instances in which RACE is needed and can be performed in 1–3 days (Scotto-Lavino, Du et al. 2006).

#### **B. 3' RACE**

Having knowledge of the entire 3' sequence of a cDNA is often important because the non-coding terminal region can contain signals that regulate the stability or subcellular localization of the mRNA. Also, some messages use alternative genomic sites for cleavage and polyadenylation that can alter the above properties, or change the encoded

protein. Full-length cDNAs can be obtained from complex mixtures of cellular mRNA using rapid amplification of cDNA ends (RACE) PCR as long as part of the mRNA sequence is known; adding non-specific tags to the ends of the cDNA allows the regions between the known parts of the sequence and the ends to be amplified. In 3' RACE, the poly(A) tail functions as a non-specific tag at the 3' end of the mRNA. cDNA ends can be obtained in 1–3 days using this protocol (Scotto-Lavino, Du et al. 2006).

### **C. “New” RACE**

‘New RACE’ (rapid amplification of cDNA ends) PCR is a method for obtaining full-length cDNA for mRNA for which only part of the sequence is known. Starting with cellular mRNA, PCR is used to amplify regions between the known parts of the sequence and nonspecific tags at the ends of the cDNA. In ‘new RACE’, an anchor is ligated to the 5' end of the mRNA before reverse transcription, resulting in the selective production of full-length 5' cDNA ends. Although ‘new RACE’ can also be used to amplify 3' ends, only the protocol for obtaining 5' ends is presented here. This protocol can be completed in 1–3 day (Scotto-Lavino, Du et al. 2006).